THE MODIFICATION, DESIGN AND DEVELOPMENT OF A SCALED-DOWN INDUSTRIAL FURNACE WITH INTERCHANGING BURNERS FOR ACADEMIC USE

by

Antonio Jose Mendes

A thesis submitted to the Department of Chemical Engineering

In conformity with the requirements for

the Degree of Master of Applied Science

Queen's University

Kingston, Ontario, Canada

July, 2010

For My Parents:

Antonio Freitas Mendes & Almerinda Linhares da Costa Mendes

Abstract

Industry is heavily dependent on the process of combustion and with a projected rapid increase for the demand of combustion-derived energy it is imperative to expose a new age of engineering professionals to the discipline of combustion engineering.

One purpose of this study was to modify an existing scaled-down industrial furnace and to retrofit it with the ability to interchange burners for academic application and combustion testing. A number of available industrial burners are presented and their qualities and drawbacks discussed. The modification of an existing scaled-down industrial tunnel furnace is proposed in this work with the objective of providing users with exposure to the control and safe operating strategies associated with industrial combustion.

The furnace system simulates a square-shaped tunnel geometry commonly found in industrial applications. A single nozzle mix burner is mounted along the furnace axis and operated with supporting equipment such as a burner control safeguard, a gas train, and an air supply. Details of the furnace are provided in this work. The concept of radiative heat transfer within a combustion enclosure is demonstrated through furnace simulation with Hottel's Zone Method.

Acknowledgements

In the research and writing of this paper I received moral, intellectual, and emotional support from numerous people. Among these, the following people stand out and through this mean of communication I manifest my sincere appreciation.

Firstly, I express my deepest gratitude and appreciation towards my supervisor, Dr. Edward W. Grandmaison of the Department of Chemical Engineering, Queen's University, primarily for giving me the opportunity to study under his guidance and for his continuous encouragement and assistance throughout the period of completing this project. His patience, advice and support have made this work very educational and enjoyable. I thank him for the support he extended during times when I most needed his help and for his assistance in teaching me a great deal about research, knowledge and development. I also thank him for the freedom and trust he placed in me during this project – our project.

I am very much in debt to my research fellow, Yong Jin Lee, for his never ending help and encouragement throughout this project. He gave me directions to places I thought I would never go. Thanks are also due to Dr. M. D. Matovic, York He, Graham Payne, and Zy Hu from the Department of Mechanical Engineering, Queen's University for their unceasing advice and support. I would also like to express my sincere gratitude to the administrative and technical staff of the Department of Chemical Engineering for their continuous support in ways that are too many to mention here.

Last, but certainly not least, I am truly thankful to my parents (Antonio and Almerinda) and brothers (Francisco Paulo and Moises Duarte) for their tremendous encouragement and moral support during the period of this research work. They knew I could accomplish this monumental undertaking before I did.

Table of Contents

List of Figures

List of Tables

Chapter 1

Introduction

As we continue to make our way into the twenty-first century, the dependence and importance of energy for industry, transportation, and electricity generation is very profound. Fossil fuels and their combustion has been by far the most predominant source of energy and will most likely continue that way for many years to come (Baukal and Schwartz, 2001). The field of industrial combustion is very broad and touches all aspects of our lives. The majority of the materials that we use in our day-to-day activities have been prepared through some type of heating process (Baukal, 2003). Combustion has been the foundation of worldwide industrial development for over the past 200 years (U.S. DOE, 1998). For all practical purposes, it was not until the onset of the Industrial Revolution in the nineteenth century that mankind learned how to harness power from combustion. The applications of combustion have progressed rapidly since that time of history, and many of today's industries have come into existence as a direct result of this achievement (Baukal and Schwartz, 2001).

Industry is heavily dependent on the process of combustion as shown Table 1.1. Common heating applications and examples in the process industry are listed in Table 1.2 while the major uses for combustion in process heating are shown in Table 1.3.

Table 1.1: The Importance of Combustion in Industry (U.S. DOE, 1998)

	Percentage of Total Energy Form		
Industry	**Steam**	**Heat**	**Combustion**
Petroleum Refining	29.6	62.6	92.2
Forest Products	84.4	6.0	90.4
Steel	22.6	67.0	89.6
Chemicals	49.9	32.7	82.6
Glass	4.8	75.2	80.0
Metal Casting	2.4	67.2	69.6
Aluminum	1.3	17.6	18.9

Table 1.2: Examples of Processes Requiring Industrial Combustion (U.S. DOE and EIA, 1999)

Process Industry	**Examples of Processes Using Heat**
Steel Making	Smelting of ores, Melting, Annealing
Chemicals	Chemical reactions, Pyrolysis, Drying
Nonmetallic Minerals (Bricks, Glass, Cement)	Firing, Kilning, Drying, Calcining, Melting, Forming
Metal Manufacture (Iron and Steel, Nonferrous Metals)	Blast furnaces, Soaking and heat treatment, Melting, Sintering, Annealing
Paper and Printing	Drying

Table 1.3: Process Heating Operations (U.S. DOE, 1998)

Metal Melting
- Steel making
- Iron and steel melting
- Nonferrous melting

Metal Heating
- Steel soaking, reheat, ladle preheating
- Forging
- Nonferrous heating

Metal Heat Treating
- Annealing
- Stress relief
- Tempering
- Solution heat treating
- Aging
- Precipitation Hardening

Curing and Forming
- Glass annealing, tempering, forming
- Plastic fabrication
- Gypsum production

Fluid Heating
- Oil and Natural Gas Production
- Chemical/Petroleum feedstock preheating
- Distillation, visbreaking, hydrotreating, hydrocracking, delayed coking

Bonding
- Sintering
- Brazing

Drying
- Surface film drying
- Rubber, plastic, wood, glass products drying
- Coal drying
- Food processing
- Animal food processing

Calcining
- Cement, lime, soda ash
- Alumina
- Gypsum

Clay Firing
- Structural products
- Refractories

Agglomeration
- Iron
- Copper
- Lead

Nonmetallic Materials Melting
- Glass

Other Heating
- Ore heating
- Textile manufacturing
- Food production
- Aluminum anode baking

Moreover, due to the high dependence of industry on combustion, Figure 1.1 tells us that our demand for energy is expected to increase rapidly. Eighty-eight percent (88%) of all sources of energy are produced by the combustion of fossil fuels such as oil, natural gas, and coal (Baukal, 2003). According to a joint effort between the U.S. Department of Energy and the Energy Information Administration (1999) the energy demand in the industrial sector is projected to increase by 0.8% per year to the year 2020.

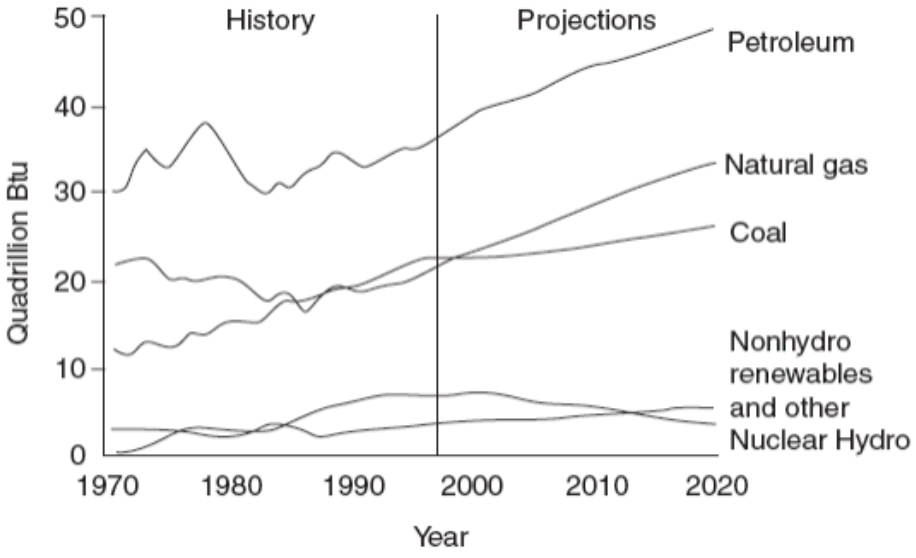

Figure 1.1: Historical and Projected World Energy Consumption (U.S. DOE, 1998)

Power generation, oil refining, and chemical processes - to name a few - are all energy intensive industries with combustion applications in burners, process heaters, boilers, cogenerative systems, thermal oxidizers, and flares. Combustion in the industries mentioned in Table 1.2 and Table 1.3 presents unique challenges related to the variety of fuel compositions encountered. For all circumstances, combustion equipment must be flexible to be able to operate in a safe, reliable, efficient, and environmentally responsible

manner under a wide array of fuel compositions and conditions (Baukal and Schwartz, 2001).

Over time, demands placed on combustion systems become more stringent and change continuously. Combustion safety has always been paramount and essential, but emphases on heat transfer effectiveness, temperature uniformity, efficiency, controls, and, more recently, environmental emissions have evolved with time. Such demands create great challenges for those who are interested in the discipline of combustion, namely combustion engineers. These challenges have been successfully met in most applications by combining sound engineering practices with creative and innovative problem solving (Baukal and Schwartz, 2001). Transmitting these findings to a new age of combustion engineers has proven difficult. Combustion engineering is a "dying form of art" that is losing its position as a mainstream form of engineering in today's higher learning institutes. Combustion is an exciting and intellectually challenging field containing plenty of opportunities to enhance fundamental and practical knowledge. The passing on of this knowledge to a new and upcoming generation of combustion personnel will ultimately lead to the development of new products with improved performances.

1.1 Motives

With a projected rapid increase for the demand of combustion derived energy it is imperative, and thus the main motive of this project, to expose undergraduate engineering students to the discipline of combustion engineering. The fields of general combustion investigations are very broad. For the purposes of this thesis, the research activity in the

discipline of industrial combustion technology focuses on three important areas of study. They are as follows:

1. The reduction and control of emissions released from the energy and heating industry.
2. Combustion safety and control.
3. Industrial combustion control and energy efficiency.

Environmental quality and Greenhouse Gases (GHG) are currently the key factors that are shaping the future of industrial combustion (Baukal, 2004). The desire to reduce and ultimately control emissions is determined primarily by governmental and environmental regulations. In their 2005 Greenhouse Gas Inventory report, Environment Canada (2007) has indicated that the total GHG emissions for Canada have increased by 25.3% since 1990. These emissions can also be expressed in terms of GHG intensities, which provide an estimate of the GHG emissions normalized with respect to the gross domestic product (GDP).

Table 1.4: Trends in Emission Intensities (Environment Canada, 2007)

	1990	1995	2000	2001	2002	2003	2004	2005
Total GHG (Mt)	**596**	**646**	**721**	**714**	**720**	**745**	**747**	**747**
Change since 1990 (%)	N/A	8.3	21.0	19.8	20.9	25.0	25.4	25.3
Annual Change (%)	N/A	2.8	3.7	-0.9	0.9	3.4	0.3	-0.1
GDP (Billions 1997$)	**708**	**773**	**946**	**961**	**989**	**1013**	**1046**	**1079**
Change since 1990 (%)	N/A	9.2	33.7	35.7	39.8	43.1	47.8	52.5
Annual Change (%)	N/A	2.6	5.5	1.5	3.0	2.4	3.3	3.2
GHG Intensity (Mt/$B GDP)	**0.84**	**0.84**	**0.76**	**0.74**	**0.73**	**0.74**	**0.71**	**0.69**
Change since 1990 (%)	N/A	-0.8	-9.5	-11.7	-13.5	-12.7	-15.1	-17.8
Annual Change (%)	N/A	0.2	-1.7	-2.4	-2.1	1.0	-2.8	-3.1
GDP: Industrial Sector Real Gross Domestic Product								

Table 1.4 indicates that the GHG emission intensities in Canada have decreased a total of

17.8% over this fifteen-year period. Although these results indicate promising progress in diminishing industry GHG emissions, there will be a long-term requirement for increased reductions to meet future regulatory policies. This need for increased reductions in GHG emissions is particularly important for CO_2 emissions, which can be obtained by various strategies such as improved combustion efficiency (Burggraaf et al., 2007) and CO_2 sequestration (bu-Khader, 2006).

Nitrogen oxides (NO_x) are an exceptionally important air pollutant (Grandmaison, 2007). NO_x is a standard term representing mono-nitrogen oxides (NO and NO_2) that are produced during combustion at high temperatures, such as the type found in industrial combustion processes (Branch Environmental Corp., 2009). In the presence of excess oxygen, the majority of nitrogen oxides are emitted into the atmosphere as nitric oxide, NO, and converted to nitrogen dioxides, NO_2.

As mentioned previously, thermal NO_x (mainly NO) is produced during high temperature combustion processes that allow nitrogen to be oxidized. The formation of NO by oxidation of atmospheric nitrogen can be expressed in terms of the overall reaction as follows:

$$\frac{1}{2}\,N_2 + \frac{1}{2}\,O_2 \rightleftharpoons NO$$

The rate of formation of NO is a function of temperature and residence time of nitrogen at high operating temperatures. At these high temperatures, usually above 1400^{o}C (Gupta and Lilley, 1992), nitrogen (N_2) and oxygen (O_2) molecules in the combustion air

disassociate into their atomic states and undergo a series of reactions known as the Zeldovich Mechanism. The Zeldovich Mechanism (Zeldovich, 1946) is the most commonly used method to model the formation of NO. The following chemical reaction pathways and their activation energies describe the Zeldovich Mechanism.

$$N_2 + O \rightleftharpoons NO + N \qquad E_A = 315 \text{ KJ/mol}$$

$$N + O_2 \rightleftharpoons NO + O \qquad E_A = 26 \text{ KJ/mol}$$

$$N + OH \rightleftharpoons NO + H \qquad E_A = 0 \text{ KJ/mol}$$

From this reaction mechanism, NO formation is controlled by the first reaction due to its high activation energy (E_A = 315 KJ/mol). For fuel-rich combustion processes, the concentration of oxygen is low making the second reaction of the Zeldovich Mechanism less important than in fuel-lean combustion. The last reaction of atomic nitrogen with the hydroxyl radical (OH) becomes the major sink for nitrogen radicals (N) (Grandmaison, 2007).

NO_x emissions along with volatile organic compounds (VOCs) are major precursors of smog. Reactions between NO_x, particulate matter, and VOCs in the presence of sunlight create ground-level ozone, leading to photochemical smog (Badjagbo et al., 2007; Grandmaison, 2007; and Turns, 2000). Nitrous oxide (N_2O) is also of interest as a major GHG and air pollutant. When N_2O enters the lowest portion of the earth's atmosphere, known as the troposphere (0 to 17 km above earth's surface), it is converted to NO by way of reacting with oxygen (known as photolysis), becoming an ozone depleting

substance (Kramlich and Linak, 1994).

The Kyoto Protocol, initially adopted on 11 December 1997, went into effect on 16 February 2005 with an aim at combating global warming and achieving the "stabilization of greenhouse gas concentrations in the atmosphere at a level that would prevent dangerous anthropogenic interference with the climate system" (United Nations, 1998). On 17 December 2002, Canada ratified the treaty with a commitment requiring it to reduce GHG emissions to 6% below 1990 levels during the 2008 - 2012 commitment period (Graves and Boucher, 2002 and Wang and Wiser, 2002). Global warming is a direct result of GHG emissions. As suggested by its name, greenhouse gases trap the sun's energy within the Earth's atmosphere increasing the global surface temperature as a result. This effect is depicted in Figure 1.2.

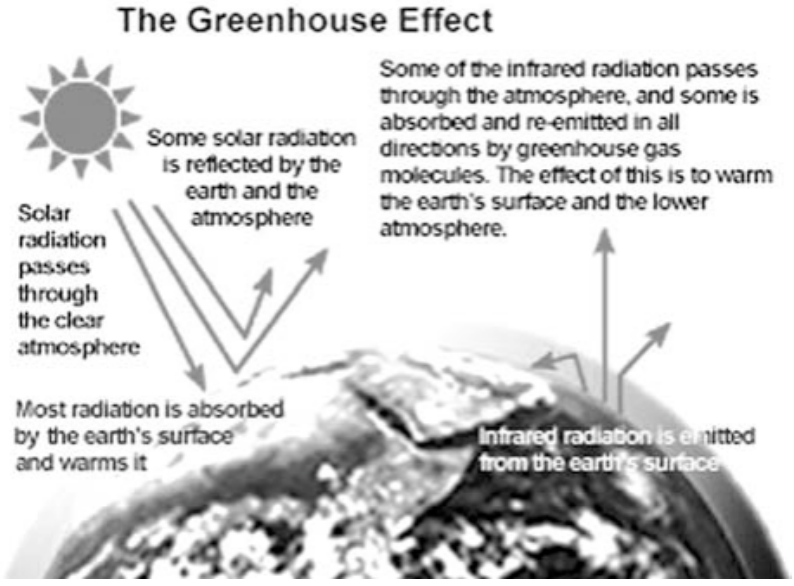

Figure 1.2: The Greenhouse Gas Effect (U.S. EPA, 2007)

Figure 1.3 displays the rise of global temperature from the years 1880 through 2000,

which consequently indicates a rise in global surface temperatures of 0.5°F to 1.0°F (0.3°C – 0.6°C) since the late 19th century. With the demand of industrial combustion generated energy expected to increase, the concentration of GHG is also expected to increase as a consequence. As a result, it is argued that if the concentration of these gases continues to increase, then global warming will accelerate. Thus the need to reduce and control the emissions released from the energy and heating industry.

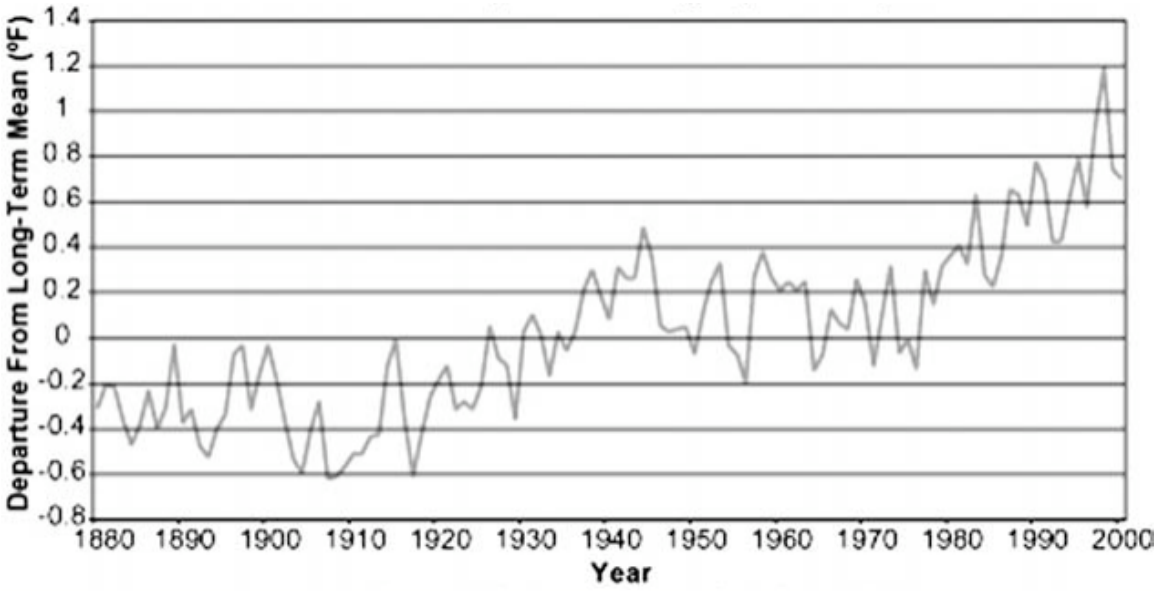

Figure 1.3: Global Temperature Changes From 1880–2000 (U.S. EPA, 2007)

Aside from emission control, it is also the motive of this thesis to expose engineering students to the safety aspect of industrial combustion technology. In spite of extensive research and development for more than 100 years to prevent and mitigate fires and explosions in the process industries, these hazards continue to threaten industries that manufacture, use and/or handle flammable gases, liquids, and dusts of combustible materials. Fire and Explosion mechanisms almost always lead to serious financial losses

in terms of damage to facilities and down time. They also often cause serious injuries to personnel to the extent of fatalities (Eckhoff, 2005).

Regrettably, process industries are not immune to accidents, as evidenced by fires and explosions that have been well documented by Richardson (1991), Sanders (1999), and many others. Numerous factors can contribute to an accident. Kletz (1994 and 1991) and the Centre for Chemical Process Safety (1994) have suggested a number of potential factors that cause industrial accidents. These factors are summarized by Baukal and Schwartz (2001) in the following list.

- Human error
- Equipment malfunction
- Upset plant conditions
- Other fires and/or explosions near the apparatus in question
- Improper procedures
- Severe weather conditions

Garrison (1988) reviewed the largest losses of the hydrocarbon process industry from 1957 through 1986 and found that vapour cloud explosions caused 42% of all accidents (refer to Figure 1.4). Garrison classifies vapour cloud explosions as gas explosions within buildings as well as outdoors or unconfined explosions. Run-away reactions, explosions in solids, Boiling Liquid Expanding Vapour Explosions (BLEVEs), loss of containment, and gas explosions internally in process equipment are classified as "Explosions" and constitute 22% of all accidental events (Eckhoff, 2005).

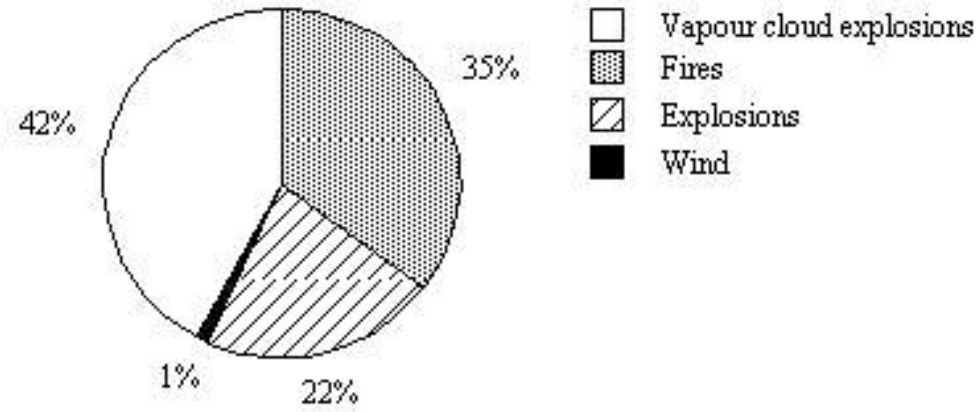

Figure 1.4: Accidental Factors for the 100 Largest Losses in the Hydrocarbon Process Industry from 1957 to 1986 (Garrison, 1988).

In similar fashion, the American Petroleum Institute (1979) reported the following causes of industrial incidents noted for 88 accidents that occurred in chemical and refining unit operations from 1959 through 1978. The percentages represent the rate of occurrence of each factor between the aforementioned timeline.

- 28% due to human error
- 28% due to equipment failures
- 13% due to faulty design
- 13% due to improper education
- 11% due to inadequate procedures
- 5% due to insufficient inspection
- 2% due to upsets in processes

Looking into the details of accidental fires and explosions, one finds a large variety in size of fires/explosions and their loss experience. Accident records enables one to learn that fires and explosions have a tendency to repeat themselves under similar conditions.

Therefore, it is important that accidents are reported and their causes disclosed so as corrective actions can be taken to minimize and perhaps prevent losses from future incidents (Eckhoff, 2005).

Aside from the factors that can contribute to accidents, there are also many potential dangers that are caused by fires and explosions: flying shrapnel, pressure waves from an explosion, high heat loads from flame radiation, and high temperatures (Crocker and Napier, 1986 and Center for Chemical Process Safety, 1996 and 1989). All these potential dangers, as well as others not mentioned here, may have severe consequences for both people and process equipment. Hence, all dangers must be considered when minimizing the probable impact of an accident (Baukal and Schwartz, 2001).

The consequences of a gas explosion depends on numerous factors, such as: type of fuel and oxidizer; size and fuel concentration of a combustible cloud; location and strength of an ignition source; size, type, and location of an explosion vent area(s); location and size of building elements and process equipment; and mitigation and prevention schemes. Gas explosions are very sensitive to these factors. Therefore it is not a straightforward or simple task to estimate the consequences of a gas explosion.

The risk of a fire and explosion can be defined as "the product of the probability of a fire and/or explosion and its expected consequence" (Eckhoff, 2005). In fire and gas explosion risk management the basic principle is to minimize the probability of a fire and of an explosion, which is in turn related to the explosion consequences. Both active and passive measures are used to reduce the consequences of a fire or explosion. The most

important means of preventing and mitigating or controlling fires and explosions can be found in the following overall goals that have high priority in fire and explosion management (Eckhoff, 2005):

- Prevention and control of potential leaks of combustible gases.
- Good ventilation to minimize extent and duration of explosion due to gas releases.
- Prevention and control of possible ignition sources.
- Minimize equipment blockage to ease explosion venting and to minimize flow turbulence during gas cloud formation and explosion.
- Installation of blast and fire barriers.

In similar fashion, Lee (2005) concentrates on three preventive and controlling measures for fire and gas explosions. The three measures are as follows: Elimination/control of flammable gas concentration; Elimination/control of oxidant concentration; and Elimination/control of ignition sources.

Combustion safety considerations as well as the reduction of emission release from energy and heating industries are both managed through control system processes. Hence, another motive for this thesis is to introduce combustion control systems to those interested in industrial combustion technology. Baukal (2003) notes that various control system components, concepts, and philosophies necessary for understanding how control systems work, what the systems are designed to accomplish, and what criteria the controls engineer uses to design and implement a system is imperative for personnel entering a combustion relied industry. According to Baukal and Schwartz (2001) the

purpose of a control system is to "start, operate, and shut down the combustion process and any related auxiliary processes safely, reliably, and efficiently."

Control systems are composed of various logical and physical components that are set-up according to a predefined design philosophy. They are arranged in such a manner that the control system provides its user with an informative, consistent, and easy-to-use interface (Baukal and Schwartz, 2001). Combustion control has increased in interest as of late. Improving a system performance and efficiency, such as reducing the levels of pollutant emissions, and decreasing the risk factor of fires and explosions due to high operating temperatures allows combustion control to have an objective – an objective of optimizing combustor operation, monitor its process, and alleviate instabilities and their severe consequences (Docquier and Candel, 2002).

A combustion control system consists of three feed lines that all converge at one or more burners: a fuel supply line, a combustion air supply line, and an ignition system. During the system start up, and for the duration of normal operation, the control system verifies the status of these three lines or systems and changes their condition and action as needed (Baukal, 2003). The combustion control system must follow specific procedures before, during, and after operation or risk causing catastrophic damage to structures, process equipment, and/or personnel. The most common source of furnace explosions, for example, is the use of an improper lighting procedure. Baukal and Schwartz (2001) as well as Niemkiewicz and Becker (1998) outline a safe furnace lighting procedure for a combustion chamber containing piloted burners. The generalized steps in this procedure

is as follows (taken from Baukal and Schwartz, 2001):

1. Confirm that the burner fuel lines are completely isolated from the furnace (either by disconnection, blind flange, or a double block and bleed valve assembly).
2. Confirm that all auxiliary furnace equipment is functioning properly, including all instrumentation and measurement devices. Open both the burner air inlet register/damper and the furnace stack damper to the fully open position.
3. Purge the furnace of any combustible or flammable substances.
4. Test the atmosphere inside the furnace to ensure that there are no combustibles present.
5. Connect the pilot fuel line(s) to the burner. Activate the permanent pilot igniter or insert a portable pilot igniter or premixed ignition torch.
6. Slowly open the pilot fuel control valve to the manufacturer-specified pilot fuel pressure; visually confirm stable ignition of the pilot flame(s).
7. Reestablish the main burner fuel supply (either by connecting the main fuel line(s), removing a blind flange, or reversing the double block and bleed valve assembly) to provide a fuel source to the furnace.
8. Slowly open the main burner fuel control valve to supply the burner with the manufacturer-specified ignition fuel pressure. Visually confirm stable ignition of the main burner flame.

In order to optimize the efficiency of a combustion system, the control system obtains various items of process information or signal inputs, such as temperatures, pressures,

and flow rates. Furthermore, the system of controls monitors all of the safety parameters that are in place at all times and will shut down the combustion process if any of the safety limits are not met (Baukal, 2003). A simplified flow diagram showing a standard burner light-off sequence is shown in Figure 1.5. This figure displays a series of sequencing steps that must be followed in order for proper shutdown and extinguishment of a furnace burner. As a rule, the control system monitors all of the inputs, and if they are all satisfactory, allows the combustion system to safely shut down. If a monitored parameter (i.e. temperature, pressure, flow rate of fuel, etc.) is on when it should be off, and vice versa, the shutdown process is aborted and the system must be reset before another shutdown is permitted. The system also controls such things as which valves are suppose to be opened and in what order they are to be opened, if and when the pilot is ignited/turned off, and if and when the main burner operation is allowed or not allowed (Baukal and Schwartz, 2001).

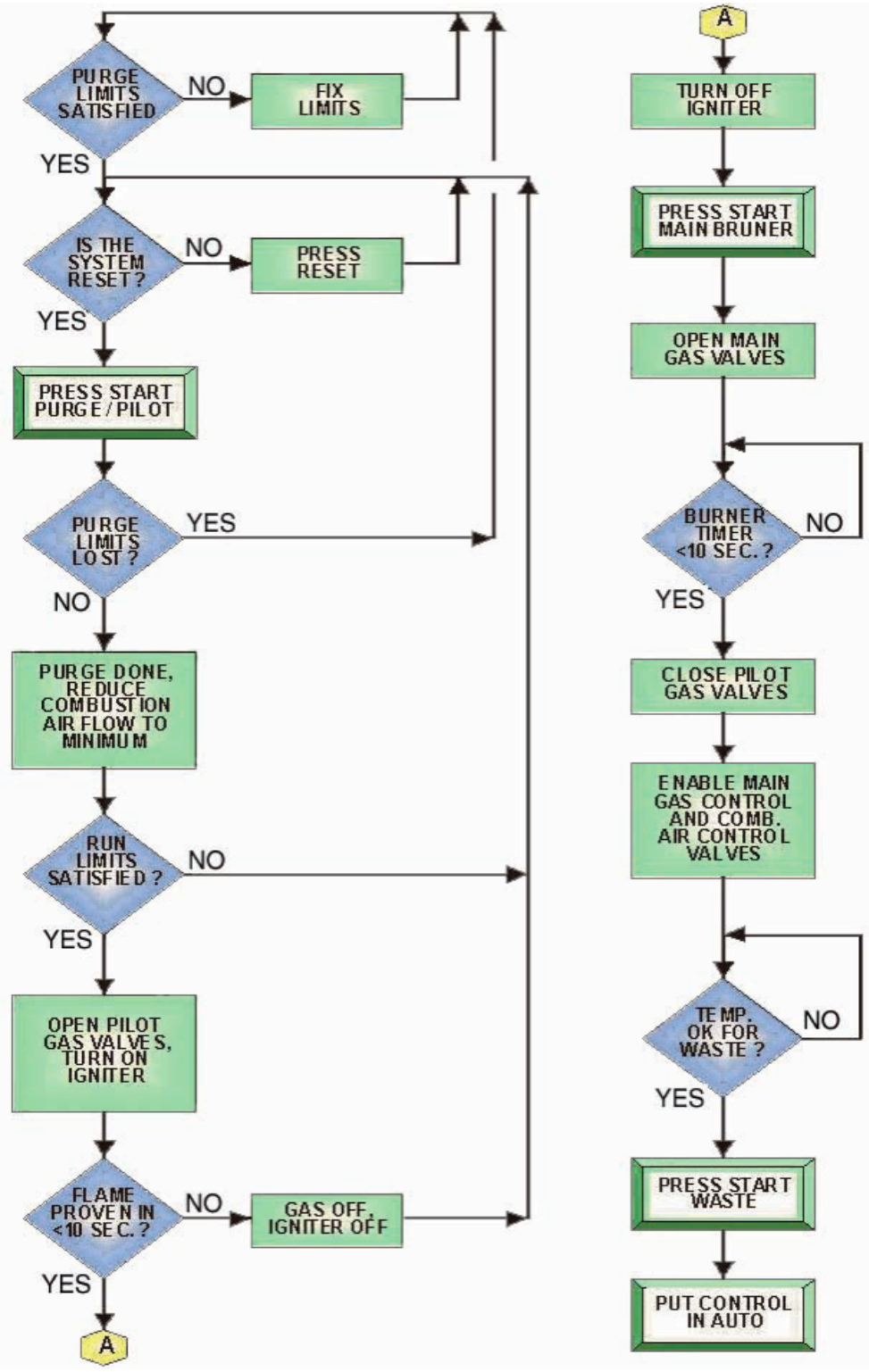

Figure 1.5: Flow Diagram of a Standard Burner Light-off Sequence (Baukal and Schwartz, 2001)

These three important areas of industrial combustion technology (reduction of pollutant emissions, combustion safety, and combustion control and efficiency) are important to understand for individuals who are interested in the field of combustion engineering. Hence, it is the motive of this thesis to expose these areas of combustion study to those wishing to follow a path of industry heating for energy intensive industries.

1.2 Objectives

In order to introduce undergraduate engineering students to the discipline of industrial combustion, it is the objective of this thesis to take an existing scaled-down industrial tunnel furnace and modify it in a manner that enables its users to interchange combustion burners. The comparison of different burners allows one to not only understand the control and safety strategies that are associated with industrial combustion but also enables one to compare and draw a distinction between the burners through their emissions and efficiencies.

1.3 Introduction to the Apparatus

The apparatus in question is a scaled down industrial type vertical tunnel furnace that was jointly commissioned by the Chemical Engineering and Mechanical Engineering Departments of Queen's University for the Center for Advance Gas Combustion Technology (CAGCT). It was initially constructed based on a design by Becker (1999) with the main goal of operating under a flameless combustion mode in the form of a Strong Jet/Weak Jet configuration. This type of configuration and mode of furnace

operation is discussed in more detail in Chapter 3 of this thesis report.

The furnace has a 400 mm square cross section with aluminum water-cooled modular sections that can be added to create a furnace of different lengths (typically ~1.4 m). In order to maintain high operating temperatures, the inner walls of the furnace are covered with a refractory or insulation lining. The furnace is aligned vertically and fired from the bottom. The furnace is equipped with view ports and sampling ports in some of the sidewall elements as well as a view port and an explosion vent at the top of the furnace and thermocouple ports for wall temperature measurements. The flue gases are removed from the furnace by an ejector system directing the exhaust gases through appropriate ductwork away from the test facility.

Pressure and gas temperature measurements within the furnace are to be taken and reported as well as the concentrations of hydrocarbon gases (HC), carbon monoxide (CO), carbon dioxide (CO_2), oxygen (O_2), and nitrogen oxides (NO_X) by means of a gas analyser. All these measurements are to be acquired in the near-burner zone of the furnace using a water-cooled sampling probe and a thin-wire thermocouple. A temperature profile of the inner walls of the furnace will also be achievable using thermocouples distributed along the axial direction of the furnace.

1.4 Outline of the Thesis

In the present thesis report, an attempt will be made to illustrate the technology of industrial combustion for the sole purpose of exposing the areas of combustion study to

those who wish to follow a path into the science of energy intensive heating industries. Chapter 2 deals with the background information of industrial furnaces and the various types of combustion burners that are available for the heating industry. Chapter 3 presents the reader with the previously mentioned furnace and its components along with design objectives and how it will be modified for future use. The concepts of the transfer of heat, in particular radiative heat transfer, as applied to combustion are discussed and analyzed in Chapter 4. Finally, in Chapter 5 a summary or restatement of the important findings presented in the previous chapters is presented along with recommendations for future work.

Chapter 2

Background

Since it is the purpose of this thesis project to introduce the science and engineering of industrial combustion, the main components of combustion system processes are presented and discussed in this chapter, with emphasis on combustion burners. The experimental set-up of the furnace apparatus will include an interchangeable burner section to allow users to compare and contrast the efficiency and emission control of various burners using the same scaled-down industrial furnace described in this thesis. Unless stated otherwise, the greater part of the information and material in the following section and subsequent subsections are cited from Baukal and Schwartz (2001) and Baukal (2000), two textbooks dealing with industrial combustion theory and practice. The emphasis is on highlighting points and details of interest to the student embarking on a combustion project.

A combustion system is composed primarily of five elements that transfer thermal energy from a combustion process to some type of heat load. This system is pictured in Figure 2.1. One component - and arguably the most important element of a combustion system – is the burner that, along with an oxidizer (i.e. air or pure oxygen), combusts with a fuel to release heat in the process. Another piece of a combustion system is the material or load that is being heated to a desired temperature. Both the burner and the

load(s) are situated in the third element of a combustion system – the combustor, which may be a furnace, heater, or dryer (for the purposes of this thesis report, a furnace will be the combustor of choice). In the majority of more advanced and costly systems, there will be a heat recovery mechanism that increases the thermal efficiency of the overall combustion system. This is the fourth component of a combustion system. Finally, the fifth section of a thermal heating device – and an important aspect for this thesis report - is a flow control system that can control the inlet and outlet streams of fuel, oxidizer, and exhausts or emissions.

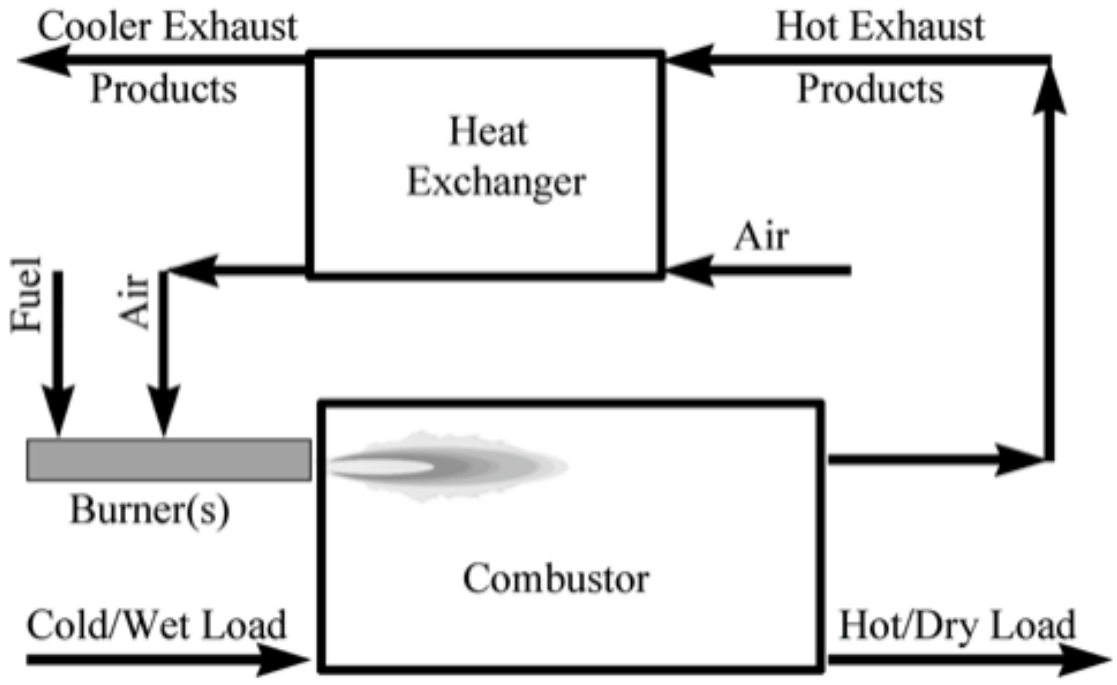

Figure 2.1: Schematic Diagram of the Major Components of a Combustion System (Baukal, 2000)

Of all the elements of a combustion system, and for the purposes of this thesis, the burner component of a combustion scheme is focused on in this chapter and is discussed in great

detail. Put simply, a burner is a device used to provide heat. It is used to combust a fuel along with the aid of an oxidizer, converting the chemical energy in the fuel into thermal energy in the process. A combustion burner provides three important design functions. These functions are as follows:

1. A burner must provide a controlled mixing of reactants, fuel, and oxidizing agent.
2. A burner must provide a stable self-renewing ignition source (i.e. pilot, spark, etc.).
3. A burner must provide a controlled region of reaction and/or controlled flame shape.

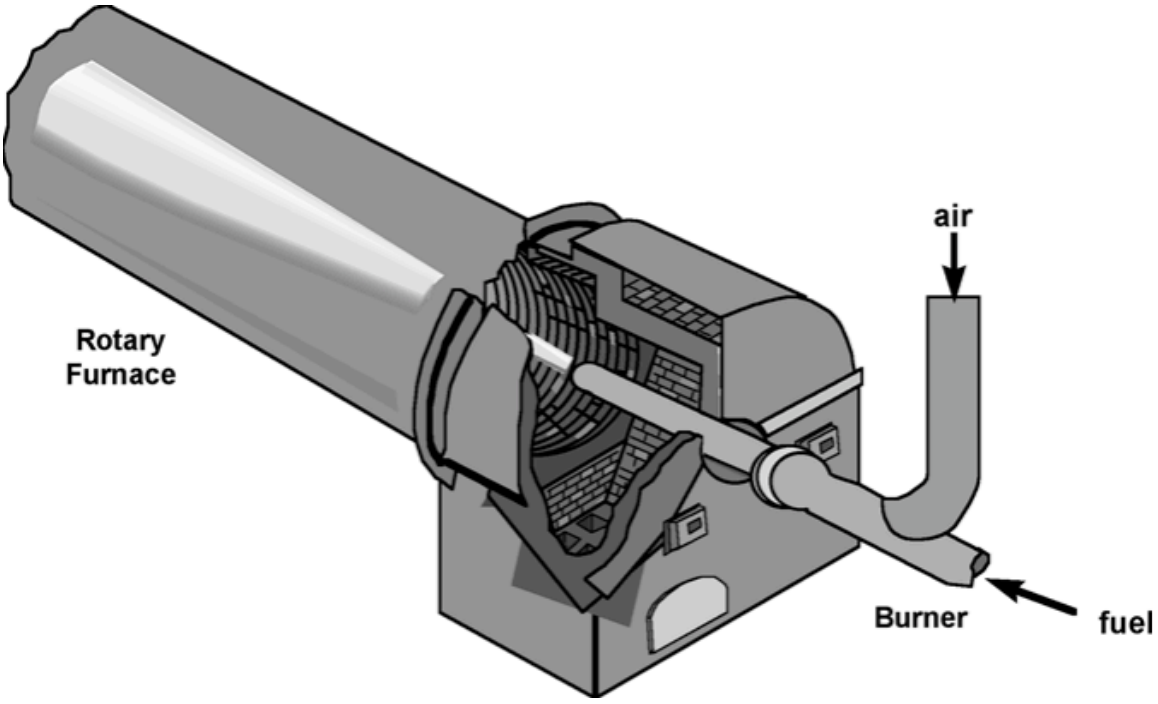

Figure 2.2: Single Burner Rotary Furnace (Baukal, 2000)

Depending on the size and type of the application, a combustion system can have single or multiple burners. In a rotary furnace or kiln, for example, a single burner is located on one end of a cylindrically shaped furnace as pictured in Figure 2.2. Its cylindrical

geometry limits the size and load type that makes use of it. Hence a rotary kiln is restricted to certain types of applications such as melting scrap aluminum or producing cement clinker. More common combustion systems consist of multiple burners and a rectangular or square geometry, such as a regenerative glass furnace as illustrated in Figure 2.3.

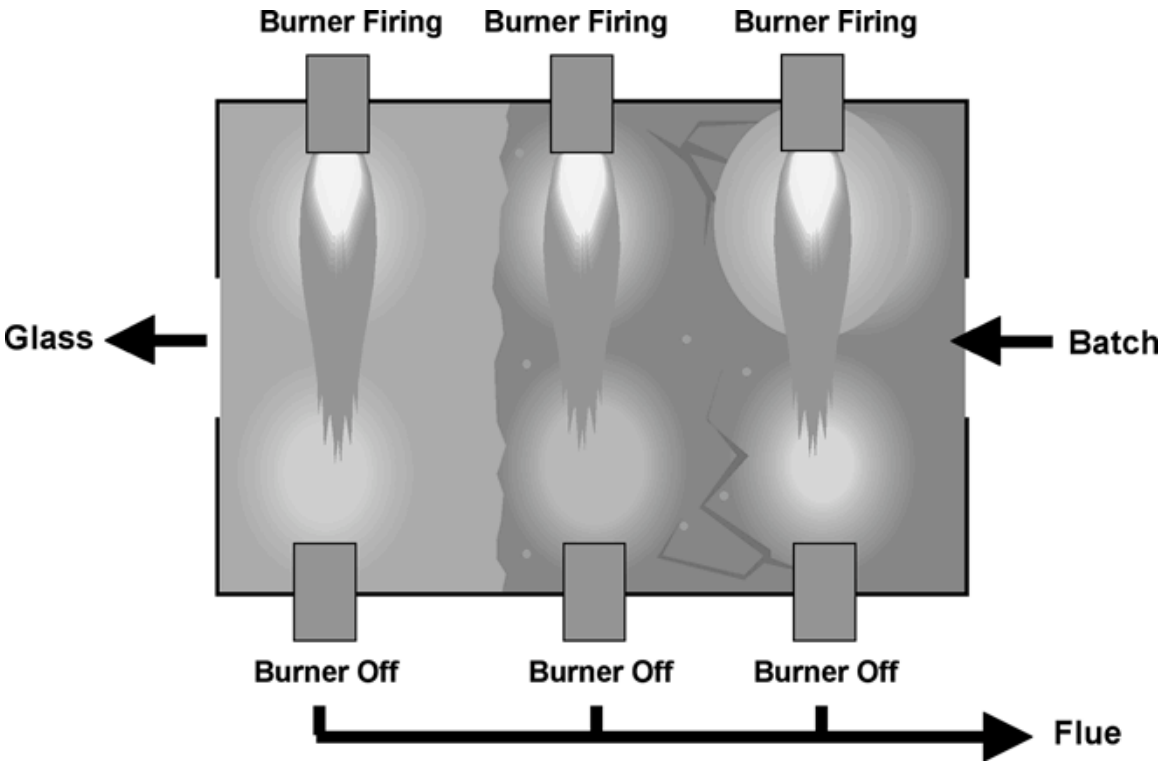

Figure 2.3: Multiple Burners in a Side-fired Regenerative Glass Furnace (Baukal, 2000)

2.1 Burner Design

A number of factors go into the design of a furnace burner. Due to the specialization of different industrial processes, and furnace designs to meet the requirements of these processes, the need for specialized burners has resulted. As mentioned previously,

burners are created and developed with the intention of providing stable working conditions as well as providing a suitable flame pattern over a predefined set of operating conditions. An industrial combustion burner must also be designed taking into account that there are specified maximum allowable levels of pollutant emissions that can be generated through a given combustion process. In order to help regulate the design of combustion burners, the American Petroleum Institute (1995) issued a guideline for burners used in industry. Burners must follow certain specifications of operating conditions as outlined by the aforesaid institute. These specifications have been summarized by Baukal and Schwartz (2001) and include the following:

- Specific types of fuels.
- Specific range of fuel compositions.
- Maximum, normal, and minimum heat release rates.
- Maximum fuel pressures available.
- Maximum atomizing medium pressures available for liquid firing.
- Fuel temperature.
- Oxidant sources - ambient air, exhaust gases, or enriched oxygen.
- Available combustion air pressure, whether forced (positive) or induced (negative).
- Combustion air temperature (ambient or preheated).
- Furnace firebox temperature.
- Furnace dimensions for flame size restrictions.
- Type of flame (configuration or shape).

An industrial burner must take into account a number of design factors as well as a quantity of competing priorities when being designed to follow these specifications.

2.1.1 Competing Priorities for Burner Design

Traditional designs of combustion burners have changed over the space of time, primarily due to the increasing popularity of reducing emissions that may pollute the surrounding environment. In its early years, a burner was designed with the sole intent of combusting a fuel efficiently and transferring the maximum amount of released energy to a heating load. More recently however, and due to new and more stringent environmental regulations, when it is designed, a burner must take into account pollutant emissions that it produces. It is therefore no surprise that reducing pollutant emissions and maximizing combustion efficiency are at odds with one another when a combustion burner design is in question.

A prime example of maximizing combustion efficiency versus minimizing pollutant emissions is a well-known technique of reducing NO_X emissions identified as staging. In this technique, the primary flame zone is deficient of either fuel or oxidizer reducing the peak temperatures in this flame zone and at the same time altering the chemistry in a way that reduces NO_X emissions - fuel-rich or fuel-lean zones are less conducive to NO_X formation than near-stoichiometric zones (Reese et al., 1994). NO_X emissions are exponentially dependent on the combustion gas temperature as shown in Figure 2.4. This figure displays the effect that the exhaust product gas has on NO_X emissions and how even the smallest reduction in the peak flame temperature can produce a dramatic

reduction in NO_X emissions.

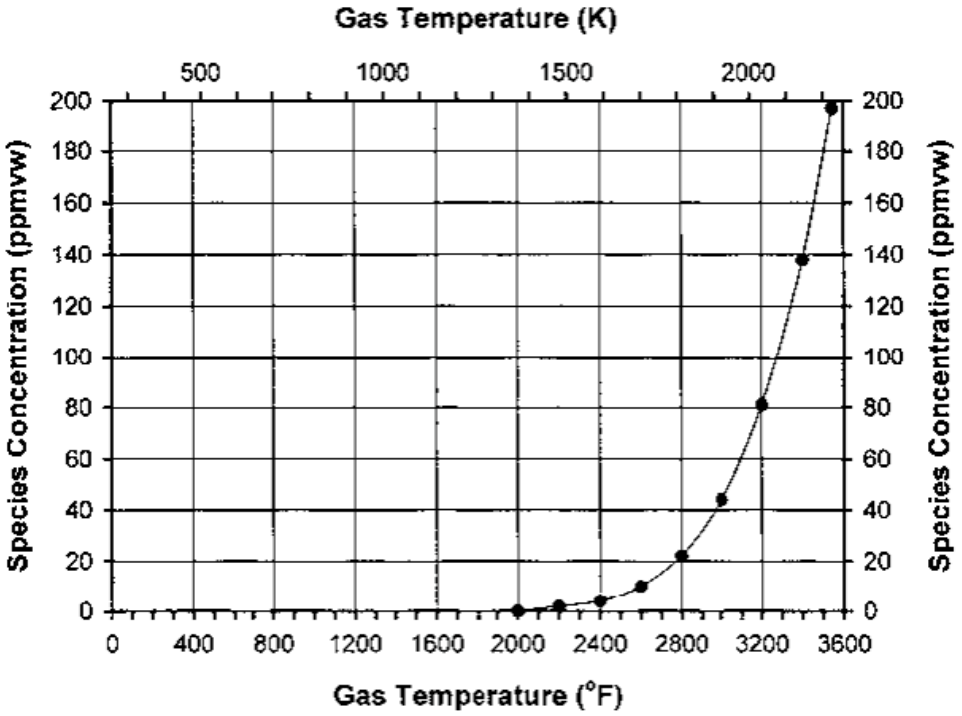

Figure 2.4: Dependence of NO_X (in parts per million on a wet basis, or ppmvw) on Gas Temperature for Adiabatic Equilibrium Combustion of Air/CH_4 (Baukal, 2000)

By lowering flame temperatures, NO_X emissions are reduced. However, lowering flame temperatures has its consequences and results in an adverse affect on combustion efficiency. Reduced peak flame temperatures causes a decrease in the radiant heat transfer from the flame given that radiation is dependent on the fourth power of the absolute temperature of combustible gases. Not only does staging minimize combustion efficiency but it also increases levels of CO emissions, which is the main indication of incomplete combustion and reduced combustion efficiency.

Another example of maximizing combustion efficiency versus minimizing pollutant

emissions is the issue of mixing between the fuel and oxidizer. Maximizing the mixing between the fuel and oxidizer has always been an essential component of ensuring complete combustion, especially if the fuel was hard to burn (i.e. low heating value fuels such as waste liquid fuels or used process gases from chemicals production).

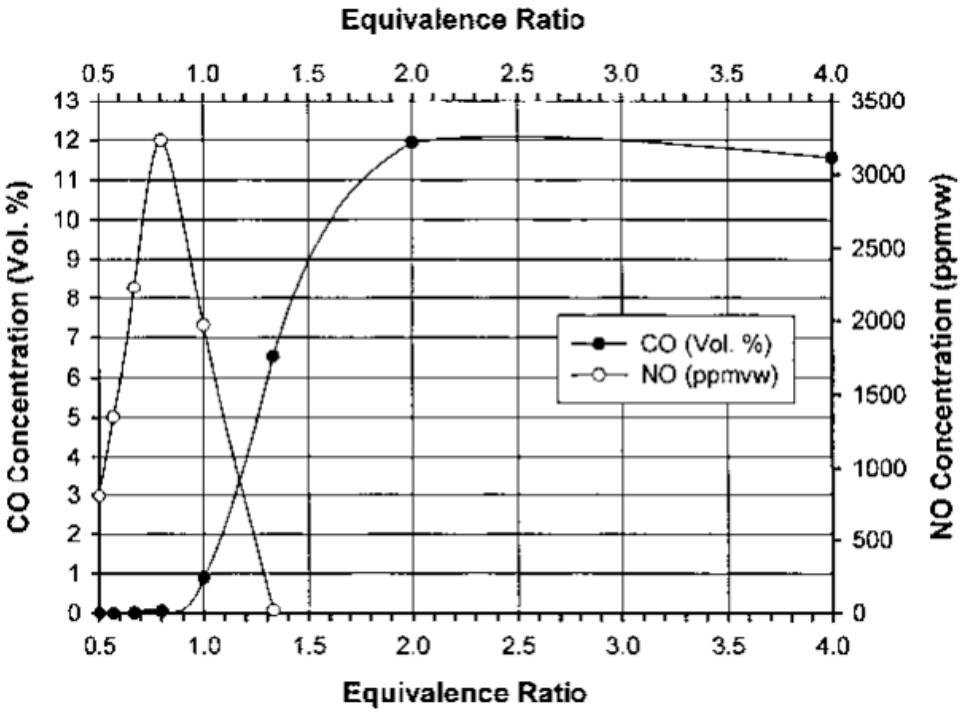

Figure 2.5: NO_X and CO Dependence on the Equivalence Ratio for Adiabatic Equilibrium Air/CH_4 Flames (Baukal, 2000)

Current trends force the engineer to design the burner in such a manner that the mixing of fuel and oxidizer be maximized while simultaneously minimizing polluting effects. This is a very hard task to achieve as pictured in Figure 2.5 where NO_X and CO emissions more often than not take opposite paths. A low NO_x emission strength may mean a high CO concentration, and vice-versa. Therefore, it is important for modern burners to be efficient at transferring heat to a load, while simultaneously maintaining an

environmentally friendly operation with the emissions they release into the atmosphere.

2.1.2 Burner Design Factors

Many designs exist for industrial burners for a number of reasons including factors that affect the types of fuels, oxidizers, environmental pollutant regulations, combustor chamber/furnace geometries, heat transfer requirements, as well as other varying types of burner design considerations. The most important design factors are discussed in this section of the chapter. In order for an industrial combustion burner to provide acceptable operation, the burner must be designed according to a number of design factors referred to as the "5 M's". These five important burner deign components are designated by Baukal and Schwartz (2001) as follows:

- **Metering:** The fuel and oxidizer must be metered into the flame zone.
- **Mixing:** The fuel and oxidizer must be mixed in such a way that the fuel is efficiently and effectively used.
- **Maintaining:** For stable burner operation, a continuous ignition zone must be maintained.
- **Molding:** The design of the burner must be able to mold the combustion flame in order to provide a proper and desired flame shape.
- **Minimizing:** It is a desire of the burner to reduce and minimize its emissions that may pollute its surroundings.

The design factors aforementioned as the "5 M's" are discussed in more detail in the following subsections.

2.1.2.1 Fuel and Oxidizer Metering

Typically, a process heater has multiple burners installed in a combustion chamber to ensure proper heat distribution. Therefore, a fuel system for such a configuration must be designed in a fashion that normally allows proper and equal fuel distribution to all burners. Fuel pressures and fuel flow to each burner are critical for the proper operation of the furnace. The total flow of fuel to the furnace operating system does not suffice. Ensuring that each burner uses the correct amount of fuel from the overall system must be taken into consideration when designing a combustion burner. The proper amount of fuel flow is controlled using a system of metering orifices or ports specifically designed for each burner. These orifices either allow fuel flow or limit the flow of fuel through each burner. Using this system ensures the passing of a known and specified amount of fuel at a given fuel pressure.

The metering ports for burners that combust gaseous fuels are installed on the burner device where the actual flame is formed. This location is known as the "burner throat". The fuel injector tips and the metering ports are either centered or located on the outside edge of the "burner throat" as displayed in Figure 2.6.

Figure 2.6: Typical Gas Burner Tips with Metering Ports (Baukal and Schwartz, 2001)

The metering system on premixed combustion burners serves dual purposes. The single metering orifice is located at the entrance of a venturi eductor that causes a pressure drop allowing the gaseous fuel discharging from the orifice to entrain air for combustion. A premixed burner metering system is shown in Figure 2.7 and displays the description from above.

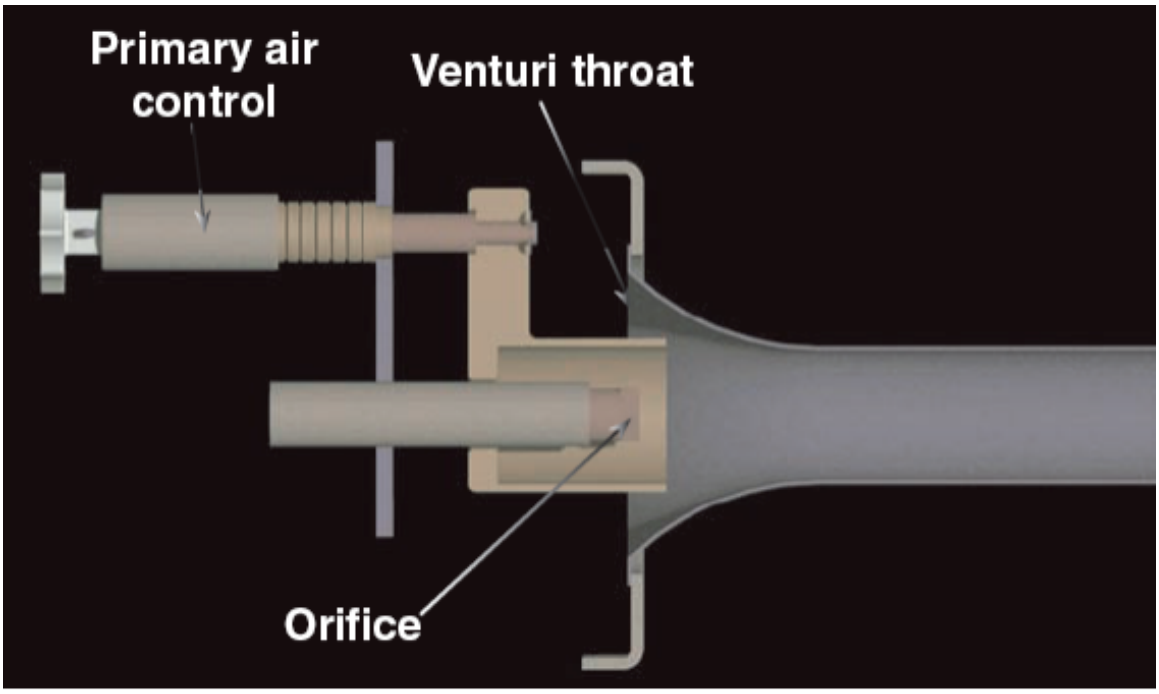

Figure 2.7: Premixed Burner Metering Port and Air Mixer Assembly (Baukal and Schwartz, 2001)

Unlike gaseous fuels, liquid fuels must be vaporized or atomized into small liquid droplets in order to burn. Burners that are designed to combust liquid fuels have an atomizer incorporated into its design. An atomizer literally sprays the liquid fuel through a single or several small openings that results in small fuel droplets, which in turn enhances the vaporization of the fuel. The need for liquid fuel atomization impacts the fuel flow metering of the burner. The metering design of an atomizing burner is more complicated due to the fact that the liquid fuel must be mixed with an atomizing medium (typically steam or air). Aside from the need for orifices designed to measure the flow of the mixture, using liquid fuel calls for two separate flow metering orifices: fuel metering orifices and atomizing media metering orifices. Figure 2.8 displays three typical liquid fuel burner atomizer configurations that can be used for more than one type of liquid fuel.

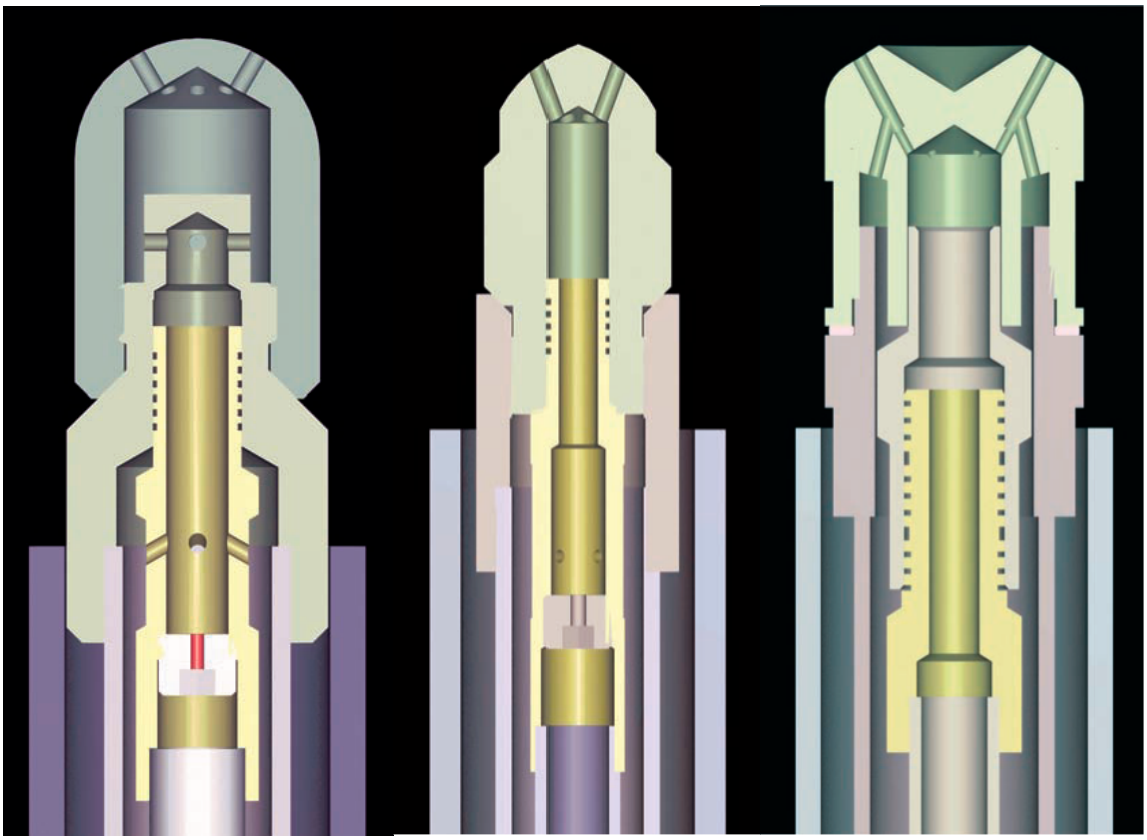

Figure 2.8: Cross Sectional Views of Liquid Fuel Burner Atomizer Tip Configurations (Baukal and Schwartz, 2001)

The combustion oxidizer or air is metered in order to ensure that proper airflow and air pressure is reaching the burner. This allows the burner to operate under safe and optimal conditions. The metering of the oxidizer is achieved at the burner "throat" as pictured in Figure 2.9. The throat is the designated part of the burner where the airflow metering takes place as well as the point where the majority of the air pressure loss is used to combust the fuel. In the majority of all burners, it is at the throat where the fuel is first injected into the air stream and it is at this location where the initiation of combustion and ignition occurs. The design of the burner throat is important for two critical and essential reasons:

1. Achieving proper flow of the combustion air is crucial to meet the demands of the combustion fuel.
2. The burner throat design plays a vital role in controlling the pattern of the burner flame.

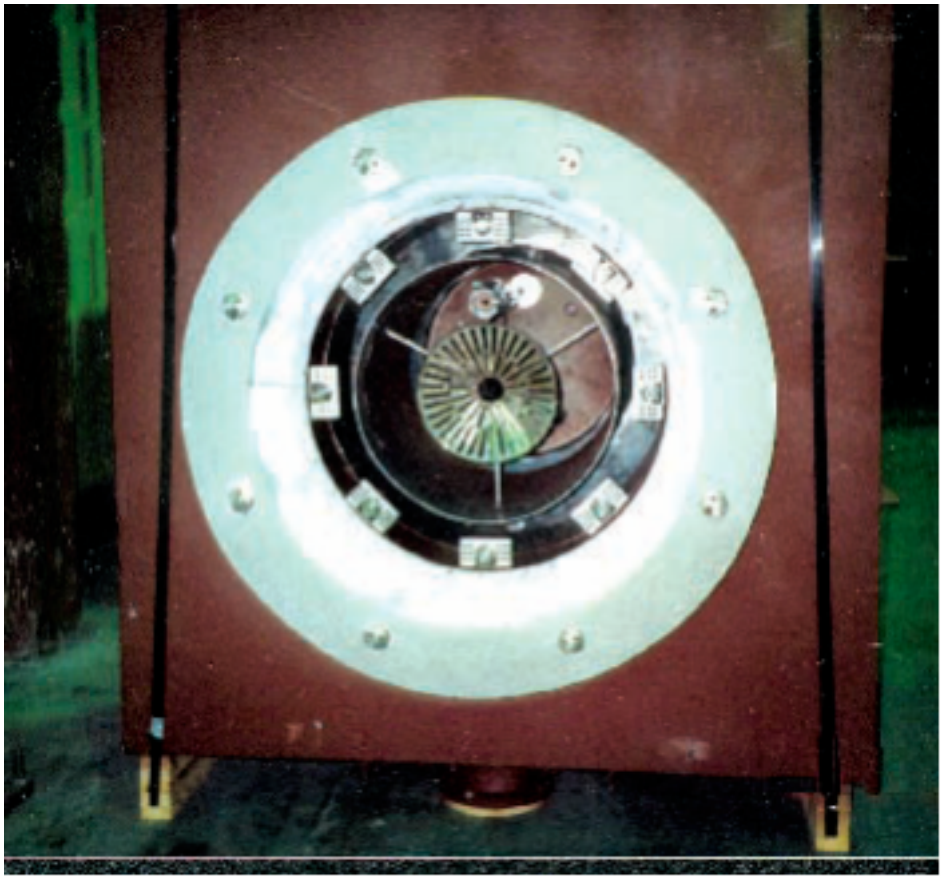

Figure 2.9: Throat of Gas Burner (Baukal and Schwartz, 2001)

2.1.2.2 Fuel and Oxidizer Mixing

In this context, the term “mixing” in the combination of fuel and oxidizer describes the ability of bringing into close molecular proximity the streams of reactant fuel and oxidant (air). The mixing of two or more different flowing fluid streams takes place at the

intersection of the streams known as the turbulent shear zone. The surface of the shear zone varies with respect to the turbulence that is in proportion to the amount of shear forces developed between the flowing fluids. Moreover, this shear zone region is described by the interaction between the mass and momentum velocity of each stream. The higher level of mixing between these streams indicates a better and more complete and intense level of combustion. It is generally accepted and considered a rule of thumb that the higher the level of shear and turbulence between the streams of combustion, the more uniform the mixture of air and fuel. More uniform mixing between air and fuel is caused by increased turbulence between the air and fuel streams and more rapid and complete combustion.

Although a high level of mixing between the two streams of combustion is desired, a number of conditions and factors must be taken into account, including the control of polluting emissions that lead to exceptions to this rule of thumb. Maximum levels of turbulent mixing between the air and fuel combustion streams do not always produce the most desirable conditions of combustion. Mixing the fuel and oxidant streams at high levels of turbulence and shear in the proper proportions will generate a maximum flame temperature, which in turn will result in the formation of higher levels of NO_X. In order to combat this problem, the emissions control is achieved by delaying the combustion process. That is to say, industrial combustion burners that produce low emissions are able to reduce the level of mixing between the fuel and oxidant streams by delaying their mixing and extending their reaction zone simultaneously.

There exist four combustion mechanisms that are used in the development of fuel and oxidant mixing:

1. **Fluid Entrainment:** A demonstration of the Law of Conservation of Momentum in which one stream, usually the fuel stream, directly influences the other. As the velocity of the fuel jet is dissipated, the mass flow of the fuel stream increases by entrainment of the oxidant stream to satisfy the conservation of momentum.
2. **Co-Flow Mixing:** The amount of shear force developed between parallel flowing streams is proportional to the differential mass velocity of the streams. At high velocity, the interface between the streams becomes turbulent allowing the streams to intermix with each other. At low velocity, the thickness of the interface between the streams is small and results in slow mixing.
3. **Cross Flow Mixing:** Having the combustion streams intersect one another creates an increase of shear energy between the flowing streams. The intersecting streams result in turbulent mixing of the oxidant and fuel streams. Moreover, the closer to perpendicular the angles of intersection are, the higher the levels of turbulent mixing.
4. **Eddy Formation:** Strategically locating obstructions along the flow of the combustion streams will provide forced changes to the streams and cause turbulence. Locating these obstacles in a region where both the fuel and oxidant streams are present will allow them to intermix with one another.

2.1.2.3 Maintaining Ignition

The continuous and reliable ignition of the fuel and oxidant mixture is considered to be the most important function that a combustion burner possesses. A burner is designed to allow the fuel and oxidant to be continuously fed into the combustion chamber at or below the mixture flame speed. This allows for a nonstop and uninterrupted ignition zone. Moreover, the ignition zone allows for the maintenance of a continuous flame and ignites a fresh fuel and oxidant mixture as it is introduced simultaneously.

Ignition safety of a fuel and oxidant mixture is highly dependent on the composition of the fuel and combustion oxidant. The stoichiometry of the combustion mixture as well as the burning characteristics of the fuel controls the rate of combustion reaction or flame speed. Moreover, the velocity and the stoichiometry of the mixture stream sustain the ignition of the combustion fuel and oxidant mixture. Finally, it is not desirable to have wide ranges in excess air requirements and fuel compositions as these create unreliable stability issues with the mixed fuel and oxidant streams.

2.1.2.4 Molding the Flame Shape

The design of industrial burners is restricted to the size, shape, and consistency of the resulting flame. The flame qualities produced by all burners that provide energy to a process be it the hydrocarbon process industry, the chemical process industry, or the power generation industry is restricted by the furnace chamber design into which it is fired. It is the main goal of all burners in all process furnaces to provide the most efficient and effective transfer of heat to the process load. The flame size and shape

play a very critical role in achieving this objective, as some of the loads being processed in these industries are sensitive to overheating. As such, there are strict industry guidelines for flame dimensions such as typical specifications for maximum flame length and flame width. Different industries indicate the number, amount of heat release, and layout of burners in the furnace as well as flame shape in order to achieve a proper heat transfer pattern for the process loads.

Proper flame patterns and shapes are achieved through the fuel injection pattern and the burner tile and flame holder that controls the airflow. The most reliable method of flame shape control is by patterning the airflow through approach distribution and exit configuration. The fuel injectors that pattern the flame shape have ports that introduce the majority of the fuel into the oxidant stream in a predetermined manner to generate the flame shape. Simultaneously, the oxidant stream obtains its pattern by flowing through passages in the burner tile and flame holder. For a round or brush-shaped flame, a round burner tile is used in the burner. Fuel is injected symmetrically through fuel injectors to achieve a round flame shape as seen in Figure 2.10 (a). In order to achieve a flat or fan-shaped flame, the burner tile is rectangular in shape and the fuel is injected in such a manner that the resulting flame is flat rather than round. A flat-shaped flame can be seen in Figure 2.10 (b).

(a) **(b)**

Figure 2.10: (a) Round-shaped Flame; (b) Flat-shaped Flame (Baukal and Schwartz, 2001)

2.1.2.5 Minimizing Pollutant Emissions

Environmental regulations that limit air-polluting emissions have perhaps the largest impact on the design of combustion equipment. We are at the point where environmental problems are of utmost importance for most societies around the world. Therefore, governments have become very critical of sources, such as industrial combustion burners, that may contaminate air, soil, or water with pollutants. Industrial combustion burners must take into account, and are restricted by, the thermo chemical reactions that form the regulated and unwanted pollutant emissions.

2.2 Burner Types

There are a number of ways to classify industrial burners. For the purpose of this thesis industrial burners will be classified based on the method used to burn a given fuel (either gaseous or liquid) and oxidizer (either air or pure oxygen). The more common types of burners are discussed in this section of the chapter, namely high velocity burners, draft

type burners, regenerative burners, oxidizer type burners, and radiant heating burners. Unless stated otherwise, the information contained within this section of Chapter 2 is interpreted from Baukal (2000 and 2003).

2.2.1 High-Velocity Industrial Burners

High-velocity burners are also known as mixing burners and are perhaps the most common type of all industrial burners. These burners are classified by how the fuel and the oxidizer mix with one another. As their name suggests, high-velocity burners are able to achieve the desired mixing of fuel and oxidant through an outlet combustion product exit velocity stream exceeding 90 m/s with nominal values within the range of 120 m/s to 150 m/s. The burner system itself is configured to allow the combustion product stream to entrain the surrounding reacted products of combustion. This phenomenon results in a perfectly mixed combustion chamber. The mutual mixing between the burner jet stream and the reacted products of combustion promotes a gaseous circulation within the combustion chamber with the aim of enhancing heat transfer and temperature uniformity.

High-velocity burners are equally capable of providing value and benefits for both low and high temperature process applications. Heating of the load in the combustion chamber is also accomplished more rapidly through the use of high-velocity burners. The high-velocity burner is capable of rapidly heating a load by being able to reduce the time required for the coldest part of the load to reach target temperature. High-velocity burners are more economical than other burners due to their low capital and maintenance costs as well as their high efficiency and productivity.

The high momentum of the gas stream from the high-velocity burners is used to drive heat into closely packed loads such as bricks or piles of aluminum scrap. The high momentum for such a burner is also used to enhance jet mixing with surrounding gases such as in fume incineration processes. Moreover, less excess air is required for high-velocity burners. This is due to the fact that the jet temperature from high-velocity burners is diluted faster by the entrainment of cooler products of combustion within the chamber surrounding. The following subsections discuss in more detail the different types of high-velocity or mixing burners, namely premix and partially premix burners, nozzle mix burners, and staged mix burners.

2.2.1.1 Premix and Partially Premix Burners

In premixed burners, the fuel and oxidizer are completely mixed before the combustion process begins. This type of burner is pictured in Figures 2.11 and 2.12. Premix burners produce shorter and more intense flames compared to other burners. Although higher temperatures and shorter flames can lead to non-uniform heating of loads and higher NO_X emissions, they are favorable in enhancing heating rates.

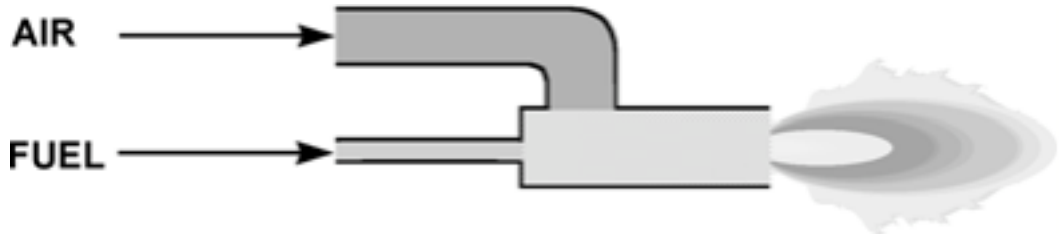

Figure 2.11: Schematic Diagram Depicting a Premix Burner (Baukal, 2000)

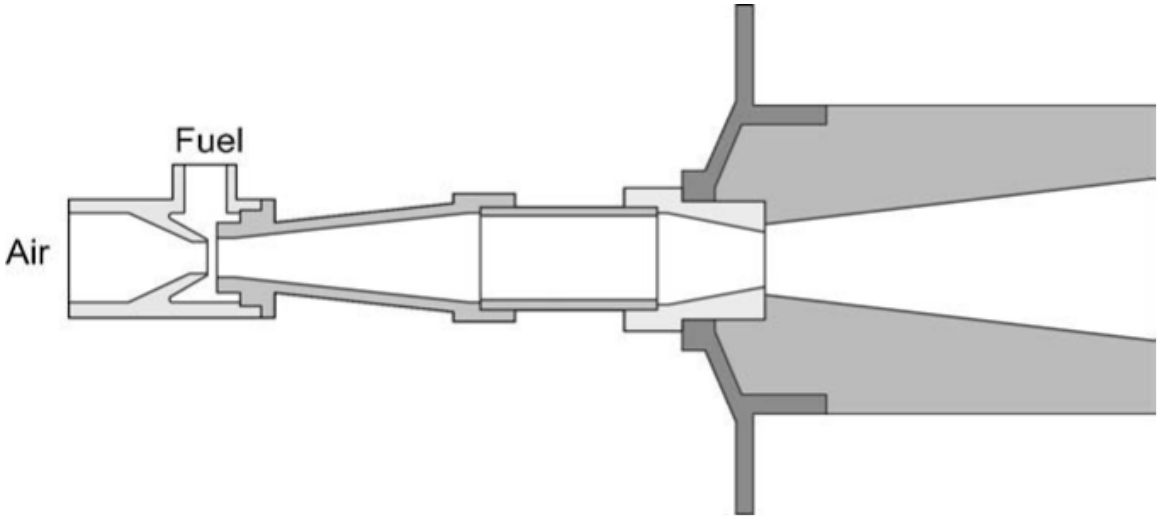

Figure 2.12: Diagram of a Premix Burner (Baukal, 2003)

Premix burners are considered to be inherently high-velocity burners due to their ability to create high-velocity gas streams. These gas streams are created from high volume expansions that result from the high temperature increase of the premix burner. Unfortunately, the high heat release from premix burners are unstable and may prove trying for the refractory lining of a combustion chamber. Also, the limited size of premix burners leads to the use of large numbers of burners in a given application. Moreover, the possibility of flashback with premix burners has made this type of burner unpopular in industry.

Partially premix burners, as shown in Figures 2.13 and 2.14, lessen the chance of flashback by having a portion of the fuel mix with the oxidizer before combustion; hence the label of "premix" on such burners. Premixing the fuel and oxidant stabilizes and anchors the resulting combustion flame for safety considerations. The flame length produced by partially premix burners is slightly longer and larger than the flame

produced by conventional premix burners. Additionally, the temperature and heat flux distribution of partially premix burners are to some extent better than that produced by premix burners.

Figure 2.13: Schematic Diagram Depicting a Partially Premix Burner (Baukal, 2000)

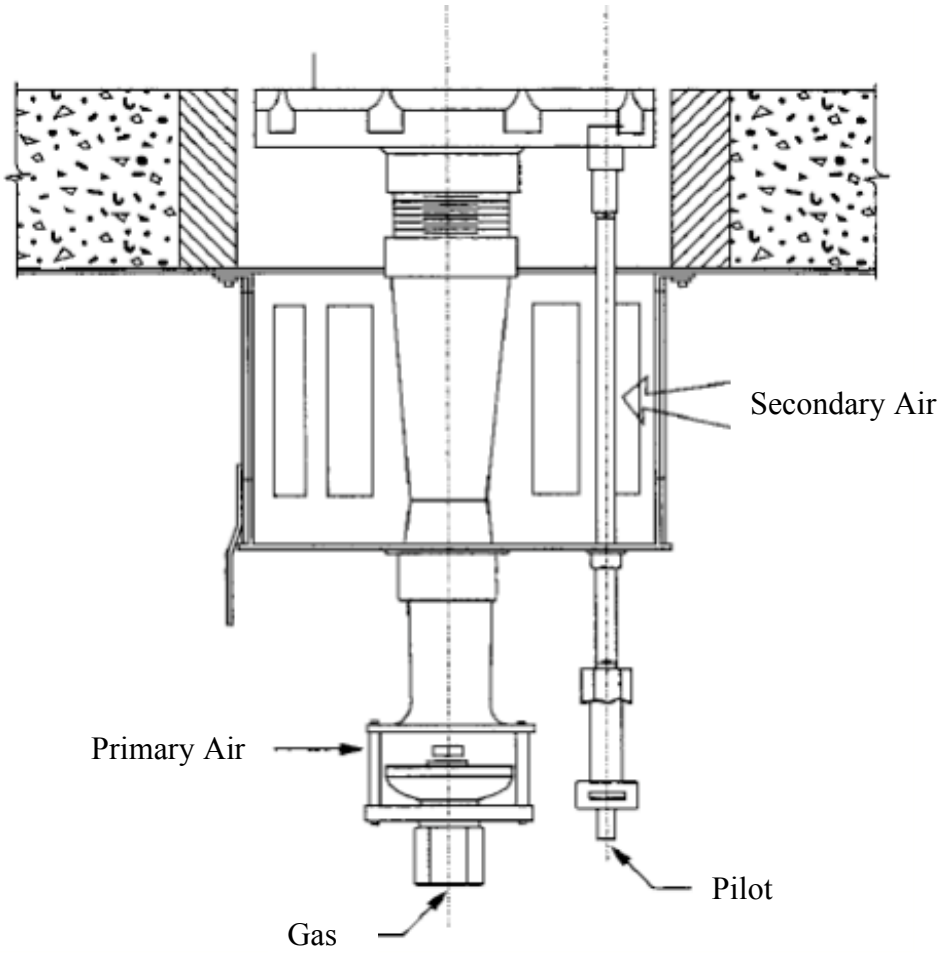

Figure 2.14: Diagram of a Partially Premix Burner (American Petroleum Institute, 1995)

2.2.1.2 Nozzle Mix Burners

Nozzle mix burners introduce the combustion fuel and oxidant into the combustion zone of the burner separately (Baukal and Schwartz, 2001). This type of high-velocity burner is pictured in Figures 2.15 and 2.16. The oxidizer and fuel are unmixed and separate from one another before combustion can take place and are only mixed at or after the ignition point of the burner (North American Manufacturing, 1995). Nozzle mix burners are also known as "Raw Gas" burners due to the fact that the fuel exiting the burner remains intact without oxidant mixed with it.

Figure 2.15: Schematic Diagram Depicting a Nozzle Mix Burner (Baukal, 2000)

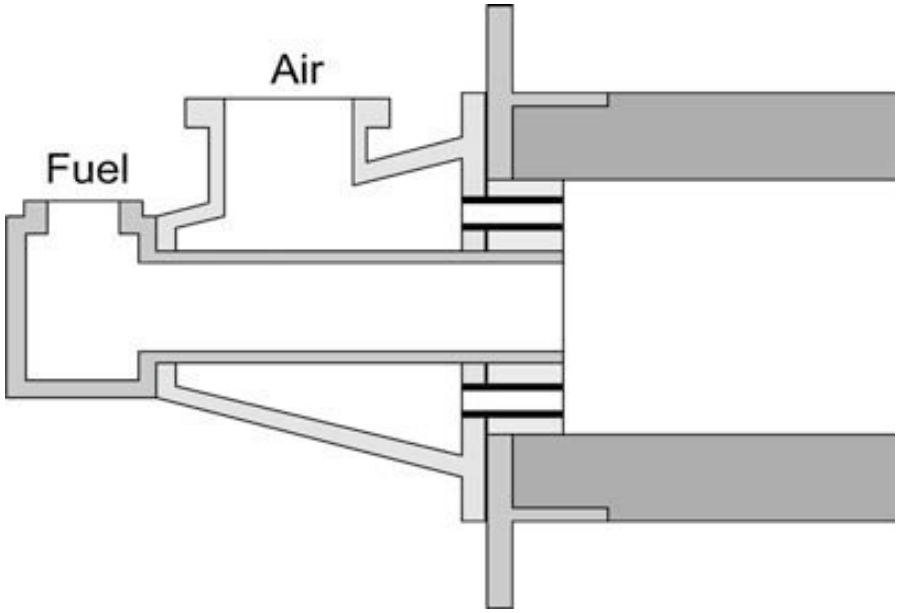

Figure 2.16: Diagram of a Nozzle Mix Burner (Baukal, 2003)

Nozzle mix burners are able to diffuse the combustion fuel and combustion oxidant streams away from the burner giving them a very wide stability range compared to other industrial burners working under the same set of operating conditions. Diffusing the streams away from the burner prevents flashbacks and explosions in potentially dangerous systems, such as a combustion chamber that operates under positive pressure. Hence, many in the industrial combustion industry have referred to nozzle mix burners as "Diffusion Mix" burners. Nozzle mix burners have longer flames than premix and partially premix burners and do not have flame hot spots, leading to a better and more uniform distribution of temperature and heat flux throughout the combustion chamber.

Nozzle mix burners can have their oxidant supply stream set to a maximum flow rate while the flow of fuel can be reduced according to the desired temperature demand. This indicates that nozzle mix burners can operate under significant and high levels of excess air allowing for the use of less fuel but equal output of heat. The excess air capability of nozzle mix burners results in high heating efficiencies with less fuel as well as higher combustion velocities due to larger amounts of combustion air. The extra velocity allows the use of fewer burners to achieve temperature consistency and heat flux uniformity, which reduces the capital and maintenance costs of a furnace.

In order to increase exit velocities, burner manufacturers started to add restrictions to the nozzle mix burner exit, as seen in Figure 2.17. The increase of burner exit velocities led to an increase of circulation of combustion product by entrainment, which in turn would reduce the amount excess air required in achieving temperature uniformity throughout a

combustion furnace. Restricted nozzle mix burners provided a very fast mixing rate between the fuel and oxidant streams that resulted in a well-defined, stable flame as well as clean burning. A stable flame and clean burning of the combustion streams are ideal conditions for a heating process but puts great stress on the refractory lining of the combustion furnace. The use of an alloy jacket between the refractory and furnace wall is the ideal method of solving this problem. The jacket seals the lining and prevents the leakage of hot gases into the surrounding furnace structure (Beer and Chigier, 1983).

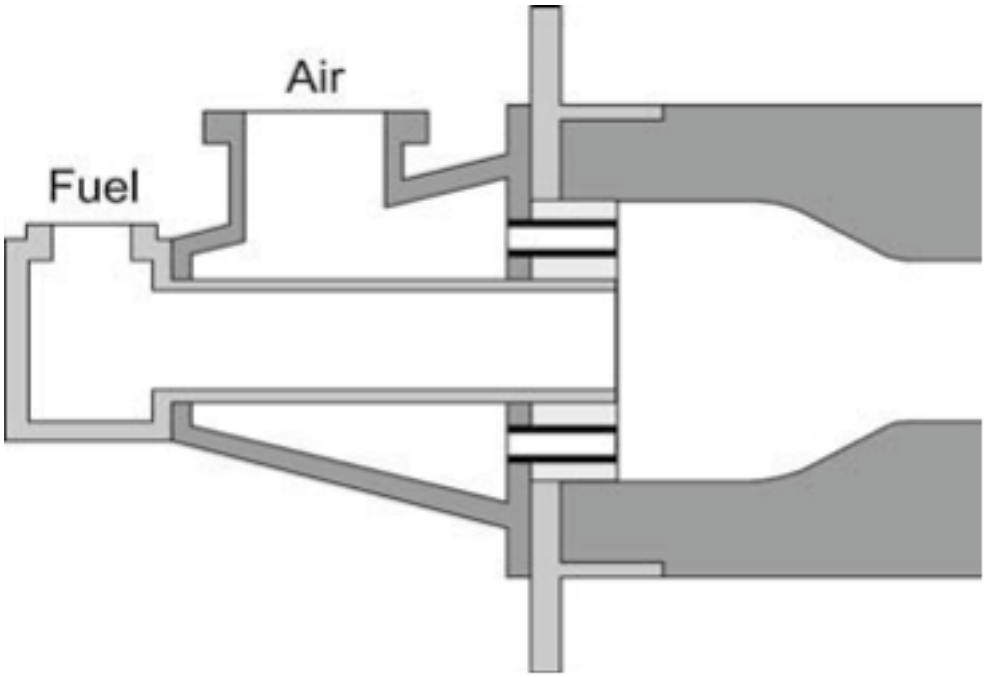

Figure 2.17: Restricted Nozzle Mix Burner (Baukal, 2003)

2.2.1.3 Staged Mix Burners

The final common type of high velocity burner based on mixing is referred to as staging. There are two types of staged mixed burners: Staged-air and Staged-fuel. Schematic

diagrams depicting both a staged-air and a staged-fuel burner are shown in Figure 2.18.

(a) (b)

Figure 2.18: Schematic Diagrams Depicting (a) Staged-air Burner and (b) Staged-fuel Burner (Baukal, 2000)

In burner staging, secondary and sometimes tertiary oxidant or fuel injectors are used to inject oxidant and/or fuel into the flame downstream from the root of the flame itself. The staging of both air and fuel streams are done with the main objective of reducing NO_X emissions. Staging in burners produces longer flames that typically have lower peak flame temperatures as well as a more uniform distribution of heat than non-staged burners.

In the first stage of a staged-air burner, all of the fuel is mixed with a portion of the combustion air. The remaining combustion air is then added in one or more additional stages until the fuel is completely used (Bloom Engineering, 2007). Figure 2.19 shows a typical example of a staged-air burner. The first stage air is introduced through the inner air jets and the second and third stage air through the outer air jets. Fuel flows through the center. A staged-fuel burner follows the same principle as that of a staged-air burner. Secondary and sometimes tertiary inlets of a staged-fuel burner deal with fuel instead of air as in the case of staged-air burners. Figure 2.20 depicts a schematic diagram of a typical staged-fuel burner.

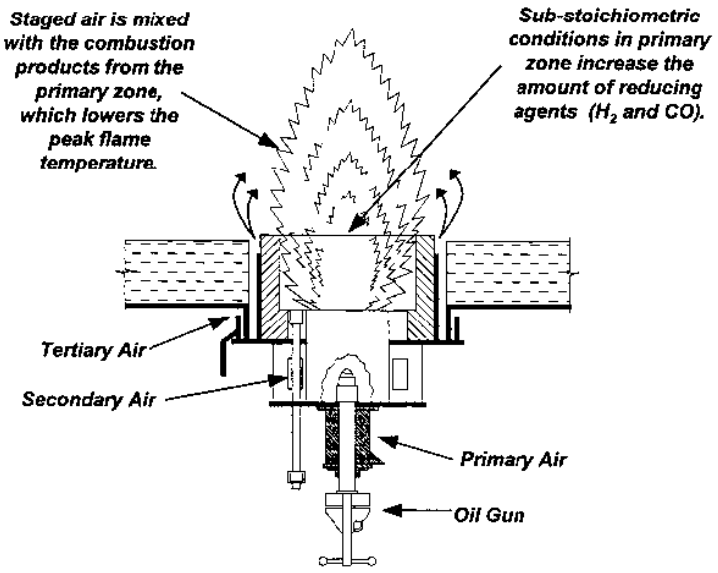

Figure 2.19: Diagram of a Staged-air Burner
(Courtesy of John Zink Company LLC, Tulsa, OK)

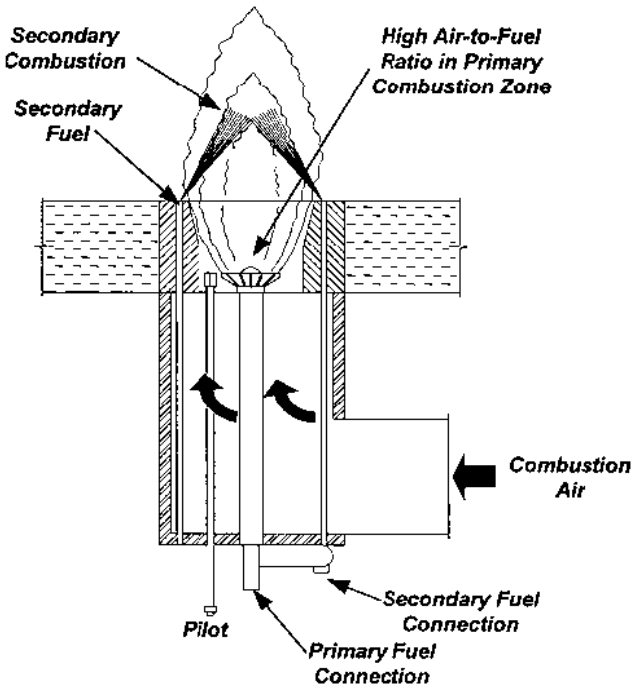

Figure 2.20: Diagram of a Staged-fuel Burner
(Courtesy of John Zink Company LLC, Tulsa, OK)

2.2.2 Regenerative Burners

An excellent explanation of what regenerative burners are and how they work is given by Bloom Engineering (2007) as follows:

> "Regeneration uses a pair of burners which cycle to alternately heat the combustion air or recover and store the heat from the furnace exhaust gases. When one regenerative burner is firing, the other is exhausting the furnace gases. Exhaust gases pass through the regenerative burner body and into a media case, which contains refractory material. The refractory media is heated by the exhaust gases, thus recovering and storing energy from the flue products. When the media bed is fully heated, the regenerative burner currently firing is turned off and begins to exhaust the flue products. The regenerative burner with the hot media bed begins firing. Combustion air passes through the media bed and is heated by the hot refractory. Air preheat temperatures within 300°F - 500°F of the furnace are achieved resulting in exceptionally high thermal efficiency."

In fact, Baukal (2003) suggests the heat recovery of a regenerator can approach 90% effectiveness, compared to approximately 40% effectiveness for a typical recuperator system. William Siemens first developed regenerative burners in 1858. The first experimental furnace built by Siemens had a sole purpose of achieving high temperatures within the furnace combustion chamber. Two years later, he patented the first regenerative furnace for melting glass. The advantages of the regeneration combustion

principle were already well understood at the time and were quickly adopted into furnaces for iron puddling, melting of steel, and reheating of steel and iron (Camp and Francis, 1925). A traditional regenerator heating system, as developed and patented by Siemens, is displayed in Figure 2.21. From this figure, one can see that the older style regenerators are large compared to the furnace itself. One can also notice the use of refractory checkerwork in the regenerators. The checkerwork is used as the heat transfer mass and also serves to control the direction of combustion oxidant and waste gas flows.

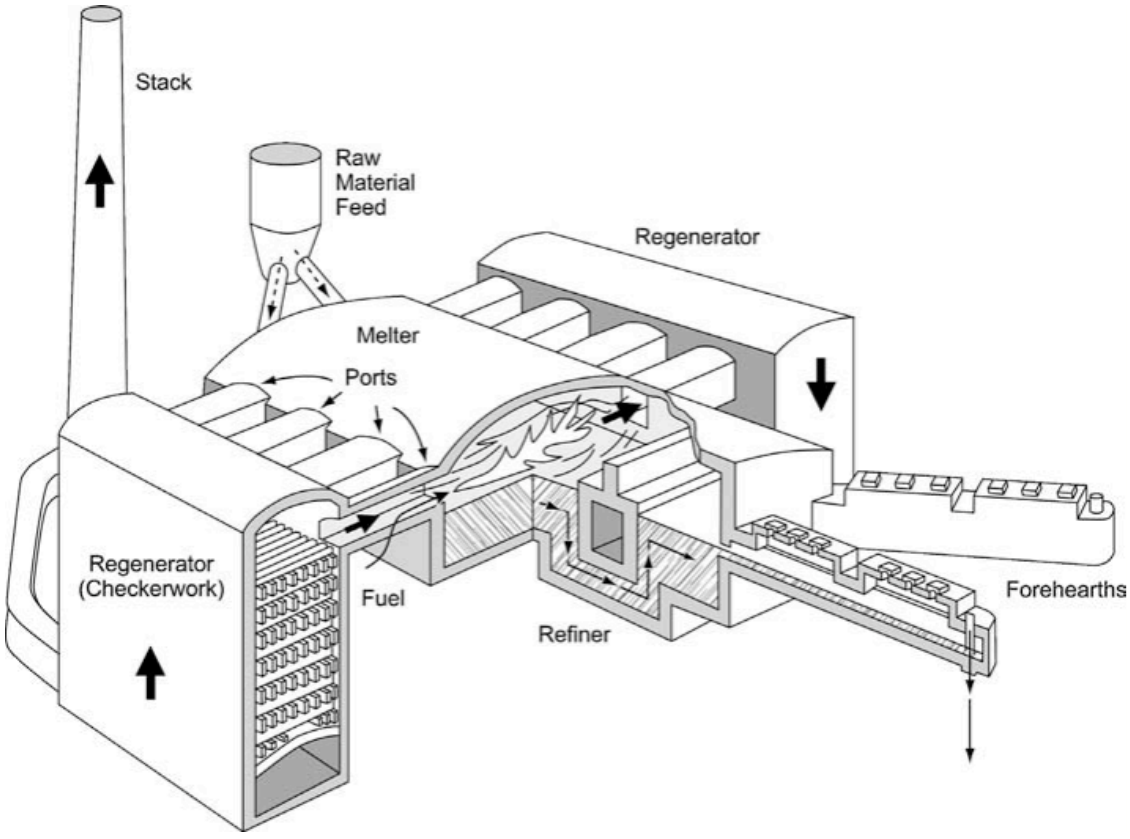

Figure 2.21: A Regenerative Burner Furnace at Work (North American Manufacturing Company, 1972)

Modern times called for modern measures, and the burner furnace depicted in Figure 2.21 was much too big and old-fashioned to be used in the progressive heat processing

industry. British Gas developed the modern and compact regenerative burner simultaneously in the early 1980's (Webb, 1983) with the North American Manufacturing Company (Davies, 1986). The first commercial installation of the modern regenerative burner took place in February 1983 and was a 1 MMBtu/hour, 1400^{o}C glass melting furnace (Webb, 1983 and Newby, 1985).

The modern version of the regenerative burner is essentially a high temperature preheated air burner coupled with a ceramic regenerator. Regenerative burners can provide preheated air in excess of 85% of the process temperature of fuel-fired applications up to 1650^{o}C. The 90% heat recovery effectiveness, along with its insensitivity to the operating environment and high preheat level combine to provide an excellent economic, trouble free and low maintenance operation. Each burner serves a double duty, acting as a flue and exhaust port from the fired combustion chamber. Two burners, two regenerators, reversing valves, and the reversing logic make up one complete single set of a compact regenerative burner. Each of these burners contains a bed of ceramic balls. As one burner of the set fires with cold air, the other acts as an exhaust from the chamber. Air flowing through the firing burner is preheated by the bed by removing heat stored in the ceramic balls while hot furnace gases are simultaneously giving up heat to the bed of ceramic balls of the exhausting burner. The burners cycle between firing and exhausting when the process application is in demand of heat. This continuous cycle of firing and exhausting is pictured in Figure 2.22 and Figure 2.23.

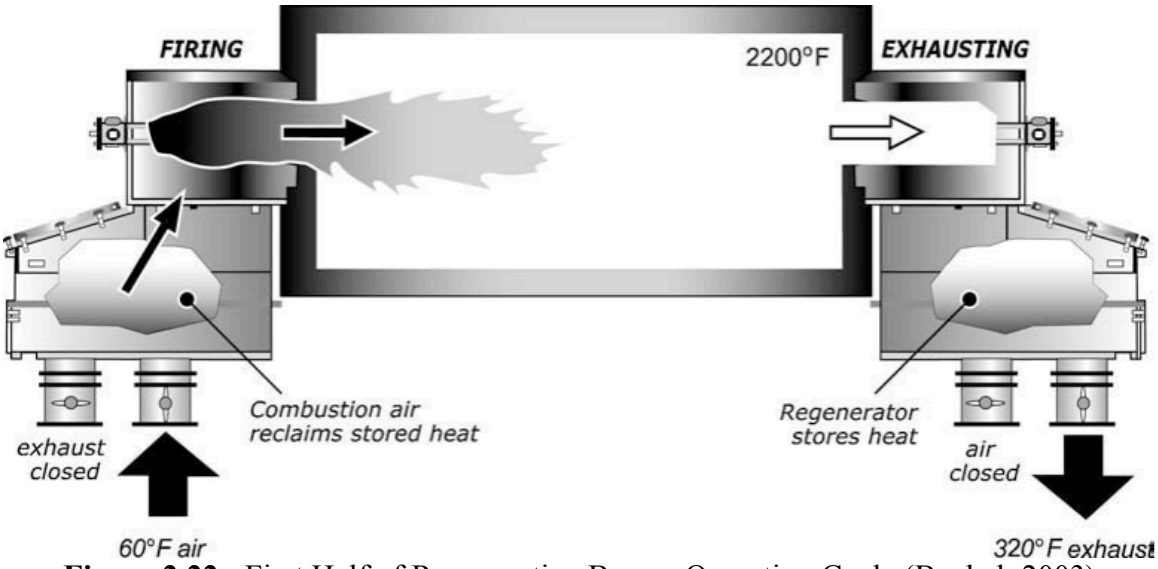

Figure 2.22: First Half of Regenerative Burner Operation Cycle (Baukal, 2003)

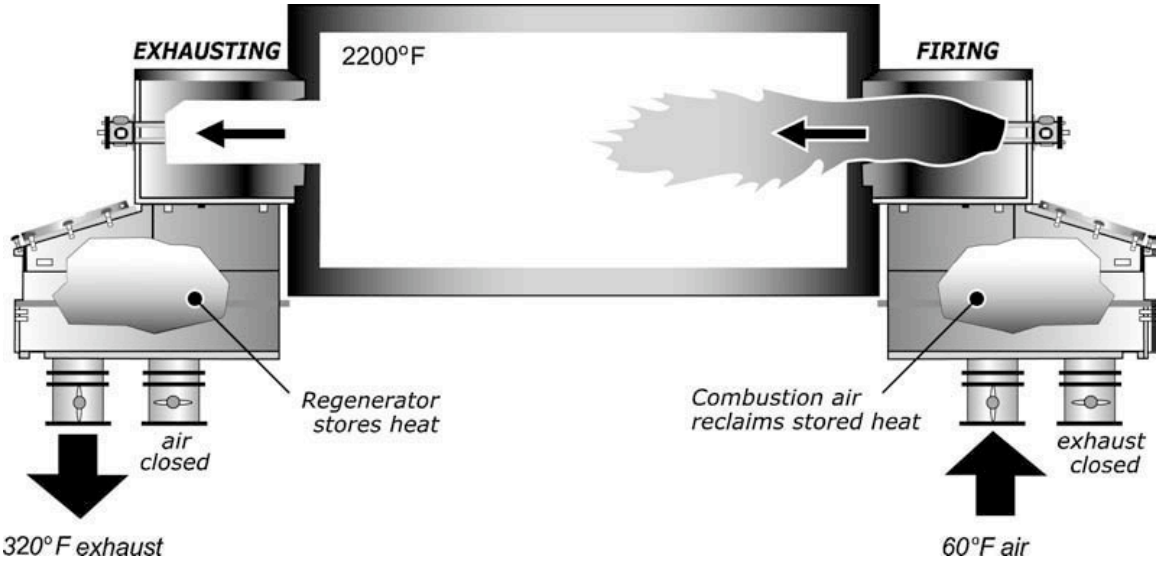

Figure 2.23: Second Half of Regenerative Burner Operation Cycle (Baukal, 2003)

2.2.3 Oxidizer Burners

The majority of combustion processes use air as the oxidant to burn hydrocarbon fuels such as natural gas to generate substantial amounts of heat. Using a higher concentration of oxygen than the amount found in air enhances the combustion process both in its

efficiency and heating effectiveness. The introduction of higher levels of O_2 into the combustion streams is referred to as oxygen-enhanced combustion or OEC (Baukal, 1998). One example of OEC is called Air-Oxy/Fuel where the oxidant consists of air blended with pure O_2 and mixed with the fuel for combustion. Another example is referred to simply as Oxy/Fuel, which consists of pure O_2 as the oxidant instead of air.

In the past, OEC was considered expensive for industrial use but with the introduction of new oxygen-generation technologies - pressure and vacuum swing adsorption for example (McGuinness and Kleinberg, 1998) - the cost of separating pure O_2 from air has decreased allowing the use of OEC to offset added costs. OEC is also used to substantially reduce polluting emissions, which in turn have increased the number of cost effective applications (Baukal, 1998). Williams et al. (1989) and Baukal et al. (1992) argue that replacing some or all of the combustion air with high purity O_2 can enhance the majority of industrial heating processes. Benedek and Wilson (1996) prepared a report in which they identified the possible industries that may enhance their processes by replacing air with pure oxygen. The processes are as follows:

- Processes with high flue gas temperatures in excess of 1090°C (1363K)
- Processes with low thermal efficiencies due to heat transfer limitations
- Processes with throughput limitations which could benefit from additional heat transfer without affecting product quality
- Processes with dirty flue gases and high NO_X emissions

There are four ways of using oxygen to enhance combustion processes. The four

methods are called air enrichment, oxygen lancing, oxy/fuel, and air-oxy/fuel and are discussed in the following sub-subsections.

2.2.3.1 Air Enrichment

Injecting O_2 into the incoming combustion air supply through a diffuser is one type of OEC. This method is referred to as air enrichment and is pictured schematically in Figure 2.24. The injection of O_2 is accomplished to ensure proper mixing and is an inexpensive retrofit that can provide substantial benefits such as shortening and intensifying the flame. The addition of too much O_2 has adverse effects such as the production of an unacceptably short flame and overheating that may damage the burner.

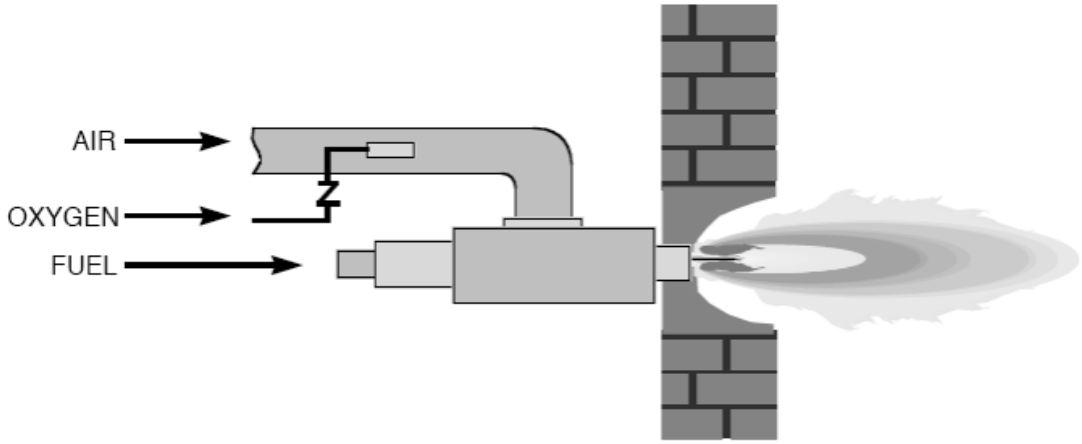

Figure 2.24: Air Enrichment Method (Baukal, 1998)

2.2.3.2 Oxygen Lancing

Oxygen Lancing is another method used to enrich an air/fuel process with pure O_2. This OEC method is pictured in Figure 2.25 and has some advantages over the air enrichment

method. O_2 lancing requires no modifications to the existing burner set-up and produces lower NO_X emissions due to its form of staging - a well-accepted technique for reducing NO_X (U.S. Environmental Protection Agency, 1994). The heat release is more evenly distributed than the air enrichment technique and O_2 lancing between the burner flame and the load causes the flame to be pulled down toward the load. This phenomenon serves for more than one purpose - to improve the heat transfer efficiency and to lessen the likelihood of overheating the burner and refractory lining of the furnace chamber.

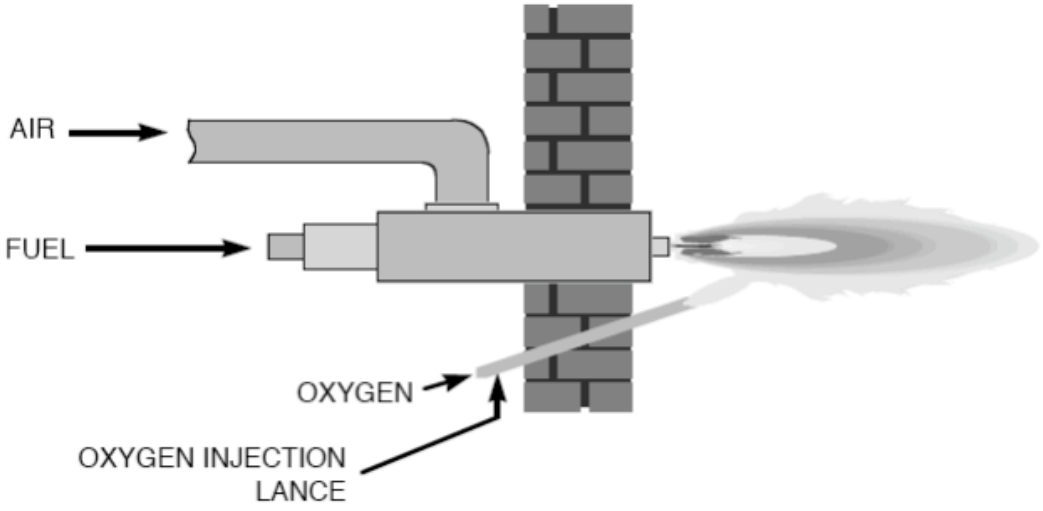

Figure 2.25: Oxygen Lancing Method (Baukal, 1998)

2.2.3.3 Oxy/Fuel

Oxy/fuel combustion is another type of OEC, which follows the nozzle mix method of combustion discussed above. The fuel and oxidant remain separate and do not mix until they reach the outlet of the burner. As its name suggests, an oxy/fuel burner uses pure oxygen as the oxidant and due to the high reactivity of pure oxygen, the combustion

streams are not premixed to avoid flashback and a potential for explosion. An oxy/fuel burner is schematically pictured in Figure 2.26. Of all the oxidizer burners, the oxy/fuel combustion method is able to improve an industrial process the most. However, it has the highest operating cost of all oxidizer burners.

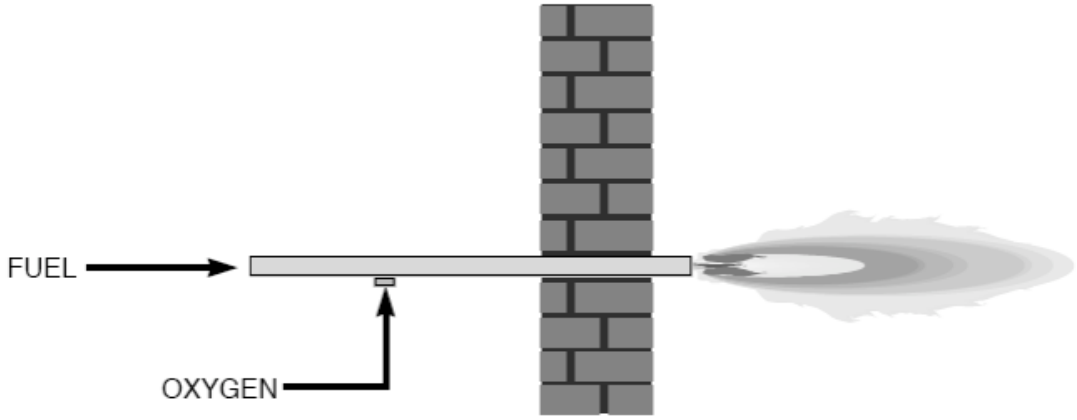

Figure 2.26: Oxy/Fuel Burner (Baukal, 1998)

2.2.3.4 Air-Oxy/Fuel

The air-oxy/fuel method of OEC deals with the separate injection of air and pure oxygen through a burner as pictured in Figure 2.27. This method is a variant of the three aforementioned methods and in most cases an air/fuel burner can be easily modified to become an air-oxy/fuel burner by inserting an oxy/fuel line (Bazarian et al., 1994). The air-oxy/fuel burner has numerous advantages:

- Uses higher levels of O_2 than air enrichment and O_2 lancing methods, which yields higher benefits than these air/fuel burners.
- Lowers operating costs compared to oxy/fuel burners.

- Adjusts the flame shape and heat release pattern by controlling the amount of O_2 in an air-oxy/fuel burner.
- Modifications for an existing burner to act as an air-oxy/fuel burner is generally inexpensive.

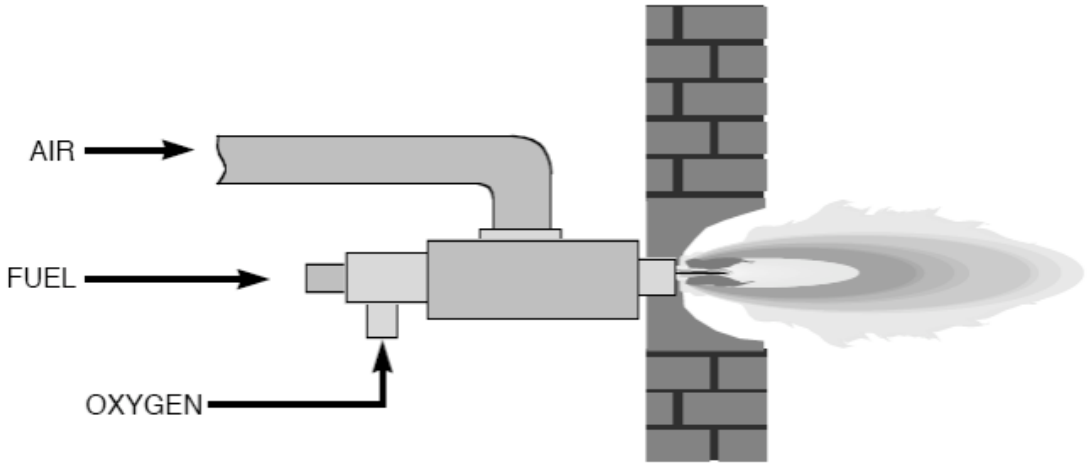

Figure 2.27: Air-Oxy/Fuel Burner (Baukal, 1998)

2.2.4 Indirect Heating Burners

Indirect heating burners work on the principle of having an intermediate surface between the burner flame and the heating load. This type of burner is used to prohibit the possible contamination of the material being heated by having the combustion products not come in contact with the load itself. Electric heaters are sometimes used for this very purpose, but the energy costs associated with electricity are considerably higher than the cost of fossil-fuel-fired heaters. The radiant tube burners are the most advantageous source of indirect heating for the majority of heat treatment processes where the work must not come into contact with the products of combustion or the flame. Radiant tubes are gas

fired and offer an extraordinarily even distribution of heat while operating at very high intensities. Radiant tube burners provide a uniform heat release profile along the length of the tube in order to achieve a constant and uniform heat distribution. An even heat flux from the tube also improves the temperature uniformity of the load, which in turn provides an improvement of product quality. Few designs come close to providing a uniform heat flux as that delivered by radiant tube burners.

Radiant tube furnaces have one or more radiant tubes within its walls to contain the combustion products. With the help of a jet, the flame is forced into tubes and the heat is conducted through the tube wall and transmitted to the load in the furnace by radiation. The biggest challenge of using radiant tube for indirect heating is the choice of construction material for the tube itself. Tubes are constructed of either high temperature metal alloys or ceramics. Both types of materials have their drawbacks. Metal alloys are expensive and do not have a continuous operating temperature as high as ceramics do. Metal alloy tubes have an operating temperature of 1400K (1127^{o}C) and normally fail at higher temperatures due to a variety of metallurgical problems. Metallurgical research into higher temperature metals continues to try and overcome this obstacle for use in metallic radiant tube burners (Liang and Schreiner, 1986 and Alliat et al., 1998). Metal tubes are used more often than ceramic tubes. Ceramic tubes have higher temperature operating limits compared to metal tubes, but are more susceptible to thermal shock.

There are three different types of radiant tube burners: Straight-through Tube Burner; Single-ended Recuperative Tube Burner; and U-tube Burner. The straight-through tube

burner is the simplest of the three types. It consists of a burner at one end of the tube with the heat and exhaust traveling through the tube and exiting at the other end. The straight-through tube burner is pictured in Figure 2.28. The main disadvantage of this type of radiant tube burner is getting a good efficiency of heat transfer from the flame and its gases to the tube. Another disadvantage of straight-through burners is their connections. The supply gas is connected on one side of the tube while the exhaust connection is on the other end of the tube. Opposite connections are troubling for installation, maintenance, and upkeep reasons.

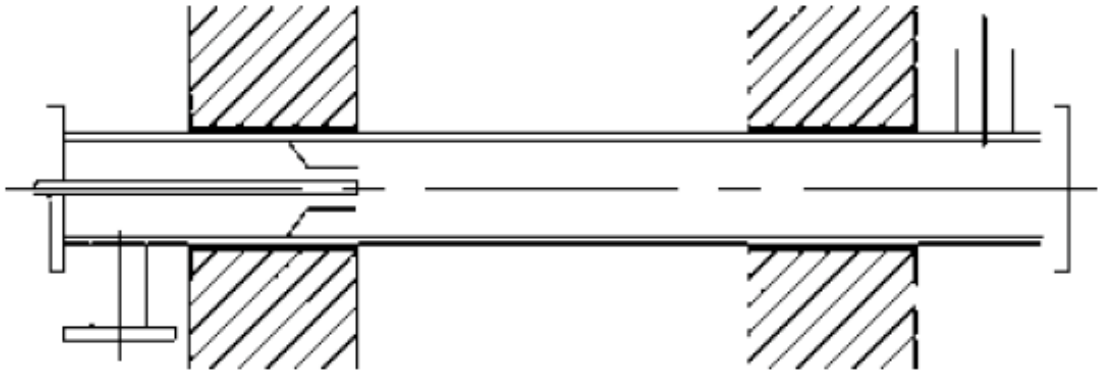

Figure 2.28: Straight-through Radiant Tube Burner (Singh and Gorski, 1990)

Another type of radiant tube burner is known as a single-ended recuperative burner and unlike the previous burner, the inlet and exhaust are located on the same side of the tube. A single-ended recuperative burner is displayed in Figure 2.29. The exhaust gases of a single-ended recuperative burner is used to preheat the incoming combustion stream by firing down an inner tube and then returning back to the starting end through an outer annulus. The preheating of the incoming fuel and oxidizer by the exhaust gases increases

the overall efficiency of the tube burner.

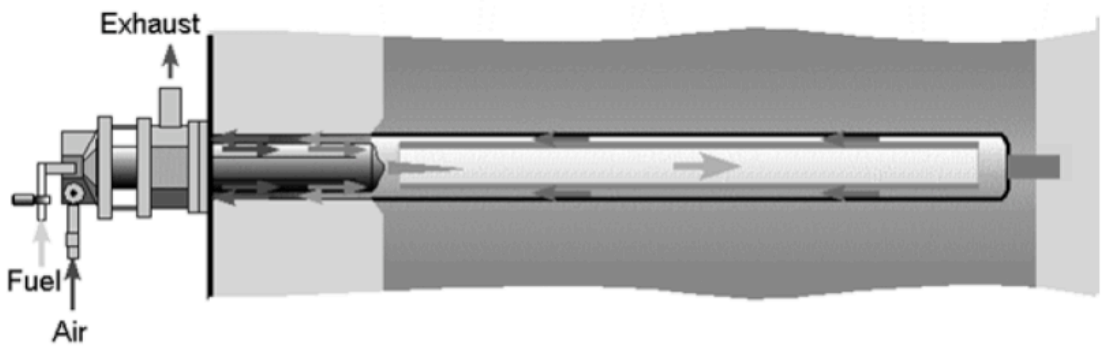

Figure 2.29: Single-ended Recuperative Radiant Tube Burner (WS Thermal Process Technology Inc., 2004)

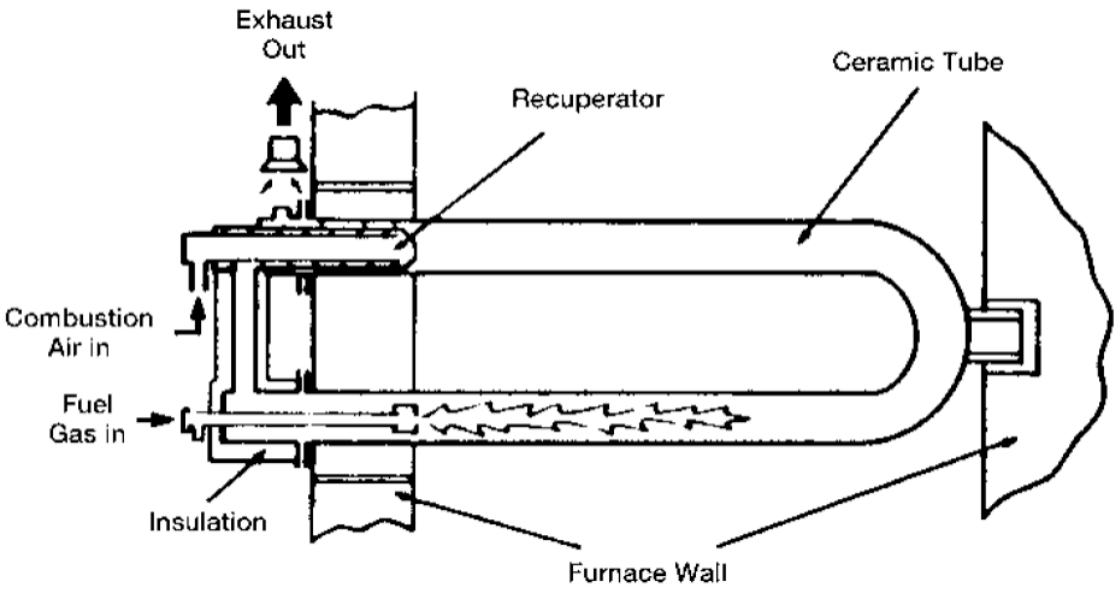

Figure 2.30: U-tube Radiant Burner (Liang and Schreiner, 1986)

The third type of radiant tube burner is named after its shape – U-tube radiant tube burner. The combustion stream inlet and exhaust outlet is on the same side of the tube. A disadvantage of the u-tube burner is its 180^{o} elbow, which increases the chances of leaks and failures. Abbasi et al. (1998) have introduced a new breed of u-tube burners.

Its design not only decreases its failure and leakage rates at their 180^{o} elbow, but also has better temperature uniformity and lower pollutant emissions than conventional burners by using internal exhaust gas recirculation.

2.2.5 Draft Burners

The majority of industrial burners are forced-draft burners; that is to say, the combustion oxidizer is supplied to the burner under pressure and is usually supplied by a high-pressure blower. Natural-draft burners, on the other hand, have their combustion oxidizer supplied to the burner by a negative draft produced in the combustion or furnace chamber. A schematic diagram of a natural-draft burner is depicted in Figure 2.31 and shown in practice in Figure 2.32.

Natural-draft burners depend on the pressure drop and combustor stack height to produce enough suction to draw sufficient combustion air into the burner. Natural-draft burners are usually used in the chemical and petrochemical industries. One consequence of natural-draft burners is based on its ability to transfer heat. Natural-draft burners produce flames that are longer than forced-draft burners. Hence, the heat flux from natural-draft flames is distributed over longer distances, often lowering the peak temperature in the resulting flame.

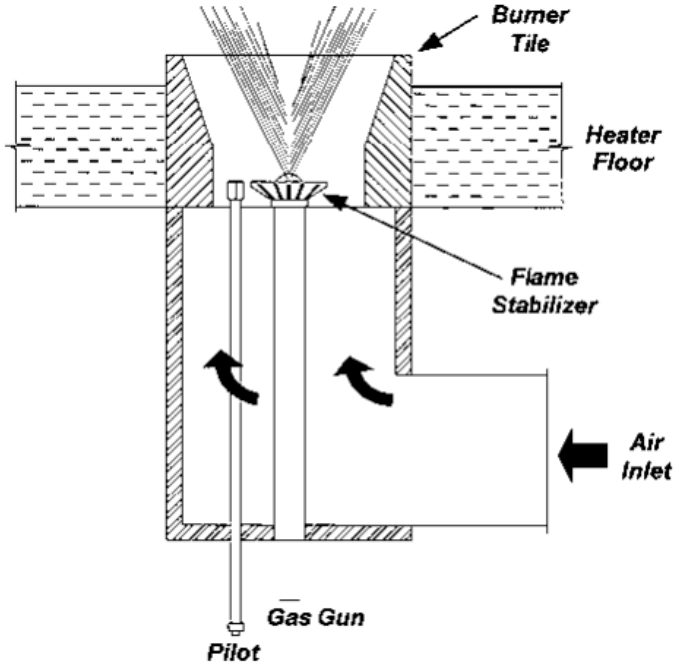

Figure 2.31: Schematic Diagram of a Natural-Draft Burner
(Courtesy of the John Zink Company LLC, Tulsa, OK)

Figure 2.32: Natural-Draft Burner in Practice
(Courtesy of the John Zink Company LLC, Tulsa, OK)

The main components associated with the operation, design and capabilities of burners currently found in industrial practice were examined in this chapter. This serves as background for possible introduction of new burners for the apparatus examined in this study. Clearly there are various areas that must be taken into account including safety, control systems, instrumentation, emissions, and background of potential users of this particular equipment. These issues are addressed in later chapters.

Chapter 3

Apparatus

This purpose of this chapter is to present the reader with the experimental apparatus that is in current use and how it will be modified to accommodate the ability to interchange different types of industrial burners. The reasoning behind the current design of the experimental apparatus and how it will benefit its future usage is also discussed in this chapter. To further the introduction of the apparatus presented in Chapter 1, a detailed explanation of both the physical and methodological features of the furnace test rig is explained in detail in the following sections of this chapter.

3.1 The Flameless Combustion Furnace

The topic of flameless combustion (FLOX®), mild combustion or high temperature air combustion (HiTAC) is of interest because of the capability of this technology to provide uniform gas temperatures in industrial furnaces (Wünning and Wünning, 1997) and low NO_X emissions with high air preheat (Sobiesiak et al., 1998), oxy-fuel combustion (Poirier et al., 2004) and regenerative burners (Milani and Saponaro, 2001). The Flameless Combustion furnace is also referred to as the Strong-Jet/Weak-Jet (SJ/WJ) furnace for reasons that will soon be discussed. This research furnace was first designed to simulate "flameless" combustion based on the concept originally incorporated in a burner developed by the Canadian Gas Research Institute (CGRI) in cooperation with the

Centre for Advanced Gas Combustion Technology (CAGCT) at Queen's University. Under flameless combustion operating mode, the fuel and air streams for the SJ/WJ furnace are supplied through separate feed streams to the furnace chamber as seen in Figure 3.1. The nozzles and resulting jet flows for these streams are similar in size. Under normal stoichiometric combustion conditions this requires a relatively low velocity (weak) fuel jet and a high velocity (strong) air jet. The fuel jet is commonly directed at an angle (θ) to the air jet. The typical angles of the fuel stream range between $5° < \theta < 20°$ (He, 2008).

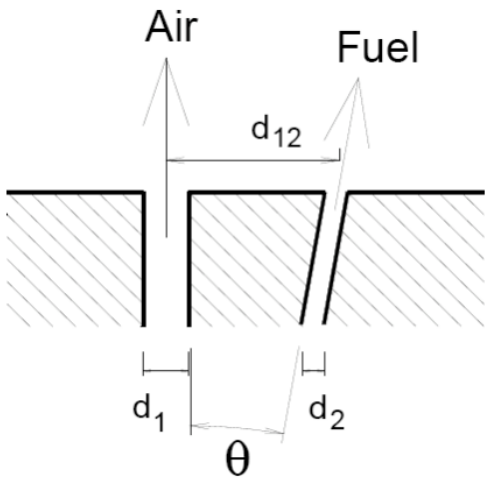

Figure 3.1: Schematic Diagram of the SJ/WJ Feed Streams (He, 2008)

Flameless combustion is a direct result of fluid entrainment. It was first developed to decrease nitrogen oxide (NO_x) emissions in high temperature gas-fired furnaces. Flameless combustion is portrayed as having uniform temperature distribution, low combustion noise, and extremely low NO_x emissions. In contrast to traditional flame combustion, flameless combustion is dilution and temperature controlled achieved by

extensive recirculation of combustion product gases as seen in Figure 3.2 (He et al, 2007). As its name suggests, flameless combustion refers to the outstanding characteristic that no visible flame emission is detectable in the oxidation region of combustion. In other words, flameless or diluted combustion occurs when the burning fuel is completely consumed without the presence of a visible flame as seen in Figure 3.3. All of the flameless combustion characteristics are primarily achieved from fluid entrainment.

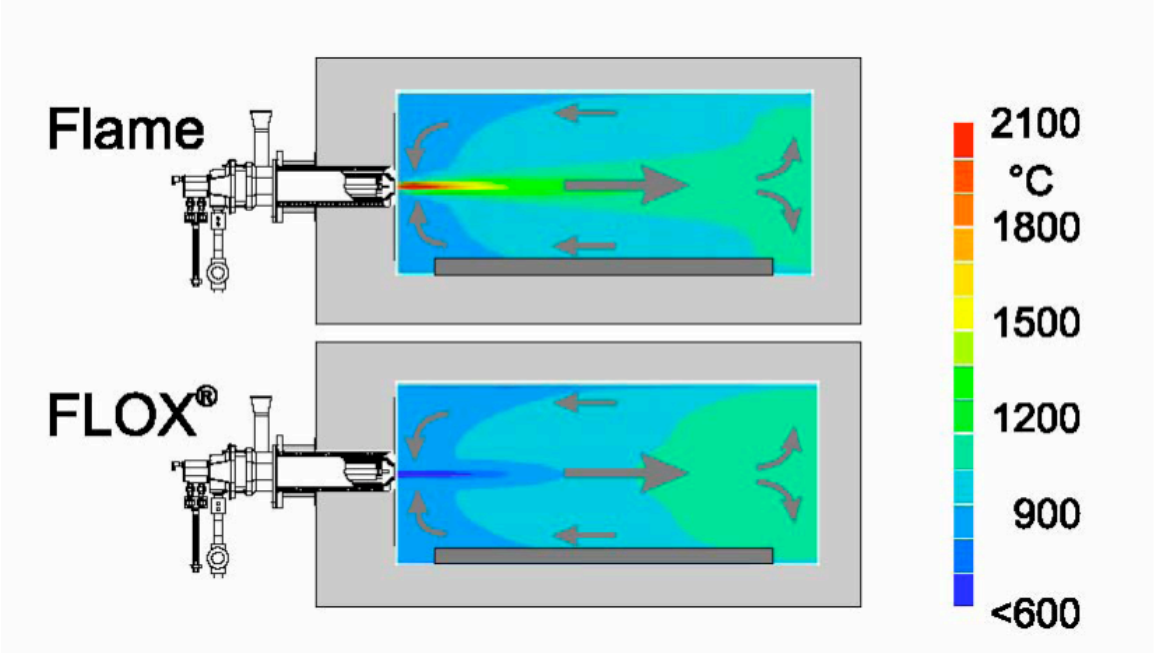

Figure 3.2: Contrasting Temperature Distributions Between Direct Flame (Top) and Flameless Combustion (Bottom) due to Extensive Recirculation of Combustion Product Gases (Wünning, 2000)

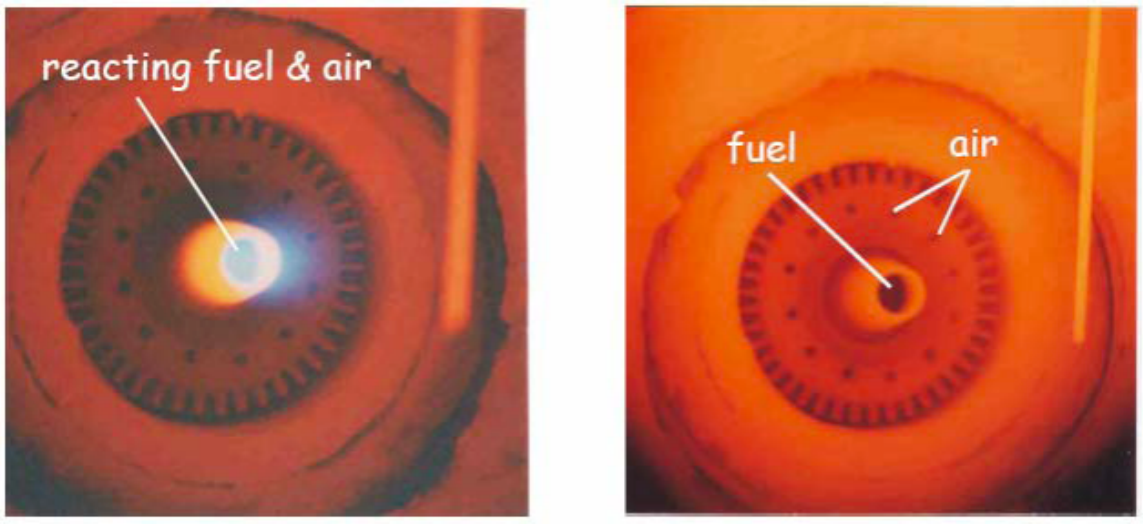

(a) **(b)**

Figure 3.3: Comparison Between (a) Direct Fired Flame and (b) Flameless Combustion (Wünning, 2003)

As mentioned before, the Strong-Jet/Weak-Jet Flameless Combustion Furnace system is composed of a dual jet system. In this system, the fuel and oxidant streams are supplied through independent jet nozzles where the fuel jet is at an angle θ from the oxidant jet. The two jet streams come together or converge downstream as shown in Figure 3.4.

The fuel stream flow rate is smaller than that of the oxidant due to stoichiometric requirements for the combustion process, hence the Strong-Jet/Weak-Jet (SJ/WJ) terminology for this type of burner design (Grandmaison et al, 1998). As a result, the strong-jet is able to entrain the weak-jet creating the curved trajectory depicted in Figures 3.4 and 3.5.

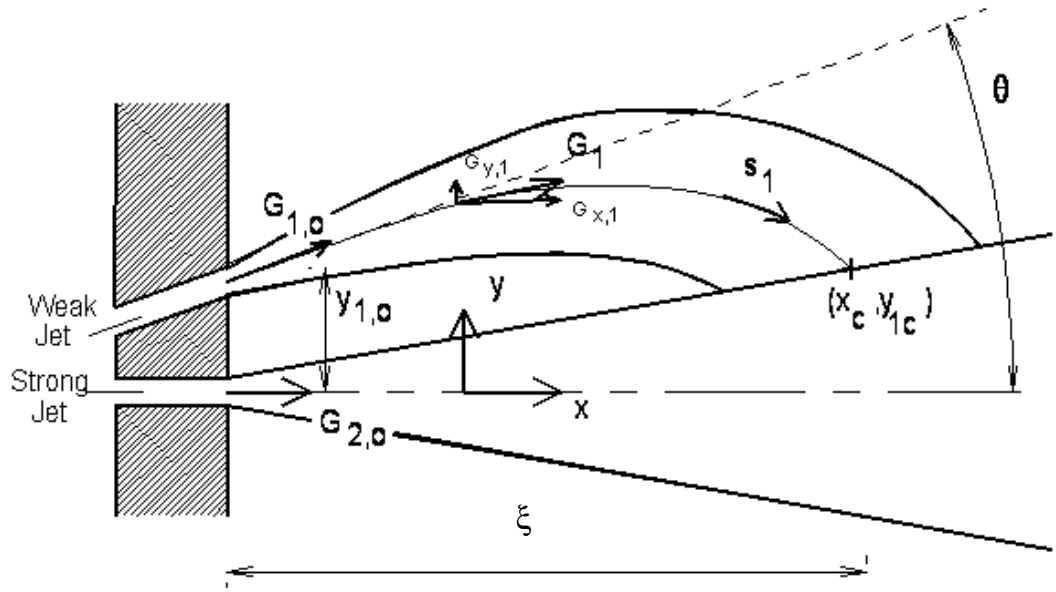

Figure 3.4: Schematic Diagram of the Strong-Jet/Weak-Jet Flow System (Grandmaison et al, 1998)

Figure 3.5: Flow Visualization of the Strong-Jet/Weak-Jet Entrainment Interaction (Yimer, 1997)

Overall, the trajectory of the weak-jet or fuel jet is directly dependent on the entrainment force that the strong-jet possesses. Entrainment, and subsequently the fuel jet trajectory, depends on the fuel jet angle θ from the oxidant jet and the momentum ratio between the two jets (Grandmaison et al, 1998).

3.2 The Flameless Combustion Furnace Configuration

The SJ/WJ furnace is a 48 kW (165,000 BTU/h) square, water-cooled, refractory lined, pilot-scale, non-preheated combustion air, natural gas-fired furnace with a single pair of jets in the SJ/WJ configuration (Becker, 1999, Li, 2005 and He, 2008). Becker (1999) first created detailed drawings of the furnace components, Li (2005) and He (2008) later transferred these drawings to Solid Edge (V17) and design modifications were made in the current work. The SJ/WJ furnace has a 400 mm square cross section with aluminum water-cooled modular sections that can be added to create a furnace of different lengths (typically 1.4 m to a maximum length of 2.0 m). The furnace is aligned vertically and fired from the bottom with the combustion product gases circulating along the length of the unit and finally withdrawn from the bottom of the furnace as shown in Figure 3.6. This flow pattern provides a strong recirculation of the combustion product gases – a key feature of this flameless combustion system. Wall panels for the lower part of the furnace are removed in this figure to show detail of the burner plate in the bottom of the furnace.

Special modular sections are available to accommodate view-ports and sampling-ports. The base surface or burner plate where the fuel and air enter the furnace can also be raised or lowered over a distance of approximately 80 mm for probing along the axis of

the combustion chamber. Additional capability to probe along the furnace axis is accommodated by moving some of the special modular sections to different downstream positions. The furnace is equipped with an explosion vent and view port at the top of the furnace chamber. The flue gases are removed from the furnace by an ejector system directing the exhaust gases through appropriate ductwork away from the test facility.

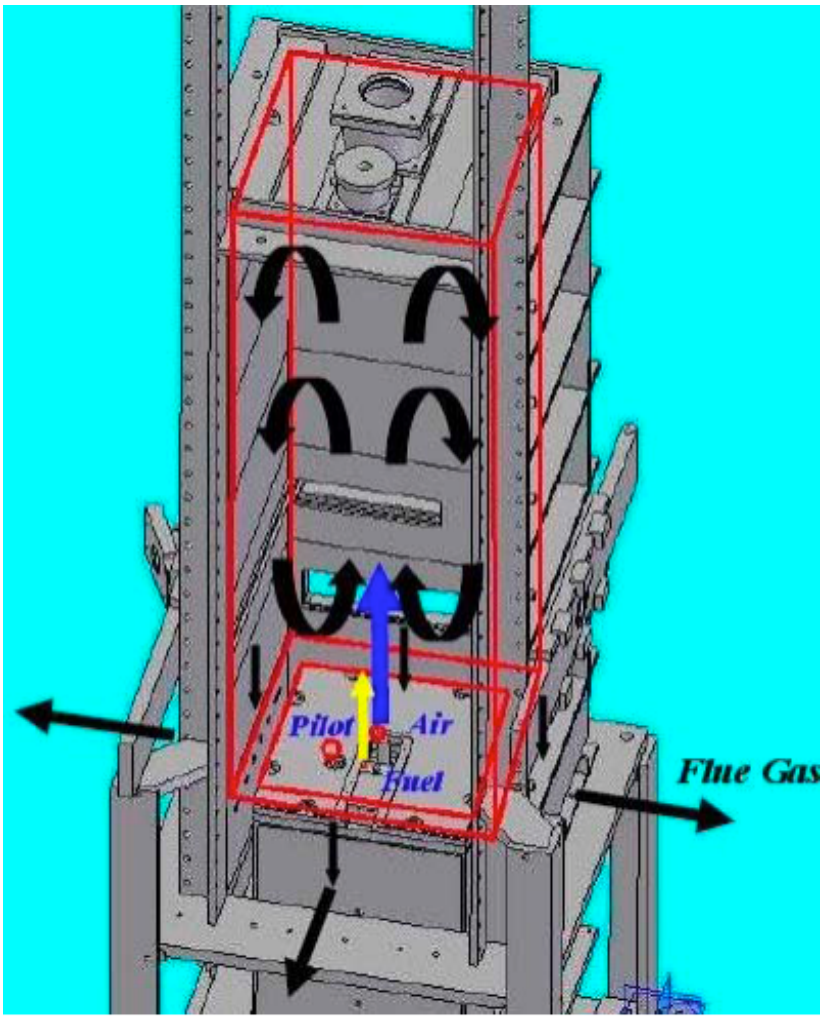

Figure 3.6: The SJ/WJ (Strong-Jet/Weak-Jet) Furnace Showing a Typical Assembly of Modular Sections (He, 2008)

The furnace assembly consists of an aluminum-mounting base, Figure 3.7 (b), with

structural angles mounted to accommodate the modular sections as shown in Figure 3.7 (c). The cross sectional elements of the furnace consist of water-cooled modular sections fabricated from aluminum plate and channel material as seen in Figure 3.7 (a). Each of these modules provides a furnace length of 200 mm and a square furnace cross section, 400 × 400 mm.

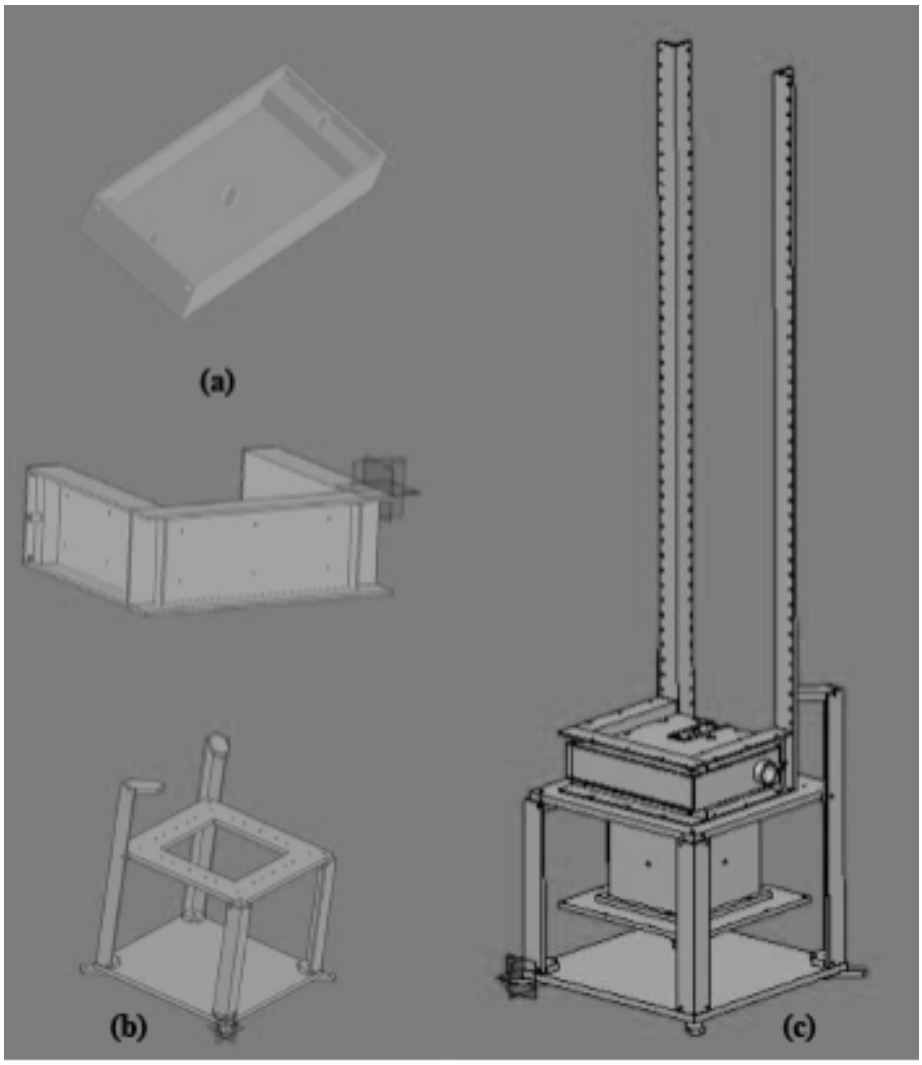

Figure 3.7: Components of the Combustion Furnace Consisting of (a) Modular Sections; (b) Mounting Base; and (c) Base with Structural Mounting Angles for Modules (He, 2008)

The furnace is equipped with view ports and sampling ports in some of the sidewall

elements as well as a view port, an explosion vent at the top of the furnace and thermocouple ports for wall temperature measurements. These features are depicted in Figure 3.8.

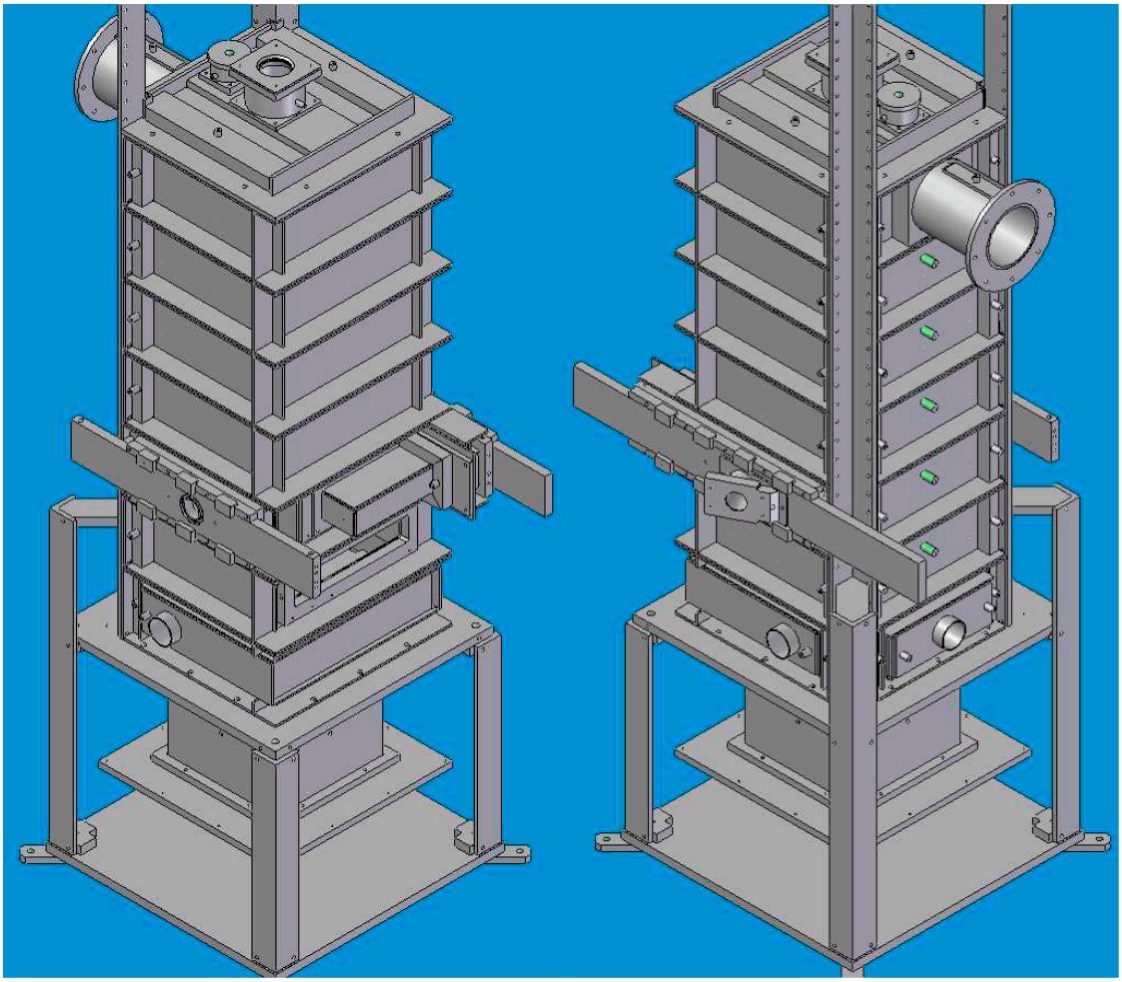

Figure 3.8: Isometric Views of the SJ/WJ Furnace Detailing Sidewall Sampling Port and View Port Modules; Explosion Vent; Top View Port; and Thermocouple Ports for Furnace Wall Temperatures (He, 2008)

Aside from the skeletal and physical aspects of the SJ/WJ combustor, a number of feed and return lines are associated with the furnace as well. The furnace assembly consists of a combustion air supply line, a natural gas supply line, a flue gas exhaust system, a pilot

supply line, and a cooling water supply system. A regenerative blower provides the air supply for the SJ/WJ burner system. The exhaust gases are removed from the furnace by an ejector supplied with air from a regenerative blower. The flow rates of the natural gas lines – for the main burner and pilot burner – as well as the cooling water line are manually monitored with rotameters. Data collection was done through a Data Acquisition Board (DAQ) and recorded to a computer. The DAQ was composed of a channel board, which collected all necessary data including temperature and pressure via electrical signal through thermocouple and pressure differentials. The entire experimental system is schematically shown in piping and instrumentation form in Appendix A.

The primary safety concern with the furnace configuration was its pilot burner. During tests with this furnace, a pilot flame was used to preheat the furnace prior to switching the furnace firing to the SJ/WJ burner operation. The pilot burner system consisted of a premixed flame stabilized on the rim of a stainless steel flame holder as shown in Figure 3.9. The air supply for this burner was provided by a portable compressor and mounted on the base plate of the furnace through a pre-drilled port as shown in Figure 3.10. This current set-up of the pilot burner poses many difficulties and safety concerns to its users. Firstly, it is very difficult to ensure that the pilot is burning its fuel and not causing an accumulation of flammable fuel within the chamber, which can lead to an explosion. Its flame stability is very untrustworthy and questionable under different firing conditions (positive, neutral, and negative combustion chambers; excess air; excess gas) due to its high levels of heat release and does not ensure instant lighting. Finally, since the current pilot burner is classified as a premixed burner, the possibility of flashback is always

present.

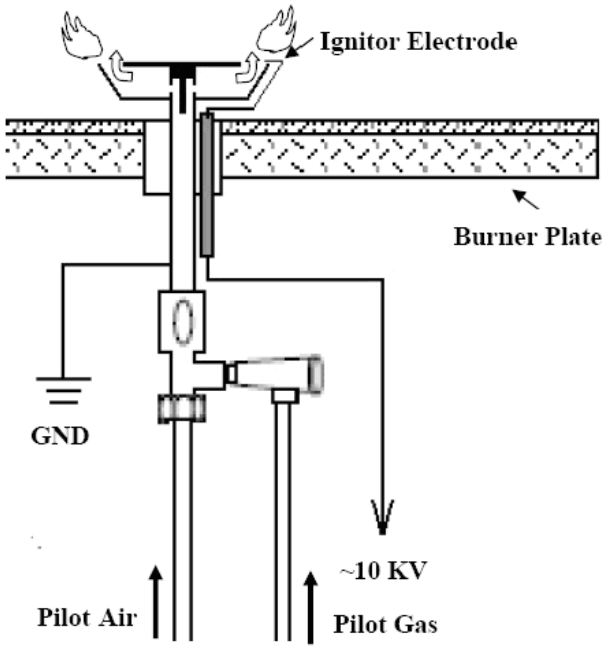

Figure 3.9: The Pilot Flame Assembly (He, 2008)

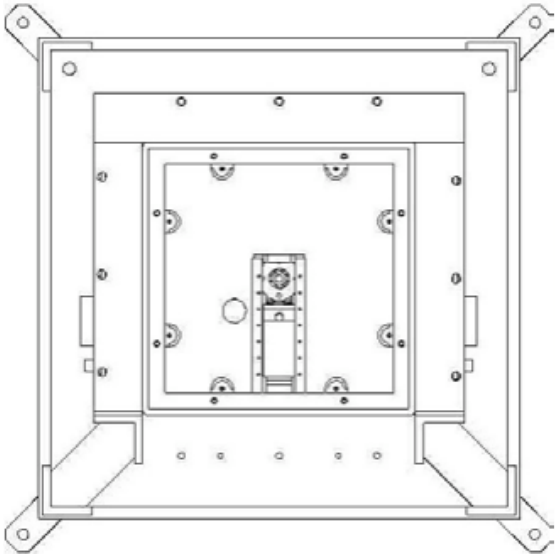

Figure 3.10: Burner Base Plate with Mounting Assembly for the SJ/WJ Burner (Centre of Burner Plate) and the Pilot Flame Port (Offset from the SJ/WJ Burner) (He, 2008)

3.3 Furnace Modifications

Due to numerous safety restrictions posed by the current SJ/WJ Furnace, it was decided to use the furnace in a different fashion that was not limited to flameless combustion. The main skeletal part of the furnace (modular sections, mounting base, structural mounting angles, etc.) will remain and be retrofitted with new DAQ and cooling water lines. The current SJ/SW burner and pilot along with all the feed and return lines will be replaced with a water cooled burner plate that can accommodate various types of different combustion burners allowing the plate to be interchangeable in nature. This burner plate is pictured in Figure 3.11 and will be placed on the furnace-mounting base.

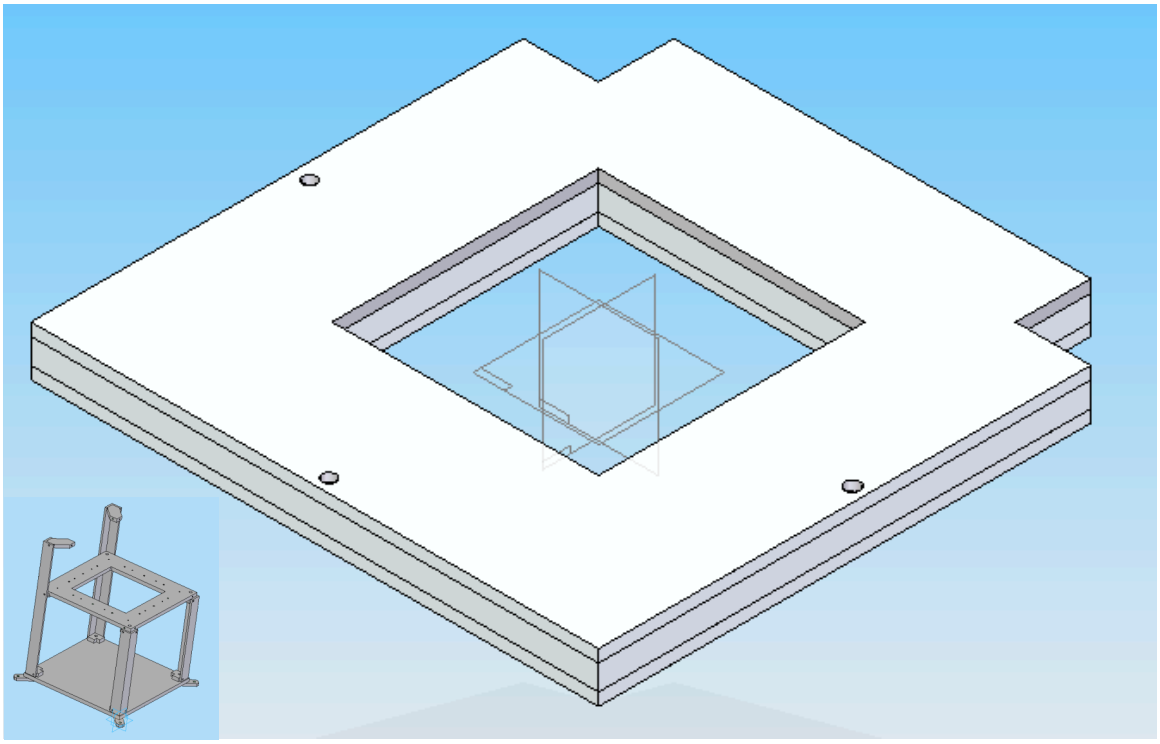

Figure 3.11: Burner Plate and Furnace Mounting Base (Inset)

To be consistent with safety requirements set by the Technical Standards and Safety

Authority (TSSA) and the Canadian Standards Association (CSA), the entire furnace system is to be overhauled with special attention focused on the main burner and pilot. Aside from a new DAQ system and a new burner/pilot arrangement and gas train, the furnace maintains essentially the same skeletal structure as the SJ/WJ furnace.

As mentioned before, the furnace will be retrofitted with a mounting base plate (Figure 3.11) that can accommodate different types of burners. One such burner that will be initially used to operate the furnace is an excess air nozzle mix burner pictured in Figure 3.12. The nozzle mix burner in question is manufactured by Pyronics Inc. and supplied by Ordan Thermal Products Ltd. As with all nozzle mix type of burners, there is no exception to safe operation with this burner, especially since this particular nozzle mix burner can operate under excess air conditions.

As previously mentioned in Chapter 2, nozzle mix burners introduce the combustion fuel and oxidant into the combustion zone of the burner separately. The oxidizer and fuel are unmixed and separate from one another before combustion can take place and are mixed only at or after the ignition point of the burner. Nozzle mix burners are able to diffuse the combustion fuel and combustion oxidant streams away from the burner giving them a very wide range of operation stability. Diffusing the streams away from the burner prevents flashbacks and explosions in potentially dangerous systems, such as a combustion chamber that operates under positive pressure. Nozzle mix burners can have their oxidant supply stream set to a maximum flow rate while the flow of fuel can be reduced according to the desired temperature demand. This indicates that nozzle mix

burners can operate under significant and high levels of excess air allowing less use of fuel but equal output of heat. The excess air capability of nozzle mix burners results in high heating efficiencies with less fuel as well as higher combustion velocities due to larger amounts of combustion air.

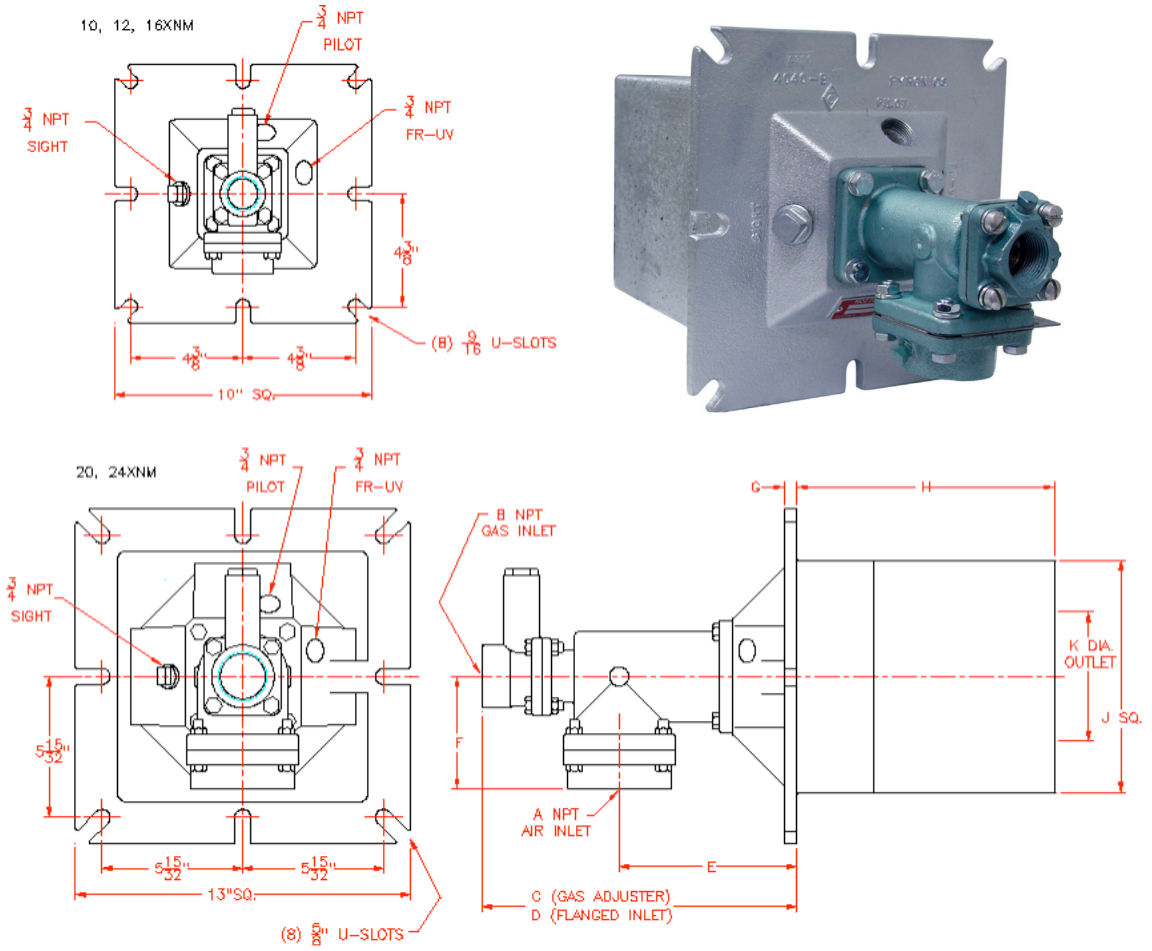

Figure 3.12: Nozzle Mix Burner – Pyronics Model 3502-XNM (Ordan Thermal Products Ltd. – Excess Air Burner, 2009)

Pyronics Inc. identifies the following favored features of their excess air nozzle mix burner, model 3502-XNM (Ordan Thermal Products Ltd. – Excess Air Burner, 2009):

- 500% - 800% excess air.
- Preheated air up to 750°F.
- Excellent flame stability with: Excess Air, Excess Gas, On Ratio Firing.
- Instant lighting at all firing ranges.
- High discharge velocities.
- Low air and gas pressures required.
- Unique stepped tunnel design.
- Operation to 2500°F.
- Rugged, heavy-duty industrial construction.
- Burner ports for pilot, flame monitoring, and sighting.
- Intermediate flame length.
- Max. Capacities: 200,000 to 6,000,000 BTU/h.

The particular nozzle mix burner at hand harbors its own pilot flame and meets the technical standards of both the TSSA and CSA by having its own gas train (i.e. the control valves and pressure regulators used to meter the fuel) for both the main burner and pilot flame. This gas train is shown in more detail in Appendix B. To complement this gas train, two important pieces of hardware are taken into account and discussed in more detail: the regenerative blower and the burner control safeguard.

The air supply for both the main burner and pilot flame will be provided by Pyronics Inc. 4120-LC blower. This type of blower, furnished by Ordan Thermal Producst Ltd., is pictured in Figure 3.13. As its name suggests, this type of blower is low in cost yet presents rugged, dependable, and constant pressure operation. It is able to deal with high capacity flow rates (116-166 cfm) at reasonable powers (1/3 – 1/2 horsepower). With a 3450 rpm motor, the blower is lightweight and requires minimum maintenance.

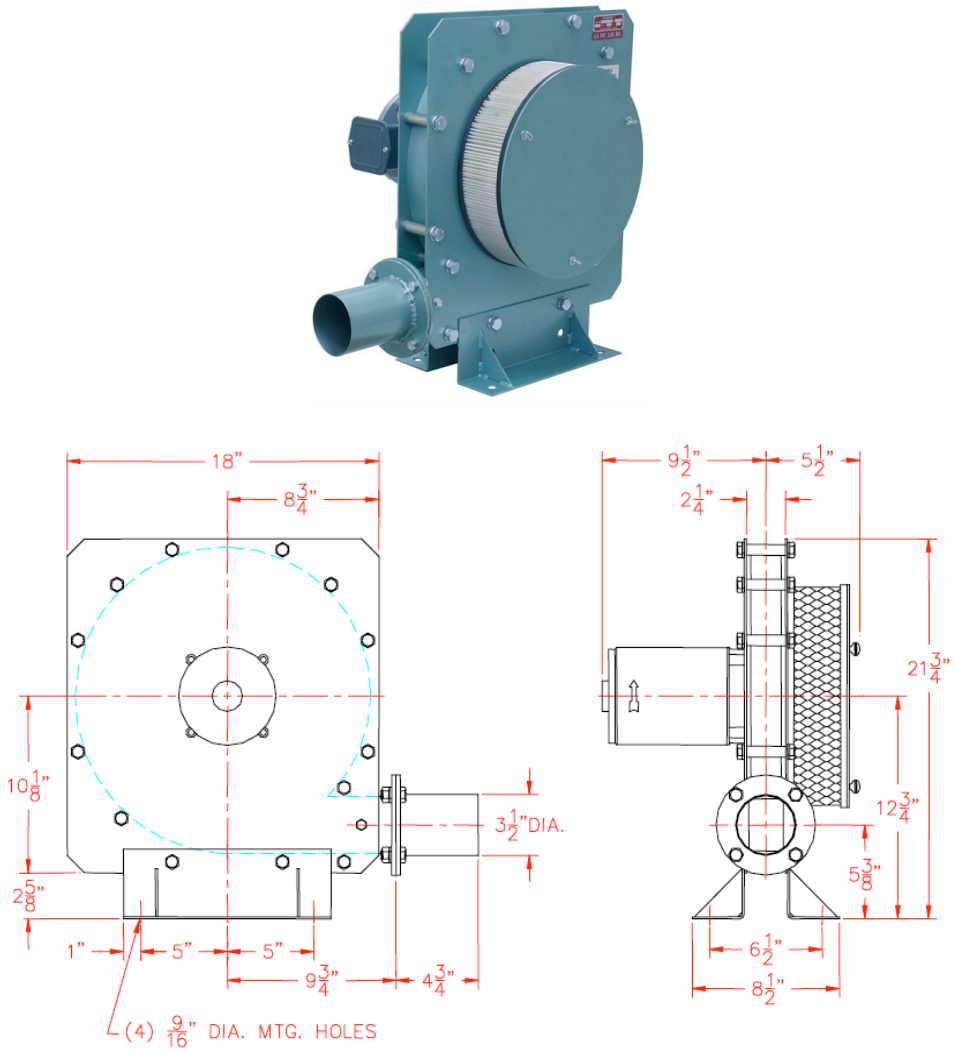

Figure 3.13: Regenerative Blower - Pyronics Model 4120-LC (Ordan Thermal Products Ltd. – Mini L.C. Blowers, 2009)

The burner control safeguard shown in Figure 3.14 is designed to provide continuous, automatic protection against the buildup of combustible fuel mixtures due to flame failure or other faults in the combustion chamber or furnace. The burner control system includes a flame safeguard function that provides an automatic sequencing of the furnace system through pre-purge, pilot trial for ignition (PTFI), main trial for ignition (MTFI), run (AUTO), and post purging (Fireye, 2007). The system can monitor one or more burners

simultaneously and will respond to the presence or absence of a flame. The control line consists of plug-in components that have high signal strength to provide safe and secure operation while minimizing the potential for system shutdown due to noise in signals.

Figure 3.14: Burner Control Safeguard – Pyronics Model 7500 (Ordan Thermal Products Ltd. – Microprocessor Burner Control, 2009)

In addition to the material presented in this chapter concerning the furnace, a more detailed presentation of the SJ/WJ furnace can be found in He (2008) and Li (2005). Now that the furnace modifications have been defined, the following chapter presents a detailed analysis on the heat transfer parameters occurring in industrial furnaces. This analysis includes a number of calculations that will allow one to determine the transfer of heat within a furnace enclosure, namely radiative heat transfer.

Chapter 4

Heat Transfer Analysis

The transfer of heat is without a doubt the most important and fundamental purpose of combustion in all of the process industries. The main objective in industrial combustion applications is to transfer energy, in the form of heat, to a type of material or load for the thermal processing of that load (Gebhart, 1971). The understanding of heat transfer is essential to the successful design and operation of fired equipment (Baukal and Schwartz, 2001). Hence, it is the intent of this chapter to discuss the concepts of the transfer of heat, in particular radiative heat transfer, as applied to combustion.

4.1 Heat Transfer in Industrial Furnaces

The majority of all process industries are based on heat as the main form of energy. Heat transfer is the science that seeks to understand and predict the energy transfer between masses resulting from differences in temperature (Holman, 1990 and Kreith and Bohn, 1986). The simplest way to explain heat transfer would be that *heat transfer is energy transfer due to a temperature difference*. There are three mechanisms or modes into which heat transfer is classified: conduction, convection, and radiation. All three modes of heat transfer are critical to the transfer of energy when applied to combustion in the process industries. Consider a typical gas fired process, such as the furnace shown in Figure 4.1. It consists of a load or heat sink to be heated, and a burner to provide the

required energy for the desired heating process. The heat transfer processes that occur in such a furnace include the following:

1. Conduction through the furnace refractory and convection from the wall of the furnace to the surrounding air.
2. Radiation exchange between the flame, the surrounding walls, load and from the wall of the furnace to the surrounding air.
3. Convection from the hot furnace gases to the refractory and load.

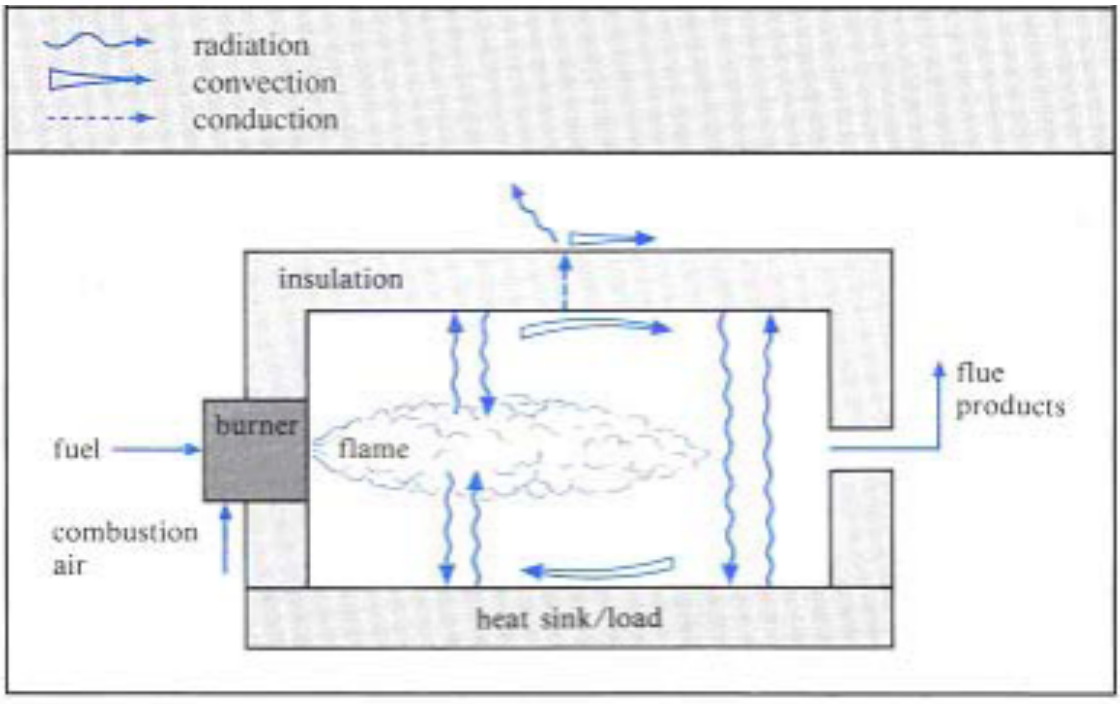

Figure 4.1: The Modes of Heat Transfer in a Simple Gas Fired Process (Tucker, 2004)

The performance of these modes of heat transfer has a direct impact on the product quality, furnace efficiency, lifespan of equipment, and overall safety. Moreover, heat transfer also has an effect on the performance of the fired equipment with respect to NO_X

emissions, flame stability, and shape of the flame (Baukal and Schwartz, 2001). In 1961, Hoyt C. Hottel developed a relatively simple equation that summarizes the overall heat transfer occurring in a simple gas fired process with respect to conduction, convection, and radiation. The equation concerns itself with the heat transfer to the load of a furnace and mathematically depicts the events of Figure 4.1. It is presented in this paper as Equation (1). The model that Hottel uses to develop this equation assumes that the gas in the combustion space is isothermal and is referred to as a one gas-zone furnace model.

$$q_l = \frac{\sigma\left(T_g^4 - T_l^4\right)}{\dfrac{1-\varepsilon_l}{A_l\varepsilon_l} + \dfrac{K_s}{4K_aV} + \dfrac{1}{A_l\varepsilon_g + \dfrac{1}{\dfrac{1}{A_lF_{l\to w}\left(1-\varepsilon_g\right)} + \dfrac{1}{A_w\varepsilon_g}}}} + h_lA_l\left(T_g - T_l\right) \qquad (1)$$

In this equation, σ is the Stefan-Boltzmann constant (5.67×10^{-8} W/m^{2}K^4); T_g and T_l are the absolute temperatures of the gas and load, respectively; ε_l and ε_g are the emissivities of the load and the gas, respectively; A_l and A_w are the surface areas of the load and the furnace wall, respectively; K_s and K_a are the scattering and absorption coefficients of the gas, respectively; V is the volume of the gas; $F_{l\to w}$ is the view factor to the wall from the load; and h_l is the convection coefficient to the load (Page 441 of Hottel and Sarofim, 1967). Although all three forms of heat transfer play a critical role in industrial combustion processes, radiation is the dominant mechanism of the transfer of heat within an industrial furnace and is focused on in this work. In so being, Equation (1) is merely presented as a manner of reference to mathematically display all the types of heat transfer

mechanisms occurring in a furnace.

4.1.1 Background Information on Radiation Heat Transfer

Radiation heat transfer is one of the most important heat transfer mechanisms in industrial furnaces (Faeth et al., 1989). As much as 90% of heat transferred to the load of a furnace can be attributed to radiation (Leblanc and Goracci, 1973) while some have reported that more than 98% of energy is transported by radiation (Brus and Szmyd, 2008). The remaining mode of heat transfer is largely due to forced convection. Radiation is a unique method of heat transfer because no medium is required for energy transport. Radiation is the transmission of energy by electromagnetic waves characterized by their wavelength or frequency as depicted by Equation (2).

$$\lambda = \frac{c}{\nu} \tag{2}$$

In this equation λ is the wavelength, c is the speed of light, and ν is the frequency. In the academic field of heat transfer, more importantly combustion, the wavelength of the transmission of energy is more commonly used to classify radiation. Various types of radiation are classified according to their wavelength in the electromagnetic spectrum found in Figure 4.2. The most important type of radiation for industrial combustion heating is infrared with a wavelength range of 0.01cm to 7×10^{-5}cm as shown in Table 4.1.

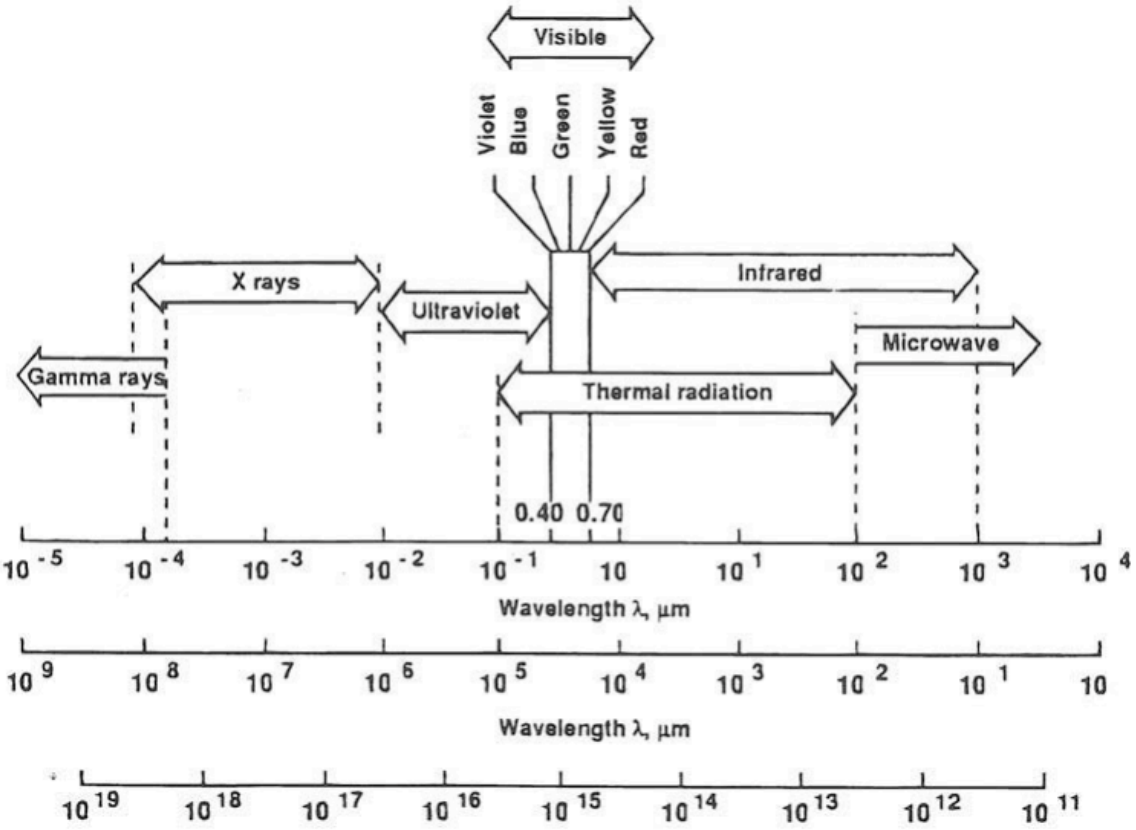

Figure 4.2: The Electromagnetic Spectrum (Hewitt et al., 1997)

Table 4.1: Spectrum of Electromagnetic Radiation (Baukal and Schwartz, 2001)

Region	Wavelength (Angstroms)	Wavelength (Centimeters)	Frequency (Hertz)	Energy (eV)
Radio	$> 10^9$	> 10	$< 3\times10^9$	$< 10^{-5}$
Microwave	10^9 to 10^6	10 to 0.01	3×10^9 to 3×10^{12}	10^{-5} to 0.01
Infrared	10^6 to 7000	0.01 to 7×10^{-5}	3×10^{12} to 4.3×10^{14}	0.01 to 2
Visible	7000 to 4000	7×10^{-5} to 4×10^{-5}	4.3×10^{14} to 7.5×10^{14}	2 to 3
Ultraviolet	4000 to 10	4×10^{-5} to 10^{-7}	7.5×10^{14} to 3×10^{17}	3 to 10^3
X-Rays	10 to 0.1	10^{-7} to 10^{-9}	3×10^{17} to 3×10^{19}	10^3 to 10^5
Gamma Rays	< 0.1	$< 10^{-9}$	$> 3\times10^{19}$	$> 10^5$

The penetration of a medium (solid, liquid, or gas) by radiant energy can result in four potential outcomes. The radiation can be either absorbed, reflected, transmitted, or a combination of the three. The three radiation incidents on a medium is depicted in Figure 4.3 and can be mathematically explained using Equation (3).

$$\alpha + \rho + \tau = 1 \tag{3}$$

The symbols of Equation (3) represent the following properties of the medium: α is the absorptivity, ρ is the reflectivity, and τ is the transmissivity.

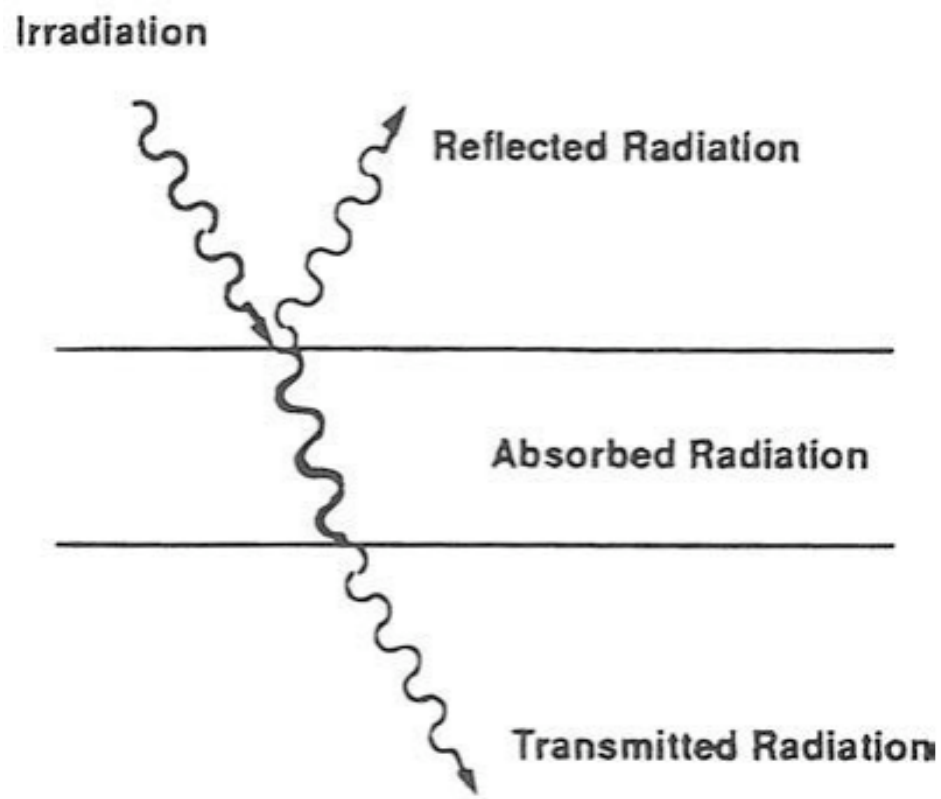

Figure 4.3: The Absorption, Reflection, and Transmission of Radiant Energy (Hewitt et al., 1997)

The absorptivity of the medium, its reflectivity, and the transmissivity, are defined as:

$$\alpha \equiv \frac{\text{absorbed part of incoming radiation}}{\text{total incoming radiation}}$$

$$\rho \equiv \frac{\text{reflected part of incoming radiation}}{\text{total incoming radiation}}$$

$$\tau \equiv \frac{\text{transmitted part of incoming radiation}}{\text{total incoming radiation}}$$

The radiative properties of materials are very important in determining how much radiation can be transferred to and from a medium. The amount of radiation transferred is further complicated due to the fact that the radiative properties may be functions of wavelength, angle of incidence, surface condition, and thickness. For example, the transmissivity of most solid materials are low except for glass and plastics. Solid materials also have low reflectivity points for the most part unless they are highly polished such as stainless steel. The transmissivity for liquids, on the other hand, are significant, especially for liquids containing high contents of water. Gases have high transmissions and negligible absorptance and reflectance.

Heat transfer within a furnace consists of direct radiation from a heating flame and its combustion products to a load. There are three forms of radiation heat transfer in industrial heating applications: Radiation from a solid surface; Non-luminous Radiation (radiation from a gaseous medium); and Luminous Radiation (radiation from particles or soot in a gaseous medium). The latter two types of radiation are of most interest for the

transfer of heat in industrial burners. Moreover, the emissivities and absorptivities of the gaseous medium and soot of both non-luminous and luminous flames play a vital role when calculating the radiative heat transfer rate to the load of a furnace. This calculation is performed using Equation (4) assuming that convective heat transfer to the load is negligible.

$$Q_{load} = \mathbb{F}A_{load}\sigma\left(T^4_{combustion} - T^4_{load}\right) \tag{4}$$

In this equation, σ is the Stefan-Boltzmann constant (5.67×10^{-8} W/m^{2}K^4); $T_{combustion}$ is a characteristic mean temperature which takes into account both the combustion products and flame temperatures; T_{load} is the absolute temperature of the load; and $\mathbb{F}A_{load}$ is the total radiation exchange area term in which $\mathbb{F}$ is Hottel's total radiation exchange factor. This term is a rather complicated function that takes into account the geometry of the furnace; load to refractory area ratio; and more importantly the gas or soot medium emissivity/absorptivity (Mengüç and Viskanta, 1987).

4.1.1.1 Surface Radiation

A blackbody can be defined as a surface that acts as a perfect emitter and absorber of radiation. The spectral emissive power of a blackbody surface depends on its radiation wavelength and absolute temperature and is calculated using Equation (5):

$$E_{b\lambda} = \frac{C_1}{\lambda^5\left(e^{\frac{C_2}{\lambda T}} - 1\right)} \tag{5}$$

In Equation (5), $E_{b\lambda}(T)$ is the spectral emissive power of a blackbody in *Btu/hr-ft^2-μm (W/m^3)*, $C_1 = 1.1870 \times 10^8$ *Btu/μm^4-ft^2-hr* (3.7415×10^{-16} *W-m^2*), $C_2 = 2.5896 \times 10^4$ *μm°R* (1.4388×10^{-2} *m-K*), T is the absolute temperature of the body in *°R(K)*, and λ is the wavelength in *μm(m)*. Figure 4.4 displays the graphical relation of Equation (5) as a function of wavelength and temperature. From this figure, one can see Plank's law which states that there is a maximum amount of radiant energy that can be emitted from a surface at a given temperature and wavelength (Sparrow and Cess, 1978). In other words, as the surface temperature increases, the peak or maximum radiation shifts to shorter wavelengths. The maximum wavelength can be computed from Wein's Displacement Law as stated in Equation (6) where $c = 5215.6$ *μm-°R* (*2897.6 μm-K*).

$$\lambda_{\max} = \frac{c}{T} \tag{6}$$

The integration of Equation (5), computed over all wavelengths, results in the hemispherical emissive power of a blackbody known as the Stefan-Boltzmann Law. This law is a function directly proportional to the fourth power of the blackbody thermodynamic or absolute temperature in Kelvin (*K*) and is described by Equation (7) where σ is the Stefan-Boltzmann constant (5.67×10^{-8} W/m^{2}K^4).

$$E_b = \sigma T^4 \tag{7}$$

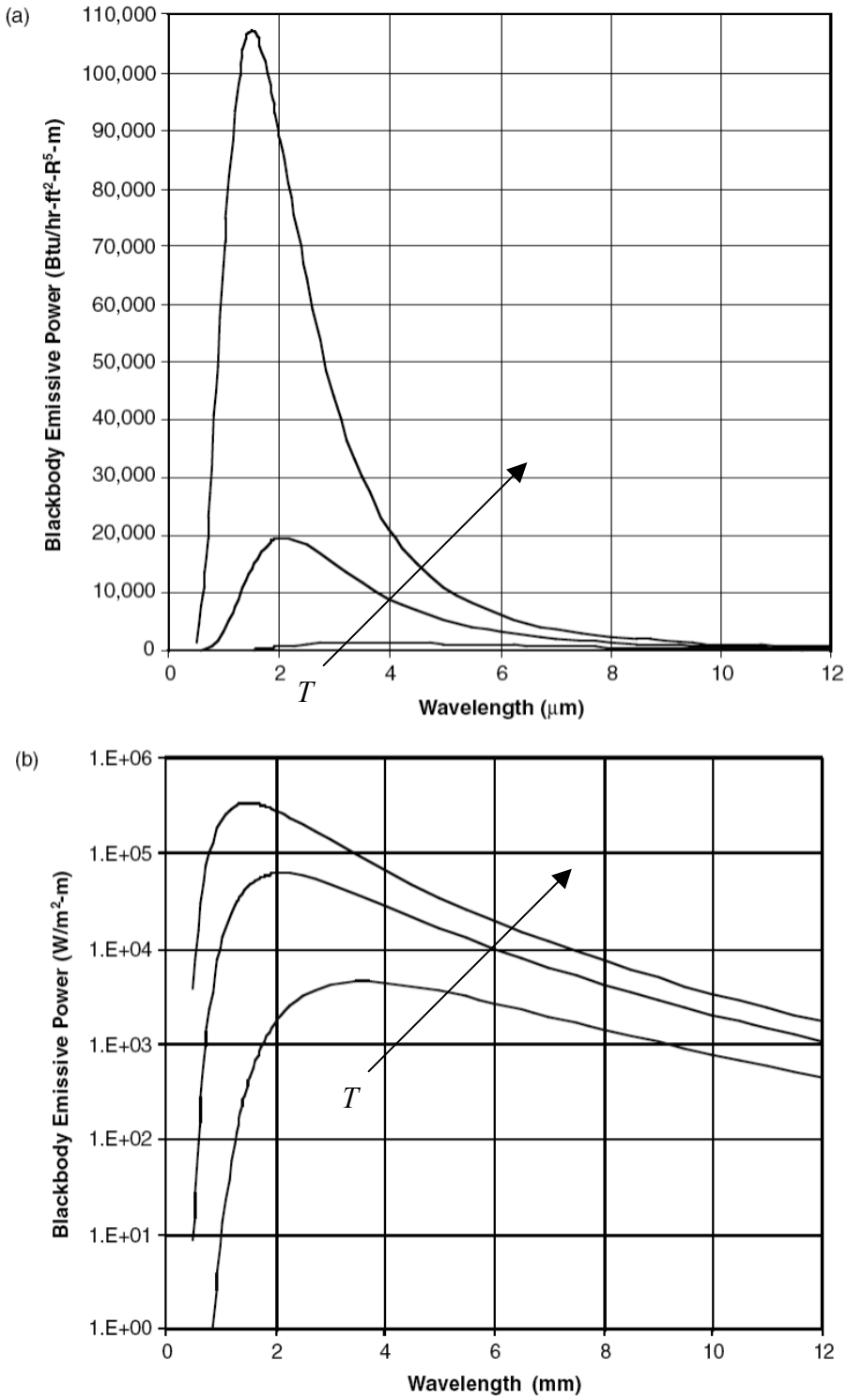

Figure 4.4: Blackbody Emissive Power in (a) English Units (Linear Scale) and (b) Metric Units (Logorithmic Scale) (Baukal, 2000)

A more general case is that of a grey surface or grey body. A grey body is one that does not absorb or emit the full amount of radiative flux. In other words, a gray surface is an imperfect emitter and absorber. They absorb and emit all wavelengths of electromagnetic radiation but absorb and emit only a fraction of the radiant energy of a blackbody (Siegel and Howell, 1992). The portion that that does not absorb or emit the full amount of radiative flux, know as irradiance, is characterized by the emissivity of the surface (ε) and is calculated using Equation (8).

$$E = \varepsilon \sigma T^4 \tag{8}$$

Irradiance has the dimensions of radiative flux or energy per time per area. In SI units, Equation (8) is measured in joules per second per square meter ($J/s\text{-}m^2$) or equivalently in watts per square meter (W/m^2). Surface emissivity is the ratio of radiant energy emitted by a gray surface to the energy emitted by a blackbody. In similar fashion, surface absorptivity (α) is the ratio of the radiant energy absorbed by a gray surface to the energy absorbed by a blackbody. If all the radiative energy arriving at a surface is absorbed by that surface, then the body is termed blackbody and has an absorptivity of unity ($\alpha = 1$). As mentioned above, a blackbody not only absorbs but also emits the maximum amount of energy possible for the given temperature. For a perfect blackbody, surface emissivity has a value of one ($\varepsilon = 1$). However, in realistic and more general cases, real bodies are not perfect emitters and absorbers of radiation and hence are not referred to as perfect blackbodies. The total absolute power of energy radiated by a body or surface takes into account the surface area, $A\ (m^2)$, and is calculated using Equation (9). Moreover, the

radiant heat transfer absorbed by real surfaces is a function of the absorptivity of the body's surface.

$$E = \varepsilon \sigma A T^4 \tag{9}$$

For some surfaces, its absoptivity and emissivity is a function of the temperature and wavelength of the radiation energy. A surface is said to be *graybody* when its absoptivity and emissivity is independent of radiation wavelength. Most surfaces are treated as *graybodies* in the majority of engineering calculations. Figure 4.5 shows examples of the spectral emissivity of some materials, namely black nickel, black chrome, white epoxy paint on aluminum, and 301 stainless steel.

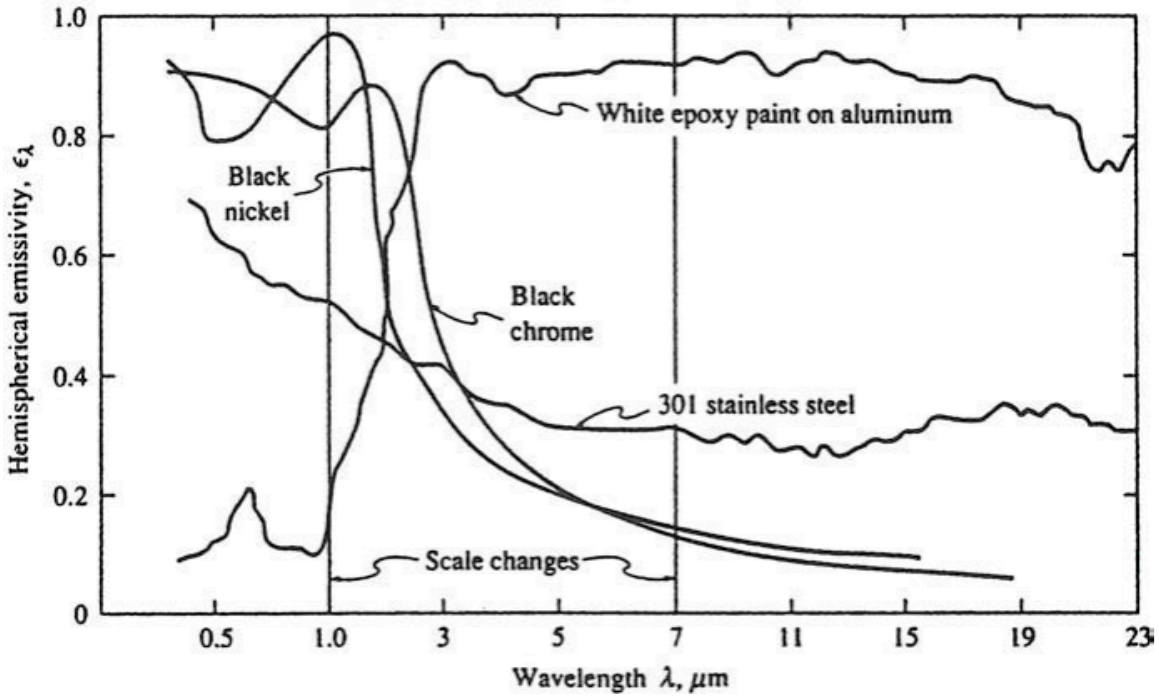

Figure 4.5: Emissivities of Several Spectrally Selective Surfaces (Kreith, 1994)

Some materials have a wide range of emissivities as shown in Figure 4.6 while other

materials, such as silicon carbide, heavily and lightly oxidized stainless steel, aluminum oxide, and tungsten have emissivities that are temperature dependent as displayed in Figure 4.7. To further the information given in Figure 4.7, Appendix C gives a list of normal total emissivities for various surfaces as a function of temperature.

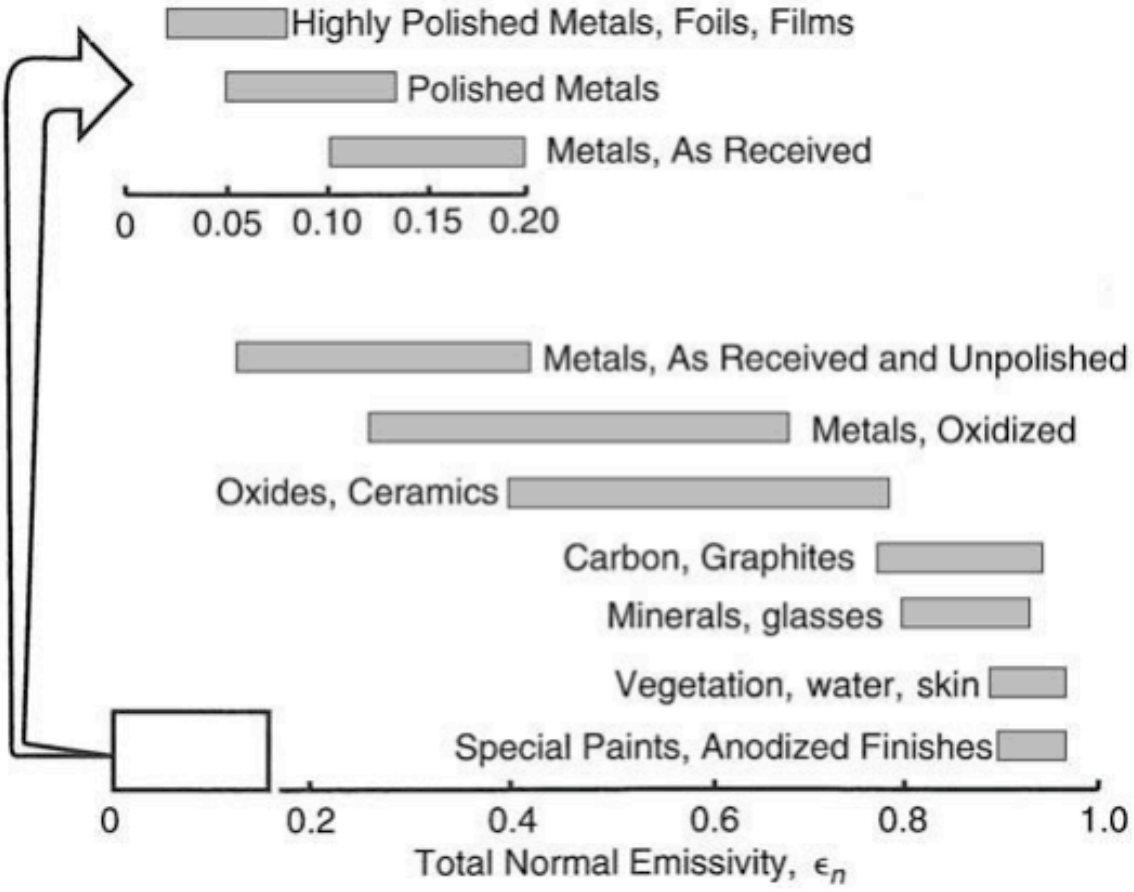

Figure 4.6: Emissivity Ranges for Various Materials (Hewitt et al., 1994)

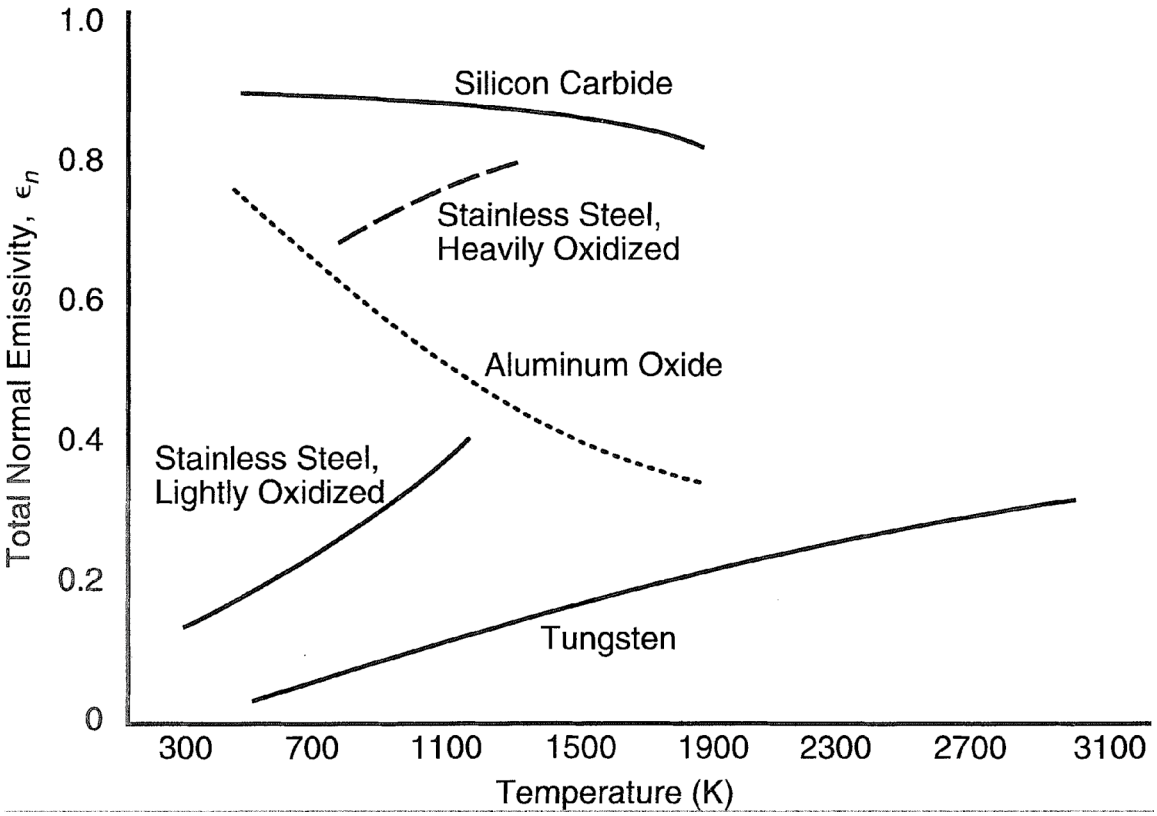

Figure 4.7: Emissivity as a Function of Temperature for Various Materials (Hewitt et al., 1994)

Surface reflectivity (ρ) is directly related to surface absorptivity. A perfect absorbing surface absorbs all incident radiant energy. A non-perfect absorbing media, also known as a gray body, is able to absorb only a fraction of the incident radiation. This, in turn, allows the remaining unabsorbed energy to be reflected onto other surfaces or media. The radiant energy that is not absorbed is known as the surface reflectivity. According to Hottel and Sarofim (1967), the absorbtivity and reflectivity of a gray body must satisfy the sum rule represented by Equation (10).

$$\rho + \alpha = 1 \tag{10}$$

An important analysis technique often used in the combustion process industry is the

calculation of radiation heat transfer within an enclosure such as a furnace. The walls of the furnace are usually higher in temperature in comparison to the load or object(s) being heated thus allowing heat energy to radiate from the furnace walls to the load. An enclosure that consists of a vacuum or a gas such as air that is transparent to radiative energies is referred to as nonparticipating media. This indicates that the media within an enclosure or furnace are unable to absorb any of the radiation passing through it. If the enclosure consists of a radiative absorbing gas such as CO_2, H_2O, or CO then the media are called participating because it is able to absorb at least some of the radiation passing through it. With respect to the combustion of fossil fuels, the resulting combustion products contain significant quantities of CO_2 and H_2O. However, it is a rule-of-thumb in the combustion industry to assume that the concentrations of participating gases are low enough due to dilution by N_2. This assumption allows one to treat the combustion space as nonparticipating, easing the mathematical analysis of the combustion chamber in the process. The net radiative heat transfer from one surface to another is calculated using Equation (11) where $q_{1\Leftrightarrow 2}$ is the net energy transferred between surfaces 1 and 2.

$$q_{1\Leftrightarrow 2} = \sigma A_1 F_{1\to 2}\left(T_1^4 - T_2^4\right) = \sigma A_2 F_{2\to 1}\left(T_1^4 - T_2^4\right) \tag{11}$$

The term $F_{i\to j}$ is referred to the configuration factor or more commonly known as the view factor and represents the diffuse radiation leaving surface *i* and received at surface *j*. Due to the reciprocity theory, Equation (12) is deemed valid.

$$A_1 F_{1\to 2} = A_2 F_{2\to 1} \tag{12}$$

Equations, charts, tables, and graphs of radiation view factors are given by Edwards (1981), Wiebelt (1966), and Hottel and Sarofim (1967) among others. One reliable, well-known and readily available source of view factor equations and graphs for different configurations is found on the World Wide Web and maintained by Howell (2001). Appendix D displays the equations and graphs of important configuration factors. In order to illustrate the view factor type of analysis, an example is given. Take for instance two identical, parallel, directly opposed rectangles as pictured in Figure 4.8.

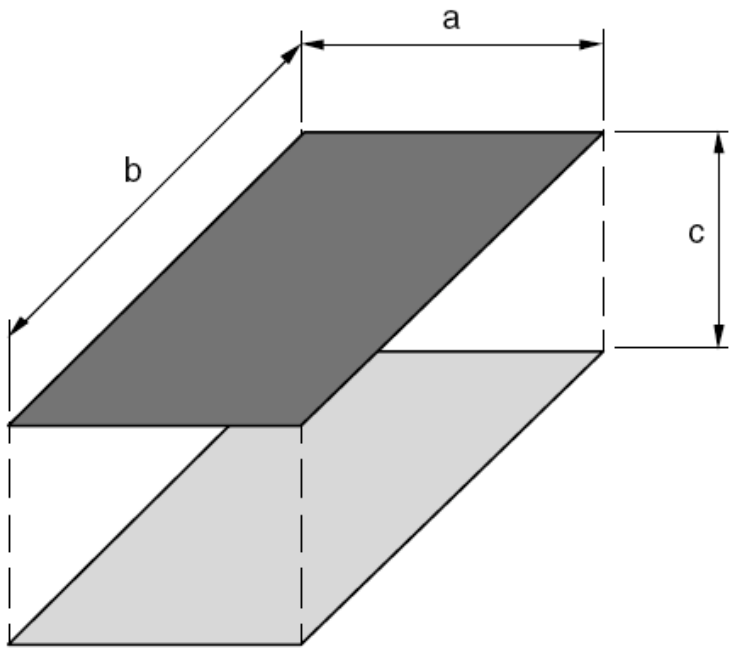

Figure 4.8: Geometry for View Factor Calculation Between Parallel Plates (Baukal, 2000)

The view factor between these two surfaces is calculated using Equation (13) where $X = a/c$, $Y = b/c$, a = length of the rectangles, b = width of the rectangles, and c = spacing between the rectangles.

$$F_{1\to 2} = F_{2\to 1} = \frac{2}{\pi XY}\left\{\begin{array}{l} \ln\sqrt{\frac{\left(1+X^2\right)\left(1+Y^2\right)}{1+X^2+Y^2}} + X\sqrt{1+Y^2}\tan^{-1}\frac{X}{\sqrt{1+Y^2}} + \\ Y\sqrt{1+X^2}\tan^{-1}\frac{Y}{\sqrt{1+X^2}} - X\tan^{-1}X - Y\tan^{-1}Y \end{array}\right\} \qquad (13)$$

One can see from Equation (13) that the view factor calculation for a relatively simple geometric configuration is complicated. Computer analysis becomes necessary for more complicated surface orientations.

4.1.1.2 Non-luminous Gaseous Radiation

As mentioned before, non-luminous gaseous radiation plays an important role in the radiative heat transfer rate from the heat source or sink to the load or material of an industrial furnace. In particular, the emissivity and absorptivity of the gaseous medium produced during combustion are essential when determining the amount of radiation given off by the gaseous medium. The complete combustion of hydrocarbon fuels produces, among other things, carbon dioxide and water vapour. These two gaseous products are the main products that generate non-luminous radiation. The gaseous medium mode of heat transfer depends on the gas temperature level, the partial pressure and concentration of each species, and the molecular path length through the gas (Baukal, 2003).

The total emissivity for a predominantly CO_2 and H_2O gaseous medium is calculated using Equation (14) where ε_{CO_2} and ε_{H_2O} are the emissivities of carbon dioxide and water vapor respectively. These values are easily obtained from graphical results in well-

known published heat transfer literature as well from simple hand calculations.

$$\varepsilon_{CO_2+H_2O} = \varepsilon_{CO_2} + \varepsilon_{H_2O} - \Delta\varepsilon \tag{14}$$

The $\Delta\varepsilon$ term of Equation (14) accounts for the overlap between the H_2O and CO_2 bands and is calculated using Equation (15) while the ξ term is calculated using Equation (16).

$$\Delta\varepsilon = \left(\frac{\xi}{10.7 + 101\xi} - 0.0089\xi^{10.4} \right) \left(\log_{10} \frac{\left(\rho_{H_2O} + \rho_{CO_2}\right) L}{\left(\rho_a L\right)_o} \right)^{2.76} \tag{15}$$

$$\xi = \frac{\rho_{H_2O}}{\rho_{H_2O} + \rho_{CO_2}} \tag{16}$$

In Equations (15) and (16), ρ represents the partial pressure of the given gas while L is the path length through the gaseous medium. Similar to the emissivity of a gaseous medium, its absorptivity is calculated using Equation (17).

$$\alpha_{CO_2+H_2O} = \alpha_{CO_2} + \alpha_{H_2O} - \Delta\varepsilon \tag{17}$$

The individual absorptivites for both CO_2 and H_2O (α_{CO_2} and α_{H_2O}) is calculated using Equation (18) where ε is the emissivity of the gas being studied, T_g the temperature of the gas, and T_s the surface temperature of the furnace wall.

$$\alpha = \varepsilon \left(\frac{T_g}{T_s} \right)^{1/2} \tag{18}$$

The $\Delta\varepsilon$ term of Equation (17) is calculated in the same manner presented in Equation (15) with the exception of the pressure path length being p_aLT_s/T_g. The equations presented above are used to calculate the absorptivity and emissivity of the gaseous medium of a non-luminous flame.

4.1.1.3 Luminous Radiation

Luminous radiation is produced by the continuous emission of particles in a flame, such as soot, that radiate as blackbodies. Blackbodies in this instance are objects that not only absorb all radiation that falls onto its surface but also allow no radiation to pass through it or reflect off of its surface. Studies on both luminous and non-luminous radiation from turbulent diffusion flames have been studied and it has been shown that soot radiation is greater than gaseous radiation. This study is displayed in Figure 4.9 where soot or luminous radiation is depicted as q_{rs} and gaseous radiation as q_{rg}. Figure 4.9 not only indicates that luminous radiation is greater than non-luminous radiation but also that the emittance of radiation increases as distance from the flame origin increases until its distance becomes so great that radiation emittance has no other choice than to decrease.

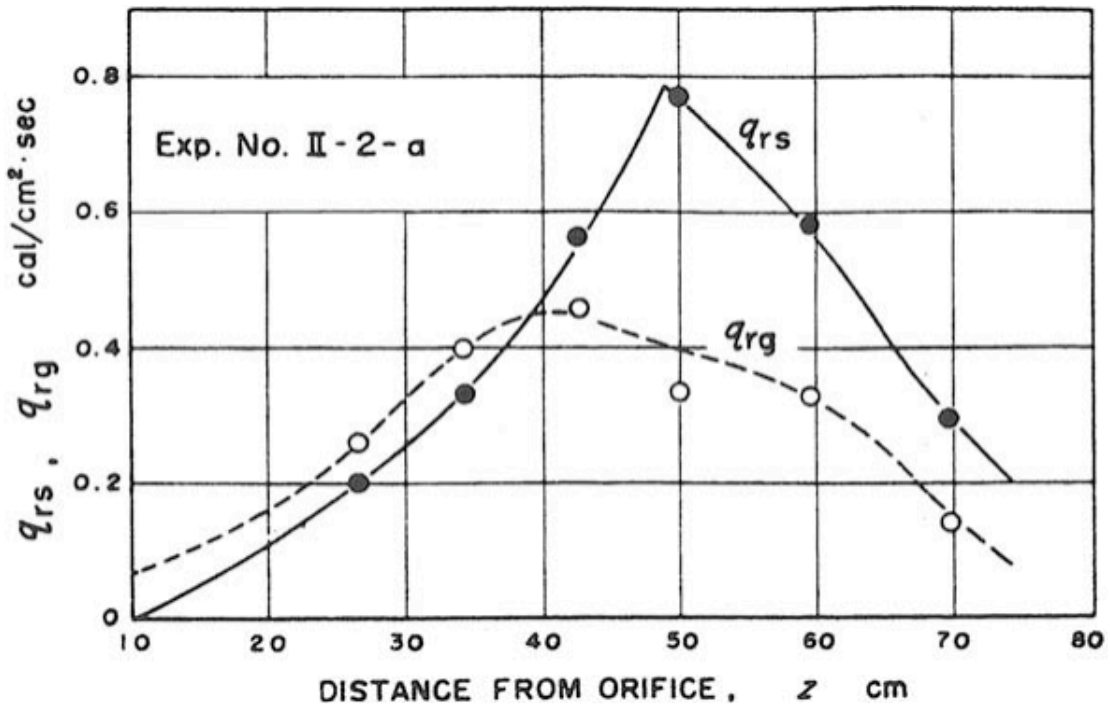

Figure 4.9: Comparison of Soot (q_{rs}) and Gaseous (q_{rg}) Radiation (Baukal, 2003)

Luminous radiation is usually only important when liquid and solid fuels, such as oil and coal, are used. This type of radiation is not significant for gaseous fuels, such as natural gas. Soot itself is composed primarily of long chains of carbon and is usually formed at temperatures ranging from 1000^0C to 2500^0C. It is also known that fuels with higher carbon-to-hydrogen (C/H) ratios produce flames with higher concentration of soot (Baukal, 2003).

It is known that flame emissivity varies with fuel type. Since fuels with higher carbon-to-hydrogen weight ratios produce sootier flames they also have higher emissivity values as a result. The emissivity of fuel gases with carbon-to-hydrogen weight ratios between 3.5 and 5.0 is calculated using Equation (19) where the MW_{fuel} term is the molecular weight

of the fuel itself.

$$\varepsilon = 0.048\sqrt{MW_{fuel}} \tag{19}$$

Examples of gaseous fuels that lie within the appropriate *C/H* weight ratio range are among others coke oven gas, ethane, propane, and butane. Similarly, the emissivity correlation for liquid fuels with carbon-to-hydrogen weight ratios between 5 and 15 is displayed in Equation (20).

$$\varepsilon = 1 - 68.2e^{-2.1\sqrt{C/H}} \tag{20}$$

Equation (20) is used to calculate the emissivities of gas oil, residual fuel oil, and pitch creosote to name a few. As is the case with non-luminous radiation, these emissivities along with the geometry of the furnace and load to refractory area ratio, are used to calculate the radiation heat transfer to the load of a furnace.

4.1.1.4 Radiation Heat Transfer to Furnace Load

Now that non-luminous and luminous emissivites-absorptivites have been accounted for, the actual radiative heat transfer to the load of a furnace can be calculated. As noted before, it is the author's interest to focus on non-luminous radiation not only because of its environmental benefits over soot heating but also due to the readily availability of gaseous fuels that it utilizes. Above all, non-luminous radiation heating is more commonplace than luminous heating in the majority of furnaces. Assuming that the combustion chamber of an industrial furnace is blackbody and that non-luminous

radiation is dominant, the heat transfer rate from the flame and its combustion products to the chamber surroundings and hence the load is calculated using Equation (21) where $\varepsilon_{CO_2+H_2O}$ and $\alpha_{CO_2+H_2O}$ are calculated using Equation (14) and Equation (17) respectively.

$$Q_{load} = \sigma A_{load}\left(\varepsilon_{CO_2+H_2O}T^4_{combustion} - \alpha_{CO_2+H_2O}T^4_{load}\right) \tag{21}$$

One can notice the similarity between Equation (21) and Equation (4) in which the emissivities and absorptivities of the non-luminous flame are able to simplify the complex functional form of Hottel's total radiation exchange factor ($\mathbb{F}$) in Equation (4). But this is only one simplified manner of computing the radiative heat transfer to the load of a furnace. Hence the $\mathbb{F}$ term changes according to the circumstances the furnace operates under.

It must be stated that much of the equations and information contained within this section, unless stated otherwise, is summarized from an important literary source cited in the reference section of this report: Baukal (2003). The information presented in this section of Chapter 4 is an important backdrop to the heating of a furnace load, namely emissivities and absortivities of luminous and non-luminous radiative effects from heating flames to a heat sink/load. The next section of this chapter will focus on the overall thermal radiation phenomena of an industrial furnace and discusses in detail radiation calculation methods and models that are used to predict radiative heat transfer in industrial furnaces.

4.2 Thermal Radiative Heat Transfer in Industrial Furnaces

In order to predict the overall thermal efficiency of a furnace an accurate radiation model is required. According to Tucker (2004), thermal radiation models allow one to successfully predict furnace production rates and polluting emissions as well as the quality of the product heated by the furnace itself. A complete heat transfer model of an industrial furnace includes the internal radiative heat transfer as well as the convective and conductive heat transfer modes into and through the load and furnace walls. More complex models take into account the turbulent flow of the mixing fluids (combustion gases – oxidant and fuel) as well as the mixing and chemical reactions that take place within the combustion chamber. Unless stated otherwise, much of the information contained within this section can be drawn from Tucker (2004).

Thermal radiative exchange is focused upon in this section due to its dominance over convection and conduction, albeit a complete heat transfer model takes into account all three mechanisms of heat transfer. Of the three methods of heat transfer, convective and conductive thermal exchanges are linearly proportional to temperature differences. Radiative heat transfer rates, on the other hand, are non-linearly proportional to temperature differences (Mishra and Prasad, 1998). In fact, the heat radiation equation contains differences to the fourth power of temperature, which in turn makes its mathematical analysis very complicated and troublesome (Chen et al., 2009). Thus, the need to determine the radiative heat transfer rate becomes important and necessary for high temperature applications such as in the case of industrial processes (heating

furnaces, incinerators, etc.).

Thermal radiative exchange is dependent on numerous factors, namely flame temperature and flame position within the furnace chamber and composition of combustion fuel. Moreover, the complexity of modeling radiative heat transfer is heightened due to its spectral and multidimensional nature. In order to arrive at a feasible thermal model of an industrial furnace, a number of mathematical techniques have been developed through the many years of combustion research. All of the known methods have introduced assumptions that have simplified the troublesome and complicated mathematical analysis associated with radiative heat transfer. What is more, the assumptions have been suited to the particular modeling approach and/or application.

Many of the numerical techniques that exist in the literature for the determination of radiative heat transfer rates are of practical importance and help find the contribution of radiative heat transfer in real life problems. Furthermore, most of the numerical techniques are used for verifying new methods and in some instances serve as benchmark tools for the development of these new methods (Mishra and Prasad, 1998). According to both Yang (1986) and Howell (1983), in order for a practical numerical radiation technique to be successful and embraced by industry, it must possess the following seven features:

1. Capability to handle multi-dimensional and complex enclosure geometry.
2. Good accuracy under all conditions: non-scattering or anisotropic scattering, gray or non-gray, isothermal or non-isothermal participating media.

3. Ease of application.
4. Ease of generalization: flexibility in choosing the different order of approximations.
5. Availability of the accurate intensity field and the integrated quantity.
6. Computational compatibility with conductive and/or convective heat transfer codes.
7. Low computation times.

As mentioned before, the prediction of radiative heat transfer is very complex primarily due to its multidimensional and spectral nature. Within a combustion enclosure, such as that of a furnace, the main sources of radiation are from the heat source (flame) or sources and from the hot combustion gases. Radiation is transferred to a load or heat sink through various complex processes. Tucker (2004) specifies these processes as follows:

- Direct radiation from the heat source and combustion products.
- Direct radiation from the walls of the enclosure.
- Indirect radiation from the combustion gases that arrives at the load after multiple reflections off of all the enclosure surfaces (this includes radiation which itself is reflected off the load and re-reflected back to the load).
- Radiation that is partially reabsorbed by the combustion gases or scattered by particles (soot or other mineral matter) as it passes through the combustion enclosure.

Taking into account the non-grey behaviour of combustion gases further complicates the problem of predicting the radiative heat transfer within a furnace. A non-grey gas is a gas whose emissivity, and consequently absorptivity, varies with radiation wavelength. Along with the fact that the heat radiation equation contains a fourth power of

temperature, this nonlinear variation complicates the mathematical analysis of radiative heat transfer. Furthermore, flame temperature and flame position within the furnace chamber and composition of combustion fuel also vary, complicating the matter even further. Simplified radiative heat transfer models assume grey behaviour along with a homogeneous flame temperature and combustion composition.

There are numerous published approaches to modeling radiative heat transfer inside furnaces. However, four techniques stand out from the rest due to their nature of closely following the seven features as outlined above by Yang (1986) and Howell (1983). The practical engineering methods are as follows with the name of its developer(s) in brackets.

- The Zone Method (Hottel and Cohen, 1958).
- The Flux Model (Fiveland, 1984 and Selçuk, 1988).
- The Monte Carlo/Statistical Technique (Howell, 1968).
- The Discrete Transfer Method – DTM (Lockwood and Shah, 1981 and Docherty and Fairweather, 1988).

The majority of these radiation models have been derived specifically for modeling the thermal exchange within industrial furnace; one such model being the Zone Method. Other engineering methods have been derived from other applications, such as the Flux Models, which resulted from astro-physics and the modeling of atmospheric radiation. The choice of method was once limited to the availability of computers with sufficient memory and speed. This is no longer the case with today's modern processing

capabilities. Mishra and Prasad (1998) indicate that there is no single radiation model that can be regarded as the best method for all types of radiative heat transfer. Each technique has its own advantages and disadvantages. Hence, in order to determine whether a particular method is worthy of a specific problem, comparisons between the four techniques have been tabulated in Table 4.2. From this table, both the Zonal Method and Monte Carlo Model are successfully applied to a large and varied class of radiative transport problems.

The Zonal and Monte Carlo methods produce solutions that serve as benchmark results for other radiative heat transfer models. These two methods can deal with relatively complex problems. This is a statement that cannot be said for the Discrete Transfer Method (DTM). The DTM provides satisfactory results for enclosures with simple boundary conditions as well as simple participating media conditions. This model combines the Zonal, Monte Carlo, and Flux models but no results have been reported for scattering media in multidimensional enclosures. On the other hand, the results produced by the DTM for one-dimensional scattering and non-scattering media did not show a level of agreement with well known and documented benchmark results. As with the DTM, the Flux Method also showed a level of flawed results in comparison to the Zone and Monte Carlo Methods (Lewis and Miller, 1984 and Lathrop, 1968). The main drawback of the Flux Method is its inability to extend its application and computation beyond Cartesian coordinates (Pomraning, 1973). This flaw is evident even in the simple cylindrical system where formulation is complicated by additional restrictions by the presence of curved surfaces (Carlson and Lathrop, 1968 and Hyde and Truelove, 1977).

Table 4.2: Comparison of Radiation Models In Furnaces (Tucker, 2004)

Model Type & Description	Advantages	Disadvantages
The Zone Method		
The furnace volume is divided into surface and volume zones. Radiation balance equations are solved using exchange factors between each zone pair.	• Can be used for single or multiple zones • Single zone models can be computed by hand • Technique has been well validated and tested. • Simple models do not require complex solution techniques • Can be applied to non-grey gases using the weighted sum of grey gases	• Cannot model non-homogeneous gas mixtures • Is not compatible with CFD equations • Large numbers of exchange areas are required to be computed and stored for large number of zones
The Flux Model		
Direct solution of the radiative transfer equation by subdividing the directional variation into a small number of angles in which radiation intensity is assumed constant.	• Can be applied to non-homogeneous media • Equations are solvable in CFD	• Results suffer from errors due complex enclosure geometry
The Monte Carlo Model		
Uses random numbers to simulate individual beams of radiation through a furnace enclosure.	• Accepts complex geometry • Handles shadowing effects • Applied to model scattering, specular reflectors and directional and spectral wall properties	• Not compatible with the form of equations solved in CFD models • Statistical errors can arise; no guarantee of convergence
The Discrete Transfer Method		
Applies features of the above three methods: • Divides space into volume and surface elements • Divides the radiation into angular regions • Tracks individual beams	• Handles non-homogeneous gases • Easy to apply • Adapts to complex geometries • If applied with CFD models the models can share common volume and surface elements	• Less accurate than the Zone method unless large numbers of elements are applied.

Of all the methods, the Zone Method may be considered as the ideal practical engineering method. The Zone Method presents publishable and applicable results; results that serve as benchmarks for other methods of modeling radiative heat transfer in furnaces. It is a method that can be computed by hand and a technique that has been well validated and tested time and time again. It is a method that does not require complex solution techniques and is one that can be undertaken and understood straightforwardly by students. Since it is the purpose of the author to introduce the nature of industrial heating processes to engineering students, a pencil-and-paper calculation of radiative exchange within a combustion enclosure would be helpful in understanding the dominant mode of thermal phenomena in an industrial furnace. Hence, the Zone Method is analyzed in more detail in the next section of this chapter.

4.3 The Zone Method

With the advancement of technology and new techniques, including the development of recuperative and regenerative burners and the installation of improved low thermal mass refractory linings, the energy consumption of industrial furnaces has been reduced significantly. The improvement of furnace control and operation still exists, however, and is for the most part achieved through the development of accurate and realistic mathematical models of heating processes. As mentioned before, the primary mode of heat transfer within a furnace is by direct radiation from the flame and combustion products, as well as by radiation exchange between the hot refractory lining. In order to accurately predict the furnace performance, it is vital to accurately find the radiative

interchange between these surfaces (Jenkins et al., 2008).

The Zone Method is deployed in order to achieve an accurate performance prediction of the scaled down industrial furnace in question. The Zone Method is also known as Hottel's Zone Method and is the most widely used method for calculating radiation heat transfer in combustion enclosures. The Zone Method was first developed by Hottel & Cohen (1958) for an absorbing-emitting and non-scattering gray gas with constant absorption coefficients. Hottel & Sarofim (1967), Nelson et al. (1986), Noble (1975), and Smith et al. (1985) extended it to deal with non-constant and non-gray absorption coefficients as well as isotropically scattering media. This method consists of subdividing an enclosure into a finite number of isothermal volume and surface area elemental zones. Each elemental zone is assumed to have an even distribution of temperature as well as uniform radiative properties (Mishra and Prasad, 1998). The governing equations to be solved are energy balances. An overall energy balance is written for each zone taking into account all the radiation arriving at that zone from all other zones and leaving that zone to all other zones within the furnace enclosure (Rhine and Tucker, 1991). Assuming the absence of free and forced convection within the enclosed surface system, an example steady-state net heat energy balance for such a surface zone is depicted in Equation (22).

$$\begin{matrix}\text{Accumulation of} \\ \text{Energy in Zone}\end{matrix} = \begin{matrix}\text{Rate of Energy} \\ \text{Arriving at Zone}\end{matrix} - \begin{matrix}\text{Rate of Energy} \\ \text{Leaving Zone}\end{matrix} \tag{22}$$

Thermal radiation travels in straight lines, hence one given surface cannot receive

radiation from another surface unless they can "see" one another as illustrated in Figure 4.10(a). Aside from direct thermal radiation exchange, transfer can also occur through partial reflection from one surface to another as shown in Figure 4.10(b).

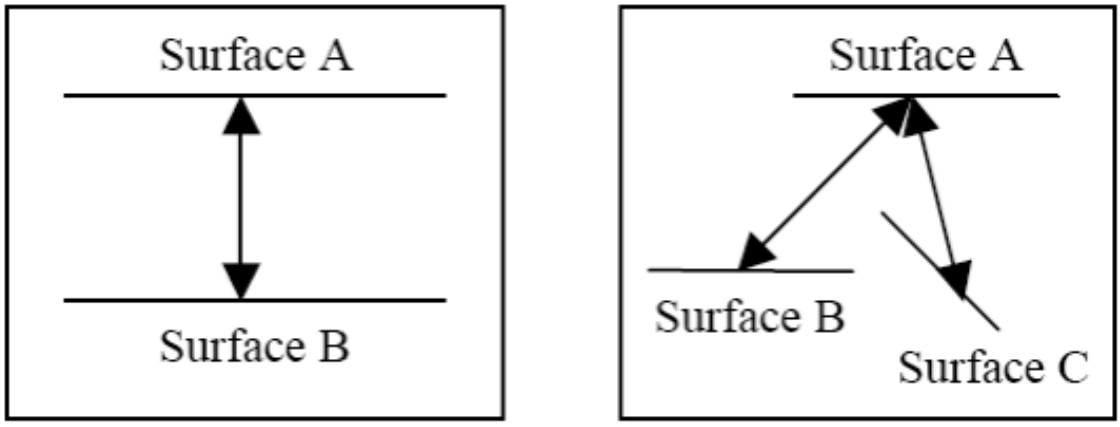

(a) (b)

Figure 4.10: (a)Direct radiation exchange since the surfaces can see one another; (b)Indirect radiation exchange due to partial reflection from a third surface (Jenkins et al., 2008).

One must note that the reflection of radiation occurs indiscriminately in all directions and is diffuse in nature. That is to say, not all the radiation leaving Surface A will arrive at Surface B. In fact, the combustion gases that have accumulated within an enclosure usually absorb some of the radiation that leaves one surface and does not reach another.

Grey surfaces partially reflect and partially absorb thermal radiation, which in turn complicates the calculation of radiation exchange between surfaces; much more so than the thermal radiation exchange between black body (complete absorption) surfaces. Hence, the total heat flux leaving a surface must be taken into account when calculating the radiation exchange of an enclosure. The total heat flux leaving any given surface is

known as radiosity and includes both emitted and reflected radiative energy as illustrated in Figure 4.11.

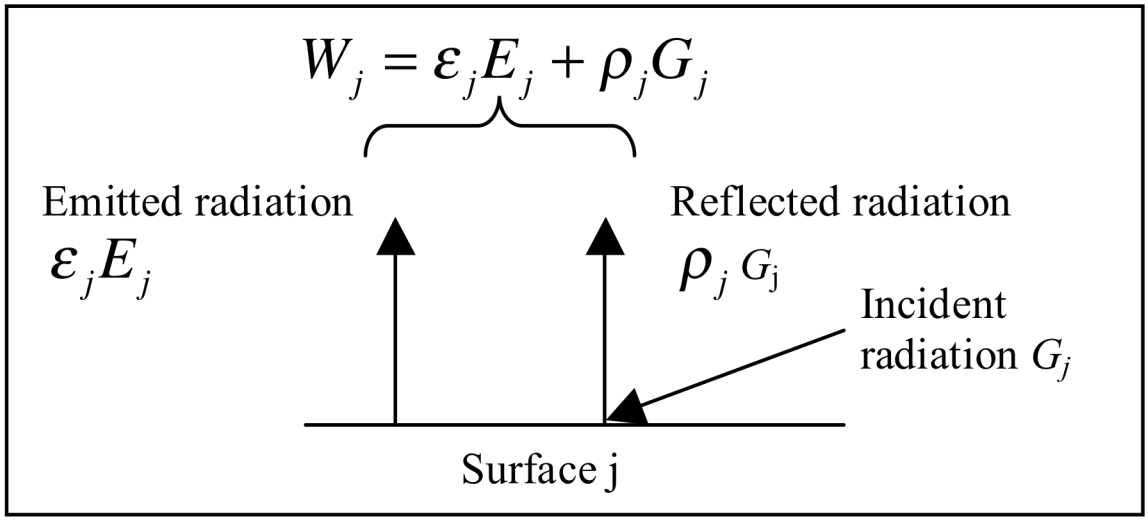

Figure 4.11: Energy Flux (Radiosity) at a Grey Surface (Jenkins et al., 2008)

Figure 4.11 depicts a grey surface, *j,* within an enclosure. The radiosity, W_j, can be expressed as Equation (23).

$$W_j = \varepsilon_j E_j + \rho_j G_j \tag{23}$$

The incident radiation from other surfaces within the enclosure is partially reflected, thus the reflected energy flux is $\rho_i G_i$ where G_j and ρ_j are the incident radiant flux density (irradiation of surface *j*) and reflectance, respectively. Radiation is also emitted at a rate per unit area of $\varepsilon_j E_j$, which is equivalent to $\varepsilon_j \sigma T_j^4$, where T is the temperature of surface *j* (Jenkins et al., 2008).

Assuming the absence of free and forced convection within the enclosed surface system,

the energy balance on any given surface yields an integral equation as seen in Equation (24) and given by Brus and Szmyd (2008). Upon further investigation, one will notice that this equation follows the worded version of Equation (22).

$$\underbrace{\int_{A_i} q_i \, dA_i}_{\substack{\text{Accumulation of Energy} \\ \text{in Zone Surface}}} = \underbrace{\int_{A_i} dA_i \int_{\lambda=0}^{\infty} \varepsilon_{\lambda i} E_{\lambda i} \, d\lambda}_{\substack{\text{Rate of Energy} \\ \text{Arriving at Zone Surface}}} - \underbrace{\int_{A_i} dA_i \int_{A_j} \int_{\lambda=0}^{\infty} \left[\frac{\left(W_{\lambda j} \cos\theta_{ij} \cos\theta_{ji} \varepsilon_{\lambda j} \right)}{\left(\pi r_{ij}^2 \right)} \right] dA_j \, d\lambda}_{\substack{\text{Rate of Energy} \\ \text{Leaving Zone Surface}}} \qquad (24)$$

In Equation (24), dA_i is the area of the free surface element; θ_{ij} is the angle between r_{ij} and the normal to dA_i; and W, λ, E, ε and q are the leaving flux density (radiosity), wavelength, black-body flux density, emissivity and heat flux, respectively. This equation specifies an energy balance on surface A_i and contains various terms such as the absorption of incidental radiation from all other surface elements, emission by surface A_i and the heat flux extracted through surface A_i (Brus and Szmyd, 2008).

Again, taking into consideration an enclosure with grey walls varying in temperature in any manner and of any shape, Equation (24) is written based on the Hottel Zone Method (Hottel and Sarofim, 1968).

$$A_i q_i = A_i \varepsilon_i E_i - \sum_{j=1}^{n} \overline{S_j S_i} E_j \qquad (i = 1, \ \ldots \ , m) \qquad (25)$$

In Equation (25), $E_i = \sigma T^4$ where E_i is the black-body flux density, T is temperature, σ is the Stefan-Boltzmann constant ($\sigma = 5.6667 \times 10^{-8}$ [$Wm^{-2}K^{-4}$]), ε_i is the emissivity of the i^{th} surface, and $\overline{S_j S_i}$ is the total interchange area between surface zones s_i and s_j. The total

interchange area between surface zones s_i and s_j is found using Equation (26).

$$\overline{S_j S_i} = \left(A_j \varepsilon_j / \rho_j\right)\left({}_{si}W_j - \delta_{ij}\varepsilon_i\right) \tag{26}$$

where

$${}_{si}W_j = \left(A_i \varepsilon_i / \rho_i\right)\left(-{}_{si}D_j / D\right) \tag{27}$$

From Equation (26) and Equation (27), ${}_{si}D_j$ represents the cofactor of the matrix $\left[\overline{s_i s_j} - \delta_{ij}\left(A_i / \rho_i\right)\right]$, δ_{ij} is the Kronecker delta (that is, $\delta_{ij} = 1$ for $i = j$ and $\delta_{ij} = 0$ for $i \neq j$) and D is the determinant of matrix $\left[\overline{s_i s_j} - \delta_{ij}\left(A_i / \rho_i\right)\right]$. The direct irradiation interchange area $\overline{s_i s_j}$ between the surface zones s_i and s_j may be evaluated by integration of Equation (28).

$$\overline{s_i s_j} = \int_{A_i}\int_{A_j}\left[\frac{\cos\theta_{ij}\cos\theta_{ji}}{\pi r_{ij}^2}\right] dA_i dA_j \tag{28}$$

From Equation (28), $\overline{s_i s_j} = F_{ij}A_i$, where F_{ij} is the configuration view factor or fraction of the energy emitted by surface i and absorbed by surface j while A_i represents the area of the i^{th} surface. For enclosed systems that contain transparent gases, the following relations must be satisfied:

$$\overline{\mathrm{s}_i s_j} = \overline{\mathrm{s}_j s_i}$$

or

$$\mathbb{F}_{ij} A_i = \mathbb{F}_{ji} A_j$$

and

$$\sum_j \overline{\mathrm{s}_i s_j} = A_i, \quad \sum_j \overline{S_i S_j} = \varepsilon_i A_i$$

The preceding equations and technical information of this section was acquired from Hottel and Sarofim (1968) with the help of Brus and Szmyd (2008) and Jenkins et al. (2008). With the governing equations pertaining to Hottel's Zone Method presented, one will now backtrack and discuss further the development of these abovementioned equations in more detail as outlined by the work performed by Siegel and Howell (1992), Wielbelt (1966) and McAdams (1954).

4.3.1 Enclosure Analysis by Use of First Principles

Starting from first and practical principles, the terminology $q_{1\to 2}$ and $q_{1\rightleftharpoons 2}$ are needed for Hottel's Zone Method. The symbol $q_{1\to 2}$ represents the total energy flow from surface element 1 that is absorbed by surface element 2. On the other hand, the symbol $q_{1\rightleftharpoons 2}$ represents the total energy exchanged between surface elements 1 and 2. The symbol $q_{1\rightleftharpoons 2}$ is defined by Equation (29). The relationship between the net heat transfer from surface element 1 (q_{net_1}) and the term that represents the total energy exchanged between

surface elements 1 and i ($q_{1\rightleftharpoons i}$) in an n surface enclosure is given by Equation (30).

$$q_{1\rightleftharpoons 2} = q_{2\rightarrow 1} - q_{1\rightarrow 2} \tag{29}$$

$$q_{net_1} = \sum_{i=1}^{n} q_{i\rightleftharpoons 1} \tag{30}$$

From the energy quantities presented above, another definition is introduced as Equation (31) where $\mathbb{F}_{12}$ is the total view factor or the energy emitted by surface element 1 and absorbed by surface element 2. Symbol A_1 is the surface area of element 1 while symbol E_1 represents the black-body flux density and is calculated using $E_1 = \sigma T_1^4$ where T_1 is the surface temperature of element 1 and σ is the Stefan-Boltzmann constant (σ = 5.6667 × 10^{-8} [$Wm^{-2}K^{-4}$]).

$$q_{1\rightarrow 2} = \mathbb{F}_{12} A_1 E_1 \tag{31}$$

The fraction of the energy emitted by surface element 1 and absorbed by surface element 2 ($\mathbb{F}_{12}$), is dependant on the geometry of all the surfaces that make up the enclosure as well as their emissivities of all these surfaces. For gray surfaces, the emissivity and absorptivity are equal; that is to say, $\varepsilon = \alpha$ is assumed to be present. The Hottel Zone Method depends on the development and/or proof of the following three statements:

1. Determination of $\mathbb{F}_{ij}$
2. $\mathbb{F}_{ij}A_i = \mathbb{F}_{ji}A_j$
3. $\sum_{j=1}^{n} \mathbb{F}_{ij} = \varepsilon_i$

Statement number one, the determination of $\mathbb{F}_{ij}$, is found in the following manner: An enclosure with n surfaces with known surface temperatures T_n and known surface emissivities ε_n is taken into account. If any of the surfaces are reradiating or well insulated, the emittance of the surface(s) may be assumed to be zero and its temperature does not have to be known. For the development of a calculation operation, all the surfaces in the enclosure are assumed to have a temperature of absolute zero except for surface number 1 - $\mathbb{F}_{1j}$ is to be evaluated. This assumption indicates that all the energy received by an elemental surface j within the enclosure is derived from surface 1. Moreover, the energy absorbed by the elemental surface j is calculated using Equation (32) where G_j is the irradiation of surface j (also known as, and previously reported in this paper as, the direct irradiation interchange area $\overline{s_i s_j}$ between the surface zones i and j); W_j is the leaving flux density or radiosity of surface j; and A_j is the area of surface j.

$$q_{net_j} = q_{1\to j} = \left(G_j - W_j\right)A_j \tag{32}$$

Since the j^{th} surface is assumed to have a temperature of absolute zero, the following statement is derived from Equation (23).

$$\rho_j G_j = W_j \tag{33}$$

Equation (33) is only valid if surface *j* does not emit any energy. In the development of the term $\mathbb{F}_{ij}$, Hottel defines the radiosity encountered in an enclosure as the *energy leaving a surface as a result of the energy emitted by surface 1* as depicted in Figure 4.11. In other words, the energy due to radiosity reflecting in an enclosure is due to an original emission from surface 1. Thus, the total outgoing energy from surface 1 is $(E_1 + W_1)$. With the definitions given by Equation (34) and Equation (35), the irradiation *G* of any given surface is given by Equation (36).

$$q_{ij} = F_{ij} A_i E_i = \left(G_j - W_j\right) A_j \tag{34}$$

For the total outgoing energy from surface 1, $(E_1 + W_1)$. Thus,

$$q_{1j} = F_{1j} A_1 \left(E_1 + W_1\right) = \left(G_j - W_j\right) A_j \tag{35}$$

$$G_j A_j = \left(E_1 + W_1\right) F_{11} A_1 + W_2 F_{21} A_2 + W_3 F_{31} A_3 + \ldots + W_n F_{n1} A_n \tag{36}$$

For *n* surfaces the following equations can be written.

$$\begin{array}{rcl}
\rho_1\left[\left(E_1 + W_1\right) F_{11} A_1 + W_2 F_{21} A_2 + \ldots + W_n F_{n1} A_n\right] & = & A_1 W_1 \\
\rho_2\left[\left(E_1 + W_1\right) F_{12} A_1 + W_2 F_{22} A_2 + \ldots + W_n F_{n2} A_n\right] & = & A_2 W_2 \\
\vdots \qquad\qquad \vdots \qquad\qquad\qquad \vdots \qquad\qquad\qquad \vdots & & \vdots \\
\rho_n\left[\left(E_1 + W_1\right) F_{1n} A_1 + W_2 F_{2n} A_2 + \ldots + W_n F_{nn} A_n\right] & = & A_n W_n
\end{array} \tag{37}$$

The terms presented in Equation (37) can be rewritten as a more convenient augmented

matrix by using the definition $F_{ij}A_i = G_{ij}$.

$$\begin{matrix}[& W_1 & & W_2 & & W_3 & \cdots & W_n &][& \text{Constant} &]\end{matrix}$$

$$\begin{bmatrix} G_{11}-(A_1/\rho_1) & G_{21} & G_{31} & \cdots & G_{n1} \\ G_{12} & G_{22}-(A_2/\rho_2) & G_{32} & \cdots & G_{n2} \\ G_{13} & G_{23} & G_{33}-(A_3/\rho_3) & \cdots & G_{n3} \\ \vdots & \vdots & \vdots & \ddots & \vdots \\ G_{1n} & G_{2n} & G_{3n} & \cdots & G_{nn}-(A_n/\rho_n) \end{bmatrix} \begin{bmatrix} -G_{11}\varepsilon_1 E_1 \\ -G_{12}\varepsilon_1 E_1 \\ -G_{13}\varepsilon_1 E_1 \\ \vdots \\ -G_{1n}\varepsilon_1 E_1 \end{bmatrix} \quad (38)$$

Equation (38) represents n equations and is solved by using a coefficient determinant D and the determinant ${}_{s1}D_n$ where the coefficient determinant is found using Equation (39). The determinant ${}_{s1}D_n$ is solved using Cramer's Rule; that is to say, the n^{th} column is replaced by the constant column given in Equation (38).

$$D = \begin{vmatrix} G_{11}-(A_1/\rho_1) & G_{21} & \cdots & G_{n1} \\ G_{12} & G_{22}-(A_2/\rho_2) & \cdots & G_{2n} \\ \vdots & \vdots & \ddots & \vdots \\ G_{1n} & G_{1n} & \cdots & G_{nn}-(A_n/\rho_n) \end{vmatrix} \quad (39)$$

The radiosity is calculated using $W_n = -\,{}_{s1}D_n / D$, or as Hottel writes it, ${}_{s1}W_n = -\,{}_{s1}D_n / D$, where the subscript before W_n indicates that W_n is from energy that is emitted from source 1. Using Equations (32) and (33) allows us to derive the following equation:

$$q_{1\to j} = \left({}_{s1}W_j / \rho_j - {}_{s1}W_j\right)A_j \quad (40)$$

Equation (40) is rewritten in terms of Hottel's notation and represented by Equation (41).

$$q_{1\to j} = \frac{\alpha_j A_j {}_{s1}W_j}{\rho_j} \tag{41}$$

Using the expression ${}_{s1}W_n = -{}_{s1}D_n / D$ in Equation (41) results in the term expressed in this report as Equation (42).

$$q_{1\to j} = \frac{\alpha_j}{\rho_j} A_j \left(-\frac{{}_{s1}D_j}{D} \right) \tag{42}$$

or

$$\mathbb{F}_{1j} A_1 E_1 = \frac{\alpha_j A_j}{\rho_j} \left(-\frac{{}_{s1}D_j}{D} \right)$$

rearranging,

$$\mathbb{F}_{1j} A_1 = \frac{\alpha_j A_j}{\rho_j E_1} \left(-\frac{{}_{s1}D_j}{D} \right) \tag{43}$$

One will note that the constant column of the determinant matrix, Equation (38), has $\varepsilon_1 E_1$ in every element. This term can be factored out of the determinant. If the symbol ${}_{s1}D_j'$ is used for the determinant with the $\varepsilon_1 E_1$ term removed, then the following can be used: ${}_{s1}D_j = \varepsilon_1 E_1 {}_{s1}D_j'$. The incorporation of this term into Equation (43) results in the following expression denoted as Equation (44) and the first requirement of Hottel's Zone Method from the three abovementioned statements.

$$\mathbb{F}_{1j} = \frac{\alpha_j \varepsilon_1 A_j}{\rho_j A_1}\left(-\frac{{}_{s1}D_j^{'}}{D}\right) \tag{44}$$

In this form, Equation (44) has the advantage of not depending on the temperature of elemental surface area 1. In the simplification of the determinant of the form ${}_{si}D_j'$, the following can be seen. Let the determinant matrix from surface 1 to surface 3 ${}_{s1}D_3'$ be evaluated and simplified using the minor of the element technique of determinant matrices in the manner shown in Equation (45). Through this simplification, one concludes what is typical of any determinant matrix: an n^2 determinant becomes an $(n-1)^2$ determinant.

$$ {}_{s1}D_3^{'} = \begin{vmatrix} G_{11}-\frac{A_1}{\rho_1} & G_{21} & G_{11} \\ G_{12} & G_{22}-\frac{A_2}{\rho_2} & G_{12} \\ G_{13} & G_{23} & G_{13} \end{vmatrix} = \begin{vmatrix} G_{11} & G_{21} & G_{11} \\ G_{12} & G_{22}-\frac{A_2}{\rho_2} & G_{12} \\ G_{13} & G_{23} & G_{13} \end{vmatrix} + \begin{vmatrix} -\frac{A_1}{\rho_1} & G_{21} & G_{11} \\ 0 & G_{22}-\frac{A_2}{\rho_2} & G_{12} \\ 0 & G_{23} & G_{13} \end{vmatrix}$$

$$ {}_{s1}D_3^{'} = -\frac{A_1}{\rho_1}\begin{vmatrix} G_{21}-\frac{A_2}{\rho_2} & G_{12} \\ G_{23} & G_{13} \end{vmatrix} \tag{45}$$

If we take the reciprocal of this determinant from surface 3 to surface 1, the determinant matrix ${}_{s3}D_1'$ can be written in the manner expressed as Equation (46):

$$ {}_{s3}D_1^{'} = \begin{vmatrix} G_{31} & G_{21} & G_{31} \\ G_{32} & G_{22}-\frac{A_2}{\rho_2} & G_{32} \\ G_{33} & G_{23} & G_{33}-\frac{A_3}{\rho_3} \end{vmatrix} = \begin{vmatrix} G_{31} & G_{21} & G_{31} \\ G_{32} & G_{22}-\frac{A_2}{\rho_2} & G_{32} \\ G_{33} & G_{23} & G_{33} \end{vmatrix} + \begin{vmatrix} G_{31} & G_{21} & 0 \\ G_{32} & G_{22}-\frac{A_2}{\rho_2} & 0 \\ G_{33} & G_{23} & -\frac{A_3}{\rho_3} \end{vmatrix} $$

$$ {}_{s3}D_1^{'} = -\frac{A_3}{\rho_3}\begin{bmatrix} G_{31} & G_{21} \\ G_{32} & G_{22}-\frac{A_2}{\rho_2} \end{bmatrix} \tag{46} $$

The skew symmetry between Equation (45) and Equation (46) shows the relation $\left(\rho_{3\ s3}D_1^{'}\right)/A_3 = \left(\rho_{1\ s1}D_3^{'}\right)/A_1$ and although this relation does not prove the following, the skew symmetry of all ${}_{si}D_j$' determinants results in the subsequent expression.

$$ \frac{\left(\rho_{i\ si}D_j^{'}\right)}{A_i} = \frac{\left(\rho_{j\ sj}D_i^{'}\right)}{A_j} \tag{47} $$

Using Equation (47) in conjunction with Equation (44) results in Equation (48).

$$ \mathbb{F}_{ij}A_i\alpha_i\varepsilon_j = \mathbb{F}_{ji}A_j\alpha_j\varepsilon_i \tag{48} $$

Since the assumption for a gray surface holds ($\varepsilon = \alpha$) Equation (48) reduces to the second requirement of the three statements from above denoted here as Equation (49).

$$ \mathbb{F}_{ij}A_i = \mathbb{F}_{ji}A_j \tag{49} $$

The third and final requirement of Hottel's Zone Method is to prove the following

expression.

$$\sum_{j=1}^{n} \mathbb{F}_{ij} = \varepsilon_i$$

The third requirement of the Zone Method is proven by taking into account the meaning of the term $q_{i\to j}$. As previously mentioned, $q_{i\to j}$ represents the energy leaving surface *i* and absorbed by surface *j*. The sum of all the energy flows is written as:

$$\sum_{j=1}^{n} q_{i\to j}$$

The summation for all the surfaces in an enclosure must equal all of the energy emitted by elemental surface area *i* as described by Equation (50).

$$\sum_{j=1}^{n} q_{i\to j} = \varepsilon_i A_i E_i \tag{50}$$

The combination of Equation (31) and Equation (50) results in the proof of the third requirement of the Zone Method statements expressed in this chapter by Equation (51).

$$\sum_{j=1}^{n} \mathbb{F}_{ij} = \varepsilon_i \tag{51}$$

4.3.2 Enclosure Analysis by Use of Total View Factors, $\mathbb{F}$

Siegel and Howell (1992) present an in-depth analysis of various computational techniques used to solve the governing equations produced by Hottel's Zone Method.

The more common method is the enclosure analysis through the use of the total view factors, $\mathbb{F}$. The total view factors are defined by stating that q has the form of Equation (52).

$$q_{ij} = A_i \sum_{j=1}^{n} \mathbb{F}_{ij} \sigma \left(T_i^4 - T_j^4 \right) \qquad (1 \le i \le n) \tag{52}$$

In comparison to previously derived equations, Siegel and Howell (1992) denote that

$$\mathbb{F}_{ij} = \varepsilon_i G_{ij} \tag{53}$$

The total view factor can obviously be calculated by first obtaining the irradiance term G. With the aid of Equations (49) and (51), an equivalent approach of solving the total view factors is to let $\sigma T_n^4 = 1$ for the n^{th} surface and $T = 0$ for all other surfaces. By doing this, Equation (52) yields Equations (54) and (55).

$$\mathbb{F}_{in} = -q_i \tag{54}$$

$$\mathbb{F}_{nn} = -q_n + \varepsilon_n \tag{55}$$

An expression representing a system of equations relating surface heating q and surface temperature T was developed by Siegel and Howell (1992) and identified in this thesis as Equation (56).

$$\sum_{j=1}^{n} \left(\frac{\delta_{ij}}{\varepsilon_j} - F_{ij} \frac{1 - \varepsilon_j}{\varepsilon_j} \right) \frac{q_j}{A_j} = \sum_{j=1}^{n} \left(\delta_{ij} - F_{ij} \right) \sigma T_j^4 = \sum_{j=1}^{n} F_{ij} \sigma \left(T_i^4 - T_j^4 \right) \tag{56}$$

By letting $\sigma T_n^4 = 1$ for the n^{th} surface and $T = 0$ for all other surfaces, Equation (56) yields Equations (57) and (58).

$$\sum_{j=1}^{n}\left(\frac{\delta_{ij}}{\varepsilon_j} - F_{ij}\frac{1-\varepsilon_j}{\varepsilon_j}\right)q_j = -F_{in} \qquad (i \neq n) \tag{57}$$

$$\sum_{j=1}^{n}\left(\frac{\delta_{nj}}{\varepsilon_j} - F_{nj}\frac{1-\varepsilon_j}{\varepsilon_j}\right)q_j = 1 - F_{nn} \tag{58}$$

If Equations (57) and (58) are solved for q, these are a function of the surface view factors F and emissivities ε. The total view factors are found from q by using Equations (54) and (55). Hence, the total view factors of an enclosure are found from F and ε and are not dependent on surface temperatures.

The coefficient matrix ∂ for the set of expressions represented by Equations (57) and (58) is denoted here as Equation (59).

$$\partial = \begin{bmatrix} \frac{1}{\varepsilon_1} & -\rho_2\frac{F_{12}}{\varepsilon_2} & -\rho_3\frac{F_{13}}{\varepsilon_3} & \cdots & -\rho_n\frac{F_{1n}}{\varepsilon_n} \\ -\rho_1\frac{F_{21}}{\varepsilon_1} & \frac{1}{\varepsilon_2} & -\rho_3\frac{F_{23}}{\varepsilon_3} & \cdots & -\rho_n\frac{F_{2n}}{\varepsilon_n} \\ -\rho_1\frac{F_{31}}{\varepsilon_1} & -\rho_2\frac{F_{32}}{\varepsilon_2} & \frac{1}{\varepsilon_3} & \cdots & -\rho_n\frac{F_{3n}}{\varepsilon_n} \\ \vdots & \vdots & \vdots & \ddots & \vdots \\ -\rho_1\frac{F_{n1}}{\varepsilon_1} & -\rho_2\frac{F_{n2}}{\varepsilon_2} & -\rho_3\frac{F_{n3}}{\varepsilon_3} & \cdots & \frac{1}{\varepsilon_n} \end{bmatrix} \tag{59}$$

The matrix for the right side coefficients of Equations (57) and (58) to determine $-q$ is expressed as Equation (60).

$$M = \begin{bmatrix} -1 & F_{12} & F_{13} & \cdots & F_{1n} \\ F_{21} & -1 & F_{23} & \cdots & F_{2n} \\ F_{31} & F_{32} & -1 & \cdots & F_{3n} \\ \vdots & \vdots & \vdots & \ddots & \vdots \\ F_{n1} & F_{n2} & F_{n3} & \cdots & -1 \end{bmatrix} \tag{60}$$

In order to relate the –q and $\mathbb{F}$ from Equations (54) and (55), and emissivity matrix is required as denoted by Equation (61).

$$\varepsilon = \begin{bmatrix} \varepsilon_1 & 0 & 0 & \cdots & 0 \\ 0 & \varepsilon_2 & 0 & \cdots & 0 \\ 0 & 0 & \varepsilon_3 & \cdots & 0 \\ \vdots & \vdots & \vdots & \ddots & \vdots \\ 0 & 0 & 0 & \cdots & \varepsilon_n \end{bmatrix} \tag{61}$$

Then according to Equations (54) and (55), the total view factors are obtained from the matrix operations as represented by Equation (62).

$$\mathbb{F} = \partial^{-1} M + \varepsilon \tag{62}$$

With the total view factors calculated, the transfer of heat q from one surface to another is computed using Equation (52).

With the definitions and proofs of all the required equations complete, one can now proceed with a practical mathematical example that incorporates Hottel's Zone Method

and its algebraic expressions. The following section outlines a detailed solution guide and worked out problem of radiation exchange within a grey furnace enclosure using both the first principles method and total view factors method.

4.4 Furnace Modeling Via Zoning

As an example of the use of Hottel's Zone Method, consider the enclosing geometry of the current furnace system. However, due to its flameless combustion nature and uniform temperature distribution, it is very difficult, if not impossible, to accurately and precisely simulate the radiation exchange of the existing furnace. Hence, in the interest of this project, rather than comparing calculated results to experimental results obtained from the current furnace system, a thorough step-by-step calculation of the radiation exchange within a furnace enclosure is performed and compared to published results. The enclosure in question is geometrically and dimensionally similar to the current furnace system and was used by Clark and Korybalski (1974) in their methods of radiation calculations.

The furnace enclosure, as seen in Figure 4.12, is a fourteen-surface grey enclosure and consists of the following dimensions:

- 1.0 ft or 0.3048 m in the x - direction
- 1.0 ft or 0.3048 m in the y - direction
- 2.0 ft or 0.6096 m in the z – direction

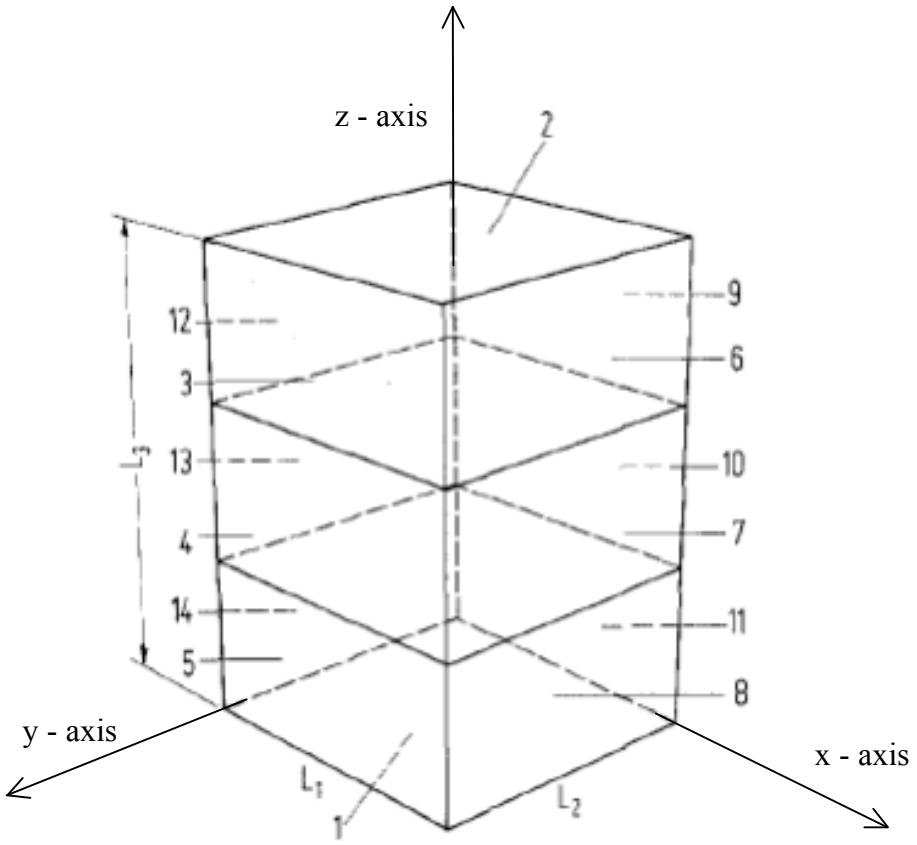

Figure 4.12: Fourteen-Surface Grey Furnace Enclosure (Clark and Korybalski, 1974)

From Figure 4.12, elemental surface zone 1 is the floor or load of the furnace enclosure while surface zone 2 is its roof. Zonal elements 1 and 2 both have surface areas of 1.0 ft^2 (0.0929 m^2). Elemental zones 3 through 14 are identically sized furnace sidewalls with surface areas of 0.667 ft^2 (0.0619 m^2) each. The surface temperatures as well as their emissivities (ε) and corresponding reflectances $(\rho = 1 - \varepsilon)$ are specified and reported in Table 4.3.

Table 4.3: Properties of 14-Surface Grey Furnace Enclosure

$T_1 = 833$ K		$A_1 = 0.0929$ m^2
$T_2 = 333$ K		$A_2 = 0.0929$ m^2
$T_3 - T_{14} = 444$ K		$A_3 - A_{14} = 0.0619$ m^2
$\varepsilon_1 - \varepsilon_{14} = 0.6500$		$\rho_1 - \rho_{14} = 0.3500$
$L_1 = 0.3048$ m	$L_2 = 0.3048$ m	$L_3 = 0.6096$ m

A detailed list of assumptions attributed to this model is given below.

- The furnace is divided into elemental surface zones.
- The temperature of each surface zone is constant.
- All the surfaces within the furnace enclosure are grey and diffuse, thus the surfaces emit and absorb all wavelengths of radiation equally in all directions.
- The surface emissivities and absorptivities are independent of temperature.
- The irradiation and radiosity are constant over each surface.
- The furnace operates under steady state conditions with no fluctuations in heat.

The numerical results obtained for the configuration factors or view factors were calculated using the equations provided by Wiebelt (1966) and Howell (2001) and displayed in Table 4.4.

Table 4.4: View Factor Values Obtained From Computation

F_{ij}	j = 1	2	3	4	5	6	7	8	9	10	11	12	13	14
i =1	0	0.069	0.016	0.047	0.170	0.016	0.047	0.170	0.016	0.047	0.170	0.016	0.047	0.170
2	0.069	0	0.170	0.047	0.016	0.170	0.047	0.016	0.170	0.047	0.016	0.170	0.047	0.016
3	0.024	0.255	0	0.000	0.000	0.171	0.048	0.009	0.148	0.089	0.028	0.171	0.048	0.009
4	0.070	0.070	0.000	0	0.000	0.048	0.171	0.048	0.089	0.148	0.089	0.048	0.171	0.048
5	0.255	0.024	0.000	0.000	0	0.009	0.048	0.171	0.028	0.089	0.148	0.009	0.048	0.171
6	0.024	0.255	0.171	0.048	0.009	0	0.000	0.000	0.171	0.048	0.009	0.148	0.089	0.028
7	0.070	0.070	0.048	0.171	0.048	0.000	0	0.000	0.048	0.171	0.048	0.089	0.148	0.089
8	0.255	0.024	0.009	0.048	0.171	0.000	0.000	0	0.009	0.048	0.171	0.028	0.089	0.148
9	0.024	0.255	0.148	0.089	0.028	0.171	0.048	0.009	0	0.000	0.000	0.171	0.048	0.009
10	0.070	0.070	0.089	0.148	0.089	0.048	0.171	0.048	0.000	0	0.000	0.048	0.171	0.048
11	0.255	0.024	0.028	0.089	0.148	0.009	0.048	0.171	0.000	0.000	0	0.009	0.048	0.171
12	0.024	0.255	0.171	0.048	0.009	0.148	0.089	0.028	0.171	0.048	0.009	0	0.000	0.000
13	0.070	0.070	0.048	0.171	0.048	0.089	0.148	0.089	0.048	0.171	0.048	0.000	0	0.000
14	0.255	0.024	0.009	0.048	0.171	0.028	0.089	0.148	0.009	0.048	0.171	0.000	0.000	0

With the above stated assumptions in mind, and using the properties stated in Table 4.3, one will now proceed with a step-by-step calculation of the radiation exchange within the 14-surface grey furnace enclosure depicted in Figure 4.12 using both the first principles method and total view factor method.

4.4.1 Furnace Zone Modeling using First Principles

With the view factor values of Table 4.4, the coefficient matrix *D* (below) is found to have a determinant value of 5.638×10^{-11}.

$$D = \begin{vmatrix}
-0.265 & 0.006 & 0.001 & 0.004 & 0.016 & 0.001 & 0.004 & 0.016 & 0.001 & 0.004 & 0.016 & 0.001 & 0.004 & 0.016 \\
0.0064 & -0.265 & 0.016 & 0.004 & 0.001 & 0.016 & 0.004 & 0.001 & 0.016 & 0.004 & 0.001 & 0.016 & 0.004 & 0.001 \\
0.0022 & 0.016 & -0.177 & 0.000 & 0.000 & 0.011 & 0.003 & 0.001 & 0.009 & 0.006 & 0.002 & 0.011 & 0.003 & 0.001 \\
0.0065 & 0.004 & 0.000 & -0.177 & 0.000 & 0.003 & 0.011 & 0.003 & 0.006 & 0.009 & 0.006 & 0.003 & 0.011 & 0.003 \\
0.0237 & 0.001 & 0.000 & 0.000 & -0.177 & 0.001 & 0.003 & 0.011 & 0.002 & 0.006 & 0.009 & 0.001 & 0.003 & 0.011 \\
0.0022 & 0.016 & 0.011 & 0.003 & 0.001 & -0.177 & 0.000 & 0.000 & 0.011 & 0.003 & 0.001 & 0.009 & 0.006 & 0.002 \\
0.0065 & 0.004 & 0.003 & 0.011 & 0.003 & 0.000 & -0.177 & 0.000 & 0.003 & 0.011 & 0.003 & 0.006 & 0.009 & 0.006 \\
0.0237 & 0.001 & 0.001 & 0.003 & 0.011 & 0.000 & 0.000 & -0.177 & 0.001 & 0.003 & 0.011 & 0.002 & 0.006 & 0.009 \\
0.0022 & 0.016 & 0.009 & 0.006 & 0.002 & 0.011 & 0.003 & 0.001 & -0.177 & 0.000 & 0.000 & 0.011 & 0.003 & 0.001 \\
0.0065 & 0.004 & 0.006 & 0.009 & 0.006 & 0.003 & 0.011 & 0.003 & 0.000 & -0.177 & 0.000 & 0.003 & 0.011 & 0.003 \\
0.0237 & 0.001 & 0.002 & 0.006 & 0.009 & 0.001 & 0.003 & 0.011 & 0.000 & 0.000 & -0.177 & 0.001 & 0.003 & 0.011 \\
0.0022 & 0.016 & 0.011 & 0.003 & 0.001 & 0.009 & 0.006 & 0.002 & 0.011 & 0.003 & 0.001 & -0.177 & 0.000 & 0.000 \\
0.0065 & 0.004 & 0.003 & 0.011 & 0.003 & 0.006 & 0.009 & 0.006 & 0.003 & 0.011 & 0.003 & 0.000 & -0.177 & 0.000 \\
0.0237 & 0.001 & 0.001 & 0.003 & 0.011 & 0.002 & 0.006 & 0.009 & 0.001 & 0.003 & 0.011 & 0.000 & 0.000 & -0.177
\end{vmatrix}$$

Following Wiebelt's (1966) method outlined in the previous section, using the constant column of the matrix in Equation (38) and implementing the term ${}_{s1}D_j=\varepsilon_1 E_{1s1} D_j'$ results in the matrix ${}_{s1}D_2'$ whose determinant value is -1.983×10^{-12}.

$$ {}_{s1}D_2' = \begin{vmatrix}
-0.2654 & 0.0000 & 0.0015 & 0.0043 & 0.0158 & 0.0015 & 0.0043 & 0.0158 & 0.0015 & 0.0043 & 0.0158 & 0.0015 & 0.0043 & 0.0158 \\
0.0064 & 0.0064 & 0.0158 & 0.0043 & 0.0015 & 0.0158 & 0.0043 & 0.0015 & 0.0158 & 0.0043 & 0.0015 & 0.0158 & 0.0043 & 0.0015 \\
0.0022 & 0.0015 & -0.1769 & 0.0000 & 0.0000 & 0.0106 & 0.0030 & 0.0006 & 0.0092 & 0.0055 & 0.0017 & 0.0106 & 0.0030 & 0.0006 \\
0.0065 & 0.0043 & 0.0000 & -0.1769 & 0.0000 & 0.0030 & 0.0106 & 0.0030 & 0.0055 & 0.0092 & 0.0055 & 0.0030 & 0.0106 & 0.0030 \\
0.0237 & 0.0158 & 0.0000 & 0.0000 & -0.1769 & 0.0006 & 0.0030 & 0.0106 & 0.0017 & 0.0055 & 0.0092 & 0.0006 & 0.0030 & 0.0106 \\
0.0022 & 0.0015 & 0.0106 & 0.0030 & 0.0006 & -0.1769 & 0.0000 & 0.0000 & 0.0106 & 0.0030 & 0.0006 & 0.0092 & 0.0055 & 0.0017 \\
0.0065 & 0.0043 & 0.0030 & 0.0106 & 0.0030 & 0.0000 & -0.1769 & 0.0000 & 0.0030 & 0.0106 & 0.0030 & 0.0055 & 0.0092 & 0.0055 \\
0.0237 & 0.0158 & 0.0006 & 0.0030 & 0.0106 & 0.0000 & 0.0000 & -0.1769 & 0.0006 & 0.0030 & 0.0106 & 0.0017 & 0.0055 & 0.0092 \\
0.0022 & 0.0015 & 0.0092 & 0.0055 & 0.0017 & 0.0106 & 0.0030 & 0.0006 & -0.1769 & 0.0000 & 0.0000 & 0.0106 & 0.0030 & 0.0006 \\
0.0065 & 0.0043 & 0.0055 & 0.0092 & 0.0055 & 0.0030 & 0.0106 & 0.0030 & 0.0000 & -0.1769 & 0.0000 & 0.0030 & 0.0106 & 0.0030 \\
0.0237 & 0.0158 & 0.0017 & 0.0055 & 0.0092 & 0.0006 & 0.0030 & 0.0106 & 0.0000 & 0.0000 & -0.1769 & 0.0006 & 0.0030 & 0.0106 \\
0.0022 & 0.0015 & 0.0106 & 0.0030 & 0.0006 & 0.0092 & 0.0055 & 0.0017 & 0.0106 & 0.0030 & 0.0006 & -0.1769 & 0.0000 & 0.0000 \\
0.0065 & 0.0043 & 0.0030 & 0.0106 & 0.0030 & 0.0055 & 0.0092 & 0.0055 & 0.0030 & 0.0106 & 0.0030 & 0.0000 & -0.1769 & 0.0000 \\
0.0237 & 0.0158 & 0.0006 & 0.0030 & 0.0106 & 0.0017 & 0.0055 & 0.0092 & 0.0006 & 0.0030 & 0.0106 & 0.0000 & 0.0000 & -0.1769
\end{vmatrix}$$

With these two determinant values and along with Equation (44), the total view factor $\mathbb{F}_{12}$ can be calculated as follows:

$$\mathbb{F}_{12} = \frac{\alpha_2 \varepsilon_1 A_2}{\rho_2 A_1}\left(-\frac{{}_{s1}D_2'}{D}\right) = \frac{(0.65)(0.65)(0.0929)}{(0.35)(0.0929)}\left(\frac{1.983\times10^{-12}}{5.638\times10^{-11}}\right) = 0.0424$$

In the same manner, all the total view factors originating from surface element 1, $\mathbb{F}_{1j}$, are

calculated as:

$$\mathbb{F}_{1,3} = 0.0158, \mathbb{F}_{1,4} = 0.0342, \mathbb{F}_{1,5} = 0.0926, \mathbb{F}_{1,6} = 0.0158, \mathbb{F}_{1,7} = 0.0342, \mathbb{F}_{1,8} = 0.0926,$$
$$\mathbb{F}_{1,9} = 0.0158, \mathbb{F}_{1,10} = 0.0342, \mathbb{F}_{1,11} = 0.0926, \mathbb{F}_{1,12} = 0.0158, \mathbb{F}_{1,13} = 0.0342, \text{ and } \mathbb{F}_{1,14} = 0.0926$$

Then, $\mathbb{F}_{1,1}$ is determined using Equation (51) as:

$$\mathbb{F}_{1,1} = \varepsilon_1 - \sum_{j=2}^{n} \mathbb{F}_{1,j} = 0.65 - 0.6127 = 0.0373$$

By reciprocity and the use of Equation (49), $\mathbb{F}_{1,2}A_1 = \mathbb{F}_{2,1}A_2$; thus

$$\mathbb{F}_{2,1} = 0.0424, \mathbb{F}_{3,1} = 0.0239, \mathbb{F}_{4,1} = 0.0508, \mathbb{F}_{5,1} = 0.1392, \mathbb{F}_{6,1} = 0.0239, \mathbb{F}_{7,1} = 0.0508,$$
$$\mathbb{F}_{8,1} =, 0.1392, \mathbb{F}_{9,1} = 0.0239, \mathbb{F}_{10,1} = 0.0508, \mathbb{F}_{11,1} = 0.1392, \mathbb{F}_{12,1} = 0.0239, \mathbb{F}_{13,1} = 0.0508,$$
$$\text{and } \mathbb{F}_{14,1} = 0.1392.$$

Continuing this process allows all of the total view factors to be calculated resulting in the values presented in Table 4.5. It is notice from this table that the sum of the total view factors for each surface is equal to its emissivity, thus proving Equation (51).

Table 4.5: Total View Factors Calculated Between Surfaces and their Sum

$\mathbb{F}_{ij}$	j = 1	2	3	4	5	6	7	8	9	10	11	12	13	14	$\sum_{j=1}^{n} \mathbb{F}_{ij}$
i =1	0.0373	0.0424	0.0158	0.0342	0.0926	0.0158	0.0342	0.0926	0.0158	0.0342	0.0926	0.0158	0.0342	0.0926	0.65
2	0.0424	0.0380	0.0926	0.0342	0.0158	0.0926	0.0342	0.0158	0.0926	0.0342	0.0158	0.0926	0.0342	0.0158	0.65
3	0.0239	0.1392	0.0269	0.0162	0.0087	0.0947	0.0343	0.0116	0.0854	0.0499	0.0184	0.0947	0.0343	0.0116	0.65
4	0.0508	0.0508	0.0162	0.0217	0.0162	0.0343	0.0890	0.0343	0.0499	0.0792	0.0499	0.0343	0.0890	0.0343	0.65
5	0.1392	0.0239	0.0087	0.0162	0.0269	0.0116	0.0343	0.0947	0.0184	0.0499	0.0854	0.0116	0.0343	0.0947	0.65
6	0.0239	0.1392	0.0947	0.0343	0.0116	0.0269	0.0162	0.0087	0.0947	0.0343	0.0116	0.0854	0.0499	0.0184	0.65
7	0.0508	0.0508	0.0343	0.0890	0.0343	0.0162	0.0217	0.0162	0.0343	0.0890	0.0343	0.0499	0.0792	0.0499	0.65
8	0.1392	0.0239	0.0116	0.0343	0.0947	0.0087	0.0162	0.0269	0.0116	0.0343	0.0947	0.0184	0.0499	0.0854	0.65
9	0.0239	0.1392	0.0854	0.0499	0.0184	0.0947	0.0343	0.0116	0.0269	0.0162	0.0087	0.0947	0.0343	0.0116	0.65
10	0.0508	0.0508	0.0499	0.0792	0.0499	0.0343	0.0890	0.0343	0.0162	0.0217	0.0162	0.0343	0.0890	0.0343	0.65
11	0.1392	0.0239	0.0184	0.0499	0.0854	0.0116	0.0343	0.0947	0.0087	0.0162	0.0269	0.0116	0.0343	0.0947	0.65
12	0.0239	0.1392	0.0947	0.0343	0.0116	0.0854	0.0499	0.0184	0.0947	0.0343	0.0116	0.0269	0.0162	0.0087	0.65
13	0.0508	0.0508	0.0343	0.0890	0.0343	0.0499	0.0792	0.0499	0.0343	0.0890	0.0343	0.0162	0.0217	0.0162	0.65
14	0.1392	0.0239	0.0116	0.0343	0.0947	0.0184	0.0499	0.0854	0.0116	0.0343	0.0947	0.0087	0.0162	0.0269	0.65

After solving the total view factors for all the surfaces, the net heat transfer for each source or sink surface is calculated using Equation (30) in conjunction with Equation (31) where E_1 represents the black-body flux density and is calculated using $E_1 = \sigma T_1^4$ where T_1 is the surface temperature of element 1 and σ is the Stefan-Boltzmann constant (σ = 5.6667×10^{-8} [$Wm^{-2}K^{-4}$]). In more practical terms,

$$q_{net_i} = q_{1 \rightleftharpoons i} + q_{2 \rightleftharpoons i} + ... + q_{13 \rightleftharpoons i} + q_{14 \rightleftharpoons i}$$
$$q_{net_i} = F_{i,1} A_i \left(E_i - E_1\right) + ... + F_{i,14} A_i \left(E_i - E_{14}\right)$$

As an example, the net heat transfer at surface 1 is calculated as follows:

$$q_{net_1} = q_{1 \rightleftharpoons 1} + q_{2 \rightleftharpoons 1} + q_{3 \rightleftharpoons 1} + ... + q_{12 \rightleftharpoons 1} + q_{13 \rightleftharpoons 1} + q_{14 \rightleftharpoons 1}$$

$$\begin{aligned} q_{net_1} &= F_{1,1} A_1 \left(E_1 - E_1\right) + F_{1,2} A_1 \left(E_1 - E_2\right) + ... + F_{1,14} A_1 \left(E_1 - E_{14}\right) \\ &= [(0.0373)(0.0929)(27284.14 - 27284.14)] + [(0.0424)(0.0929)(27284.14 - 696.80)] \\ &\quad + ... + [(0.0926)(0.0619)(27284.14 - 2202.23)] \\ &= 0 + 104.75 + ... + 215.69 \\ &= 1433.69 \text{ W} \end{aligned}$$

The radiative heat transfer between surfaces and more importantly, the net heat transfer of each elemental surface are summarized in Table 4.6. All the heat transfer in this table has been calculated in Watts and can be noticed that the majority of radiative heat exchange within the enclosure is to and from surface elements 1 and 2. In fact, due to their geometry and placement within the furnace chamber, surface zones 3 through 14 have no interaction with one another resulting in heat transfer rates of zero between themselves.

Table 4.6: Radiative Heat Transfer Between Surfaces and Net Radiative Heat Transfer of Each Surface in Watts (W)

q_{ij}	**j = 1**	**2**	**3**	**4**	**5**	**6**	**7**	**8**	**9**	**10**	**11**	**12**	**13**	**14**	$q_{net_i} = \sum_{i=1}^{n} q_{i \rightleftharpoons j}$
i =1	0	104.75	36.81	79.71	215.69	36.81	79.69	215.77	36.82	79.69	215.77	36.81	79.69	215.69	1433.69
2	-104.75	0	-12.95	-4.78	-2.21	-12.95	-4.78	-2.21	-12.95	-4.78	-2.21	-12.95	-4.78	-2.21	-184.51
3	-37.06	12.97	0	0	0	0	0	0	0	0	0	0	0	0	-24.09
4	-78.81	4.73	0	0	0	0	0	0	0	0	0	0	0	0	-74.08
5	-216.17	2.22	0	0	0	0	0	0	0	0	0	0	0	0	-213.94
6	-37.06	12.97	0	0	0	0	0	0	0	0	0	0	0	0	-24.09
7	-78.81	4.73	0	0	0	0	0	0	0	0	0	0	0	0	-74.08
8	-216.17	2.22	0	0	0	0	0	0	0	0	0	0	0	0	-213.94
9	-37.06	12.97	0	0	0	0	0	0	0	0	0	0	0	0	-24.09
10	-78.81	4.73	0	0	0	0	0	0	0	0	0	0	0	0	-74.08
11	-216.17	2.22	0	0	0	0	0	0	0	0	0	0	0	0	-213.94
12	-37.06	12.97	0	0	0	0	0	0	0	0	0	0	0	0	-24.09
13	-78.81	4.73	0	0	0	0	0	0	0	0	0	0	0	0	-74.08
14	-216.17	2.22	0	0	0	0	0	0	0	0	0	0	0	0	-213.94

4.4.2 Furnace Zone Modeling using Total View Factors

The solution will now be obtained using the total view factor method. The coefficient matrix ∂ for the set of Equations (57) and (58) has the following composition.

$$\partial = \begin{vmatrix}
1.538 & -0.037 & -0.009 & -0.025 & -0.092 & -0.009 & -0.025 & -0.092 & -0.009 & -0.025 & -0.092 & -0.009 & -0.025 & -0.092 \\
-0.037 & 1.538 & -0.092 & -0.025 & -0.009 & -0.092 & -0.025 & -0.009 & -0.092 & -0.025 & -0.009 & -0.092 & -0.025 & -0.009 \\
-0.013 & -0.137 & 1.538 & 0.000 & 0.000 & -0.092 & -0.026 & -0.005 & -0.080 & -0.048 & -0.015 & -0.092 & -0.026 & -0.005 \\
-0.038 & -0.038 & 0.000 & 1.538 & 0.000 & -0.026 & -0.092 & -0.026 & -0.048 & -0.080 & -0.048 & -0.026 & -0.092 & -0.026 \\
-0.137 & -0.013 & 0.000 & 0.000 & 1.538 & -0.005 & -0.026 & -0.092 & -0.015 & -0.048 & -0.080 & -0.005 & -0.026 & -0.092 \\
-0.013 & -0.137 & -0.092 & -0.026 & -0.005 & 1.538 & 0.000 & 0.000 & -0.092 & -0.026 & -0.005 & -0.080 & -0.048 & -0.015 \\
-0.038 & -0.038 & -0.026 & -0.092 & -0.026 & 0.000 & 1.538 & 0.000 & -0.026 & -0.092 & -0.026 & -0.048 & -0.080 & -0.048 \\
-0.137 & -0.013 & -0.005 & -0.026 & -0.092 & 0.000 & 0.000 & 1.538 & -0.005 & -0.026 & -0.092 & -0.015 & -0.048 & -0.080 \\
-0.013 & -0.137 & -0.080 & -0.048 & -0.015 & -0.092 & -0.026 & -0.005 & 1.538 & 0.000 & 0.000 & -0.092 & -0.026 & -0.005 \\
-0.038 & -0.038 & -0.048 & -0.080 & -0.048 & -0.026 & -0.092 & -0.026 & 0.000 & 1.538 & 0.000 & -0.026 & -0.092 & -0.026 \\
-0.137 & -0.013 & -0.015 & -0.048 & -0.080 & -0.005 & -0.026 & -0.092 & 0.000 & 0.000 & 1.538 & -0.005 & -0.026 & -0.092 \\
-0.013 & -0.137 & -0.092 & -0.026 & -0.005 & -0.080 & -0.048 & -0.015 & -0.092 & -0.026 & -0.005 & 1.538 & 0.000 & 0.000 \\
-0.038 & -0.038 & -0.026 & -0.092 & -0.026 & -0.048 & -0.080 & -0.048 & -0.026 & -0.092 & -0.026 & 0.000 & 1.538 & 0.000 \\
-0.137 & -0.013 & -0.005 & -0.026 & -0.092 & -0.015 & -0.048 & -0.080 & -0.005 & -0.026 & -0.092 & 0.000 & 0.000 & 1.538
\end{vmatrix}$$

The matrix M for the right side coefficients of Equations (57) and (58) to determine $-q$ is found to be the following.

$$M = \begin{vmatrix}
-1 & 0.069 & 0.016 & 0.047 & 0.170 & 0.016 & 0.047 & 0.170 & 0.016 & 0.047 & 0.170 & 0.016 & 0.047 & 0.170 \\
0.069 & -1 & 0.170 & 0.047 & 0.016 & 0.170 & 0.047 & 0.016 & 0.170 & 0.047 & 0.016 & 0.170 & 0.047 & 0.016 \\
0.024 & 0.255 & -1 & 0.000 & 0.000 & 0.171 & 0.048 & 0.009 & 0.148 & 0.089 & 0.028 & 0.171 & 0.048 & 0.009 \\
0.070 & 0.070 & 0.000 & -1 & 0.000 & 0.048 & 0.171 & 0.048 & 0.089 & 0.148 & 0.089 & 0.048 & 0.171 & 0.048 \\
0.255 & 0.024 & 0.000 & 0.000 & -1 & 0.009 & 0.048 & 0.171 & 0.028 & 0.089 & 0.148 & 0.009 & 0.048 & 0.171 \\
0.024 & 0.255 & 0.171 & 0.048 & 0.009 & -1 & 0.000 & 0.000 & 0.171 & 0.048 & 0.009 & 0.148 & 0.089 & 0.028 \\
0.070 & 0.070 & 0.048 & 0.171 & 0.048 & 0.000 & -1 & 0.000 & 0.048 & 0.171 & 0.048 & 0.089 & 0.148 & 0.089 \\
0.255 & 0.024 & 0.009 & 0.048 & 0.171 & 0.000 & 0.000 & -1 & 0.009 & 0.048 & 0.171 & 0.028 & 0.089 & 0.148 \\
0.024 & 0.255 & 0.148 & 0.089 & 0.028 & 0.171 & 0.048 & 0.009 & -1 & 0.000 & 0.000 & 0.171 & 0.048 & 0.009 \\
0.070 & 0.070 & 0.089 & 0.148 & 0.089 & 0.048 & 0.171 & 0.048 & 0.000 & -1 & 0.000 & 0.048 & 0.171 & 0.048 \\
0.255 & 0.024 & 0.028 & 0.089 & 0.148 & 0.009 & 0.048 & 0.171 & 0.000 & 0.000 & -1 & 0.009 & 0.048 & 0.171 \\
0.024 & 0.255 & 0.171 & 0.048 & 0.009 & 0.148 & 0.089 & 0.028 & 0.171 & 0.048 & 0.009 & -1 & 0.000 & 0.000 \\
0.070 & 0.070 & 0.048 & 0.171 & 0.048 & 0.089 & 0.148 & 0.089 & 0.048 & 0.171 & 0.048 & 0.000 & -1 & 0.000 \\
0.255 & 0.024 & 0.009 & 0.048 & 0.171 & 0.028 & 0.089 & 0.148 & 0.009 & 0.048 & 0.171 & 0.000 & 0.000 & -1
\end{vmatrix}$$

To relate $-q$ and $\mathbb{F}$ from Equations (54) and (55), the emissivity matrix ε has the following structure.

$$\varepsilon = \begin{vmatrix}
0.65 & 0 & 0 & 0 & 0 & 0 & 0 & 0 & 0 & 0 & 0 & 0 & 0 & 0 \\
0 & 0.65 & 0 & 0 & 0 & 0 & 0 & 0 & 0 & 0 & 0 & 0 & 0 & 0 \\
0 & 0 & 0.65 & 0 & 0 & 0 & 0 & 0 & 0 & 0 & 0 & 0 & 0 & 0 \\
0 & 0 & 0 & 0.65 & 0 & 0 & 0 & 0 & 0 & 0 & 0 & 0 & 0 & 0 \\
0 & 0 & 0 & 0 & 0.65 & 0 & 0 & 0 & 0 & 0 & 0 & 0 & 0 & 0 \\
0 & 0 & 0 & 0 & 0 & 0.65 & 0 & 0 & 0 & 0 & 0 & 0 & 0 & 0 \\
0 & 0 & 0 & 0 & 0 & 0 & 0.65 & 0 & 0 & 0 & 0 & 0 & 0 & 0 \\
0 & 0 & 0 & 0 & 0 & 0 & 0 & 0.65 & 0 & 0 & 0 & 0 & 0 & 0 \\
0 & 0 & 0 & 0 & 0 & 0 & 0 & 0 & 0.65 & 0 & 0 & 0 & 0 & 0 \\
0 & 0 & 0 & 0 & 0 & 0 & 0 & 0 & 0 & 0.65 & 0 & 0 & 0 & 0 \\
0 & 0 & 0 & 0 & 0 & 0 & 0 & 0 & 0 & 0 & 0.65 & 0 & 0 & 0 \\
0 & 0 & 0 & 0 & 0 & 0 & 0 & 0 & 0 & 0 & 0 & 0.65 & 0 & 0 \\
0 & 0 & 0 & 0 & 0 & 0 & 0 & 0 & 0 & 0 & 0 & 0 & 0.65 & 0 \\
0 & 0 & 0 & 0 & 0 & 0 & 0 & 0 & 0 & 0 & 0 & 0 & 0 & 0.65
\end{vmatrix}$$

Then according to Equations (54) and (55), the total view factors are obtained from the matrix operations displayed in Equation (62). This computation yields a matrix of total view factor values between the enclosing surfaces.

$\mathbb{F}$ =

0.0373	0.0424	0.0158	0.0342	0.0926	0.0158	0.0342	0.0926	0.0158	0.0342	0.0926	0.0158	0.0342	0.0926
0.0424	0.0380	0.0926	0.0342	0.0158	0.0926	0.0342	0.0158	0.0926	0.0342	0.0158	0.0926	0.0342	0.0158
0.0239	0.1392	0.0269	0.0162	0.0087	0.0947	0.0343	0.0116	0.0854	0.0499	0.0184	0.0947	0.0343	0.0116
0.0508	0.0508	0.0162	0.0217	0.0162	0.0343	0.0890	0.0343	0.0499	0.0792	0.0499	0.0343	0.0890	0.0343
0.1392	0.0239	0.0087	0.0162	0.0269	0.0116	0.0343	0.0947	0.0184	0.0499	0.0854	0.0116	0.0343	0.0947
0.0239	0.1392	0.0947	0.0343	0.0116	0.0269	0.0162	0.0087	0.0947	0.0343	0.0116	0.0854	0.0499	0.0184
0.0508	0.0508	0.0343	0.0890	0.0343	0.0162	0.0217	0.0162	0.0343	0.0890	0.0343	0.0499	0.0792	0.0499
0.1392	0.0239	0.0116	0.0343	0.0947	0.0087	0.0162	0.0269	0.0116	0.0343	0.0947	0.0184	0.0499	0.0854
0.0239	0.1392	0.0854	0.0499	0.0184	0.0947	0.0343	0.0116	0.0269	0.0162	0.0087	0.0947	0.0343	0.0116
0.0508	0.0508	0.0499	0.0792	0.0499	0.0343	0.0890	0.0343	0.0162	0.0217	0.0162	0.0343	0.0890	0.0343
0.1392	0.0239	0.0184	0.0499	0.0854	0.0116	0.0343	0.0947	0.0087	0.0162	0.0269	0.0116	0.0343	0.0947
0.0239	0.1392	0.0947	0.0343	0.0116	0.0854	0.0499	0.0184	0.0947	0.0343	0.0116	0.0269	0.0162	0.0087
0.0508	0.0508	0.0343	0.0890	0.0343	0.0499	0.0792	0.0499	0.0343	0.0890	0.0343	0.0162	0.0217	0.0162
0.1392	0.0239	0.0116	0.0343	0.0947	0.0184	0.0499	0.0854	0.0116	0.0343	0.0947	0.0087	0.0162	0.0269

From these values it is evident that there is a relation $\mathbb{F}_{ij} = \varepsilon_i G_{ij}$ as in Equation (53). The radiative heat transfer q between surfaces is calculated using Equation (52), and the values are identical to the ones presented in Table 4.6.

q =

0	104.75	36.81	79.71	215.69	36.81	79.69	215.77	36.82	79.69	215.77	36.81	79.69	215.69
-104.75	0	-12.95	-4.78	-2.21	-12.95	-4.78	-2.21	-12.95	-4.78	-2.21	-12.95	-4.78	-2.21
-37.06	12.97	0	0	0	0	0	0	0	0	0	0	0	0
-78.81	4.73	0	0	0	0	0	0	0	0	0	0	0	0
-216.17	2.22	0	0	0	0	0	0	0	0	0	0	0	0
-37.06	12.97	0	0	0	0	0	0	0	0	0	0	0	0
-78.81	4.73	0	0	0	0	0	0	0	0	0	0	0	0
-216.17	2.22	0	0	0	0	0	0	0	0	0	0	0	0
-37.06	12.97	0	0	0	0	0	0	0	0	0	0	0	0
-78.81	4.73	0	0	0	0	0	0	0	0	0	0	0	0
-216.17	2.22	0	0	0	0	0	0	0	0	0	0	0	0
-37.06	12.97	0	0	0	0	0	0	0	0	0	0	0	0
-78.81	4.73	0	0	0	0	0	0	0	0	0	0	0	0
-216.17	2.22	0	0	0	0	0	0	0	0	0	0	0	0

One will notice the total view factor method to be much shorter in computation length than the first principles method. In other words, the total view factor technique of the zone method produces the same results as the first principles technique in less calculating steps. Thus, the total view factor method provides an alternative, albeit reliable, time saving route in comparison to the first principles method.

4.4.3 Results - Comparison and Validation

As previously mentioned, the net radiative heat transfer of each surface calculated by the author is validated by the results published by Clark and Korybalski (1974) under identical parameters and conditions. The results of both the author (through first principles and total view factor techniques) and of Clark and Korybalski (1974) are summarized in Table 4.7.

Table 4.7: Comparison and Validation of Results for a 14-Surface Grey Enclosure

Surface,i	Net Heat Transfer Results, $q_{net,i}$ (Watts)		
	Author	Clark and Korybalski (1974)	Discrepancy
1	1433.69	1435.84	2.15
2	-184.51	-182.75	1.76
3	-24.09	-23.06	1.03
4	-74.08	-69.52	4.56
5	-213.94	-215.50	-1.56
6	-24.09	-23.06	1.03
7	-74.08	-69.52	4.56
8	-213.94	-215.50	-1.56
9	-24.09	-23.06	1.03
10	-74.08	-69.52	4.56
11	-213.94	-215.50	-1.56
12	-24.09	-23.06	1.03
13	-74.08	-69.52	4.56
14	-213.94	-215.50	-1.56

As can be seen in Table 4.7, the results computed by the author compare favorably with those presented by Clark and Korybalski (1974). Clark and Korybalski did not provide calculated view factors for the 14-surface grey enclosure using their method of radiation calculation, which inhibited the author from comparing and validating the view factors calculated in the present work. For this reason, some numerical discrepancy, although minimal, is noted and expected between the results of Clark and Korybalski and the

present work. Thus the computational procedures in this investigation are accurate and can be used as benchmark tools for those investigating the radiative heat exchange of an industrial furnace enclosure.

The calculations from above were accomplished with the aid of MathWorks Matlab 7.10 (release R2010a for Mac) in conjunction with MS Office Excel 2004 for Mac. Calculated results are displayed in Appendix E of this report. Also, one can notice for the purposes of this chapter, and maintaining with the solution procedure outlined by first principles and total view factor techniques, the temperatures of each elemental zone surface were pre-assigned in accordance with the paper published by Clark and Korybalski (1974). However, the surface temperatures along with the net radiative heat transfer of each surface can be calculated by assuming some, if not all, the surfaces of the enclosure to be re-radiating. This leads to a system of equations that can be solved simultaneously with the aid of computer software.

This chapter has shown the importance of radiative heat transfer in the process industries. It demonstrates how combustion is able to transfer energy, in the form of heat, to a material that requires thermal processing. Radiative heat transfer in an enclosure similar to the geometry of the existing furnace has been demonstrated and compared with previously published work. These results should help potential users in the development of a Zone Method model for this furnace, fired with different types of burners.

Chapter 5

Conclusions and Recommendations

This thesis describes proposed modifications to an existing pilot scale furnace for application in academic studies. Potential users might include senior year undergraduate students in Chemical and Mechanical Engineering as well as post-graduate applications in combustion and related subjects.

Since one of the purposes of this project was to introduce the science and engineering of industrial combustion, the main components of a combustion system were presented in this thesis with emphasis on combustion burners. The experimental furnace is equipped with an interchangeable burner section to allow users to compare and contrast the efficiency and emission control of various burners.

The current furnace apparatus (SJ/WJ furnace) was originally designed to simulate "flameless" combustion. This technology was first developed as a method to decrease nitrogen oxide (NO_x) emissions in high temperature gas-fired furnaces. The SJ/WJ furnace posed numerous safety restrictions and did not meet minimum requirements posed by standard safety associations such as TSSA and CSA. As a result it was determined to use the furnace in a different fashion that was not limited to flameless combustion. The proposed furnace design maintains the primary skeletal parts with capabilities to accommodate various types of burners. One such burner initially

suggested is an excess air nozzle mix burner described in this thesis. This burner would be operated with appropriate supporting equipment including a regenerative air blower and gas train. For safety considerations, a burner control safeguard is implemented into the furnace design. The burner safeguard is designed to provide continuous, automatic protection against the buildup of combustible fuel mixtures due to flame failure or other furnace chamber faults.

Radiation is the most important heat transfer mechanism found in furnaces. In order to truly understand an industrial furnace, one must take into account the transfer of heat that takes place within it through simulation calculations. A calculation method for radiative exchange within an enclosure, Hottel's Zone Method, was demonstrated in this work. The solution procedure was outlined for a geometry similar to the current furnace dimensions. The calculations can be performed with standard software (Excel, MatLab, etc.) to allow students to gain exposure to the problems of combustion engineering.

The work performed in this project has focused on gas fired furnace applications. The potential for alternative fuels including biofuels and biomass combustion has not been explored in this work. Investigation of such fuels is a prospective undertaking for future work on the furnace. A physical set-up of the furnace with its new instrumentation will be required in future endeavors. The implementation of the control and safety system process discussed previously is also required. Finally, an experimental procedure that would allow its users to start, operate, and shut down the combustion process safely, reliably, and efficiently along with its testing would be very beneficial for future users.

References

Abbasi, H.; Kurek, H.; Khinkis, M.; Yerynov, A.E.; and Semerin, O.M. *Advanced High-Efficiency Low Emissions Burner for Radiant Tube Applications.* International Gas Research Conference, Gas Research Institute Vol. V: Industrial Utilization, Pages 147 – 157, Chicago, 1998s.

American Petroleum Institute. *Burners for Fired Heaters in General Refinery Services - First Edition.* Washington, D.C.: API 535, 1995.

American Petroleum Institute. *Safety Digest of Lessons Learned: Section 2, Safety in Unit Operations*. Washington, D.C.: Publication 758, 1979.

Badjagbo, K., Sauve, S. and Moore, S. *Real-time continuous monitoring methods for airborneVOCs.* TrAC - Trends in Analytical Chemistry, Vol. 26[9], Pages 931-940, 2007.

Baukal, Charles E. *Industrial Combustion Pollution and Control.* New York: Marcel Dekker Inc., 2004.

Baukal, Charles E. *Industrial Burners Handbook.* New York: CRC Press LLC, 2003.

Baukal, Charles E. and Schwartz, Robert E. *The John Zink Combustion Handbook*. New York: CRC Press LLC, 2001.

Baukal, Charles E. *Heat Transfer in Industrial Combustion.* Boca Raton, Florida: CRC Press LLC, 2000.

Baukal, Charles E. *Oxygen-Enhanced Combustion*. Boca Raton, FL: CRC Press LLC, 1998.

Baukal, Charles E., Eleazer, P.B., and Farmer, L.K. *Basis for Enhancing Combustion by Oxygen Enrichment*. Industrial Heating, Vol. LIX (NO. 2), Pages 22 - 24, 1992.

Bazarian, E.R., Heffron, J.F., and Baukal, C.E. *Method for Reducing NOx Production During Air-Fuel Combustion Processes*. U.S. Patent 5,308,239, 1994.

Becker, H.A. *SJWJ Combustor Design.* CAGCT Technical Memorandum TM.99.2, 1999.

Beer, J. M. and Chigier, N. A. *Combustion Aerodynamics*. Malabar, FL: Robert E. Krieger, 1983.

Benedek, K.R. and Wilson, R.P. *The Competitive Position of Natural-Gas in Oxy-Fuel Burner Applications*. Gas Research Institute Report GRI-96-0350, Chicago, IL, September 1996.

Bloom Engineering. *Industrial Burner Types.* Retrieved November, 2009: http://www.bloomeng.com/burner-types.html, 2007.

Branch Environmental Corp. *NO_x Removal.* Retrieved October, 2009: http://www.branchenv.com/nox/nox.html, 2009.

Brus, G. and Szmyd, J. S. *Numerical Modelling of Heat Transfer Processes in an Internal Indirect Reforming Type SOFC.* Given at the 5th European Thermal-Sciences Conference, The Netherlands, 2008.

bu-Khader, M. *Recent Progress in CO_2 Capture/Sequestration: A Review*. Energy Sources, Part A: Recovery, Utilization and Environmental Effects, Vol. 28[14], Pages 1261-1279, 2006.

Burggraaf, B. T., Lewis, B., Hoppesteyn, P. D. J., Fricker, N., Santos, S. and Slim, B. K. *Towards Industrial Application of High Efficiency Combustion*. IFRF Combustion Journal, Pages 1-16, 2007.

Camp, J.M. and Francis, C.B. *The Making, Shaping, and Treating of Steel - Fourth Edition.* Pittsburgh, PA: Carnegie Steel Company, 1925.

Carlson B.G. and Lathrop, K.D. *Transport Theory - The Method of Discrete Ordinates.* New York: Gordon & Breach, Pages 269-308, 1968.

Center for Chemical Process Safety. *Thermal Radiation 2: The Physiological and Pathological Effects*. New York: American Institute of Chemical Engineers, 1996.

Center for Chemical Process Safety. *Guidelines for Preventing Human Error in Process Safety*. New York: American Institute of Chemical Engineers, 1994.

Center for Chemical Process Safety. *Thermal Radiation I: Sources and Transmission*. New York: American Institute of Chemical Engineers, 1989.

Chen, Yen-Hsun; Wong, King-Leung; Kuo, I-Pin; Lin, Chuan-Huang; and Lin, Jin-Yu. *The Heat Transfer Characteristics of an Insulated Circular Duct Considering and Neglecting the Influence of Heat Radiation.* Proceedings of the International MultiConference of Engineers and Computer Scientists 2009 Vol II IMECS, Hong Kong, March 18 - 20, 2009.

Clark, John A. and Korybalski, Michael E. *Algebraic Methods for the Calculation of Radiation Exchange in an Enclosure.* Wärme-und Stoffübertragung, Volume 7, Pages 31 – 44, 1974.

Crocker, W.P. and Napier, D.H. *Thermal Radiation Hazards of Liquid Pool Fires and Tank Fires.* IChemE Symposium Series No. 97, Institute of Chemical Engineers, Pages 159-184. Oxford, U.K.: Pergamon Press, 1986.

Davies, T. *Regenerative Burners for Radiant Tubes — Field Test Experience.* Warren, PA: American Society of Metals, Pages 65-70, 1986.

Docherty, P. and Fairweather, M. *Predictions of Radiative Transfer from Non-homogeneous Combustion Products Using Discrete Transfer Method.* Combustion and Flame, Volume 71, Pages 79-87, 1988.

Docquier, Nicolas and Candel, Sébastien. *Combustion Control and Sensors: A Review.* Progress in Energy and Combustion Science, Vol. 28, Pages 107 – 150, 2002.

Eckhoff, Rolf K., *Explosion Hazards in the Process Industries*. Houston: Gulf Publishing Company, 2005.

Edwards, D.K. *Radiation Heat Transfer Notes.* Washington, D.C.: Hemisphere, 1981.

Environment Canada. *Canada's 2005 Greenhouse Gas Inventory - A Summary of Trends.* Retrieved October 2009: http://www.ec.gc.ca/pdb/ghg/inventory_report/2005/2005summary_e.cfm, 2007.

Faeth, G.M., Gore, J.P., Chuech, S.G., and Jeng, S.M. *Radiation From Turbulent Diffusion Flames*. Annual Review of Fluid Mechanics & Heat Transfer, Volume 2, Pages 1–38, 1989.

Fireye. *Flame Safeguard Burner Management with Integrated Boiler Control.* Retrieved September 2009: http://www.fireye.net/pdf/ZB110-SPEC.pdf, 2007.

Fiveland, W.A. *Discrete-ordinates Solutions of the Radiative Transport Equation for Rectangular Enclosures.* Journal of Heat Transfer, Volume 106, Pages 699-706, 1984.

Garrison, W.G. *Major Fires and Explosions Analyzed for 30-Year Period.* Hydrocarbon Process, Vol. 67(9), Pages 115 – 122, 1981.

Gebhart, B. *Heat Transfer (2nd Edition).* New York: McGraw-Hill, 1971.

Grandmaison, Edward W. *CHEE 481 – Air Quality Management (Courseware)*. Kingston, Ontario, Canada: Queen's University, 2007.

Grandmaison, E.W., Yimer, I., Becker, H.A. and Sobiesiak, A. *The Strong-Jet/Weak-Jet Modeling of the CGRI Burner.* Combustion and Flame, Volume 114, Pages 381-396, 1998.

Graves, Frank and Boucher, Christian. *Public Attitudes Towards the Kyoto Protocol.* Ekos Research Associates, Retrieved October 2009: http://www.ekos.com/admin/articles/10June02KyotoProt.pdf, 2002.

Gupta, A. K. and Lilley, D. G. *Review: The Environmental Challenge of Gas Turbines.* Journal of the Institute of Energy, Volume 65(464), pages 106-117, 1992

He, Yu. *Flameless Combustion of Natural Gas in the SJ/WJ Furnace.* PhD Thesis, Department of Mechanical Engineering, Queen's University, Kingston, ON, 2008.

He, Y., Lee, Y. J., Grandmaison, E. W., Matovic, M. D. *Experimental Study of Flameless Combustion in the Strong-Jet/Weak-Jet Furnace.* Spring Technical Meeting of the Combustion Institute (Canadian Section), Banff, Alberta. May 2007.

Hewitt, G.F.; Shires, G.L.; Polezhaev, Y.V.; and Polezhaev, Iu.V. *International Encyclopedia of Heat & Mass Transfer*. Boca Raton, FL: CRC Press, 1997.

Hewitt, G.F., Shires, G.L. and Bott, T.R. *Process Heat Transfer*. Boca Raton, FL: CRC Press, 1994.

Holman, J.P. *Heat Transfer (7th Edition)*. New York: McGraw-Hill, 1990.

Hottel, H.C. and Sarofim, A.F. *Radiative Heat Transfer*. New York: McGraw-Hill, 1967.

Hottel, H.C. and Cohen, H.S. *Radiant Heat Exchange in a Gas Filled Enclosure: Allowance for Nonuniformity of Gas Temperature.* AIChE Journal, Volume 4, Pages 3-14, 1958.

Howell, J.R. *A Catalog of Radiation Heat Transfer Configuartion Factors – Second Edition.* Department of Mechanical Engineering, The University of Texas at Austin. Retrieved January 2010: http://www.me.utexas.edu/~howell/index.html, 2001.

Howell, J.R. Radiative Transfer in Multi-Dimensional Enclosures with Participating Media. ASME, paper no. 83-HT-32, 1983.

Howell, J.R. *Application of Monte Carlo to Heat Transfer Problems.* Advances in Heat Transfer, Volume 5, Ac.Press, 1968.

Hyde, D.J. and Truelove, J.S. *The Discrete Ordinate Approximation for Radiative Heat Transfer.* Technical Report AERE-R 8502, 1977.

Jenkins, Joanna; Tan, C.K; Ward, John; and Hayward, John. *Application of a One-Dimensional Thermal Radiation Model of a Simple Furnace.* Proceedings of the 3rd Research Student Workshop, ed. P. Plassmann and P. Roach, Pages 59-63, The Research Office, University of Glamorgan, 2008.

Kletz, T. *Learning from Accidents – Second Edition.* Oxford: Butterworth-Heinemann, 1994.

Kletz, T. *An Engineer's View of Human Error – Second Edition*. Rugby, U.K.: Institution of Chemical Engineers, 1991.

Kramlich, J.C. and Linak, W.P. *Nitrous Oxide Behavior in the Atmosphere, and in Combustion and Industrial Systems.* Progress in Energy and Combustion Science, Volume 20, Pages 149-202, 1994.

Kreith, F. *The CRC Handbook of Mechanical Engineering*. Boca Raton, FL: CRC Press, 1994.

Kreith, F. and Bohn, M.S. *Principles of Heat Transfer.* New York: Harper & Row, 1986.

Lathrop, K. D. *Ray Effects in Discrete Ordinate Equations.* Nuclear Science and Engineering, Volume 32, Pages 357-369, 1968.

Leblanc, B. and Goracci, E. *Example of Applications in the Field of Heat Transfer in Hot Wall Furnaces.* La Rivista dei Combustibili, Volume 27(4-5), Pages 155–164, 1973.

Lee, Sunggyu. *Encyclopedia of Chemical Processing – Volume 1.* New York: Taylor & Francis, 2005.

Lewis, E. E. and Miller, W. F. Computational Methods of Neutron Transport. New York: John Wiley and Son, 1984.

Liang, W.W. and Schreiner, M.E. *Advanced Materials Development for Radiant Tube Applications in Industrial Combustion Technologies.* Warren, PA: M.A. Lukasiewicz, Ed., American Society of Metals, Pages 305-311, 1986.

Li, Cheng Wu. *The Investigation of Ultra Low NO_X Combustion in a Strong Jet/Weak Jet Combustor: Calibration and Numerical Studies.* Master of Science Engineering Thesis, Department of Mechanical Engineering, Queen's University, Kingston, Ontario, 2005.

Lockwood, F.C. and Shah, N.G. *Eighteenth Symposium (International) on Combustion.* The Combustion Institute, Pages 1405-1414, 1981.

McAdams, W. H. *Heat Transmission.* New York: McGraw-Hill Inc., 1954, Chapter 4 (by H. C. Hottel).

McGuinness, R.M. and Kleinberg, W.T. *Oxygen-Enhanced Combustion - Chapter 3: Oxygen Production*. Boston: CRC Press, Pages 73–135, 1998.

Mengüç, M.P. and Viskanta, R. *Radiation Heat Transfer in Combustion Systems.* Prog. Energy Combustion Science, Volume 13, Pages 97-160, 1987.

Milani, A. and Saponaro, A. *Diluted Combustion Technologies.* IFRF Combustion Journal, Article number 200101, Page 32, 2001.

Mishra, Subhash C. and Prasad, Manohar. *Radiative Heat Transfer in Participating Media – A Review.* Sadhana, Volume 23 (2), Pages 213-232, 1998.

Nelson, H.F.; Look, D.C.; and Crosbie, A.L. Two-Dimensional Radiative Back-Scattering from Optically Thick Media. Trans. ASME Journal of Heat Transfer, Volume 108, Pages 619-625, 1986.

Newby, J.N. *The reGen Regenerative Burner — Principles, Properties and Practice, in Industrial Heat Exchangers.* Warren, PA: American Society of Metals, Pages 143–152, 1985.

Niemkiewicz, M.A. and Becker, J.S. *Safety Overview in Oxygen-Enhanced Combustion*. Boca Raton, FL: CRC Press, 1998.

Noble, J.J. *The Zone Method: Explicit Matrix Relations for Total Exchange Areas.* International Journal of Heat & Mass Transfer, Volume 18, Pages 261-269, 1975.

North American Manufacturing. *North American Combustion Handbook – Volume II (Third Edition).* Cleveland, Ohio: North American Manufacturing, 1995.

North American Manufacturing Company, Ltd. *Handbook Supplement 128 – Combustion in the Glass Industry*, 1972.

Ordan Thermal Products Ltd. *Excess Air Single Tunnel Burner (Model 3502-XNM).* Retrieved September 2009: http://www.ordanthermal.com/products/nozzle-mix-burners/single-tunnel-excess-air-burners.pdf, 2009

Ordan Thermal Products Ltd. *Mini L.C. Blowers (Model 4120-LC).* Retrieved September 2009: http://www.ordanthermal.com/products/blowers/Mini-L-C-Blower.pdf, 2009.

Ordan Thermal Products Ltd. *Microprocessor Burner Control (Model 7500).* Retrieved September 2009: http://www.ordanthermal.com/products/burner-flame-management/estro-burner-control.pdf, 2009.

Poirier, D., Grandmaison, E.W., Lawrence, A.D., Matovic, M.D. and Boyd, E. *Oxygen-Enriched Combustion with the Low NO_X CGRI Burner.* IFRF Combustion Journal, Article number 200404, Page 15, 2004.

Pomraning, G.C. *The Equations of Radiation Hydrodynamics*. Oxford: Pergamon, 1973.

Reese, J.L., Moilanen, G.L., Borkowicz, R., Baukal, C., Czerniak, D. and Batten, R. *State of-the-Art of NOx Emission Control Technology*. Proceedings of Int. Joint Power Generation Conf., Phoenix, AZ, ASME paper 94-JPGC-EC-15, 3-5 October, 1994.

Rhine, J. M. and Tucker, R. J. *Modelling of Gas-Fired Furnaces and Boilers.* New York: McGraw-Hill, 1991.

Richardson, T. *Learn from the Phillips Explosion*. Hydrocarbon Processes, Vol. 70(3), Pages 83-84, 1991.

Sanders, R.E. *Chemical Process Safety: Learning from Case Histories.* Boston: Butterworth-Heinemann, 1999.

Selçuk, N. *Evaluation of Flux Models for Radiative Transfer in Rectangular Furnaces.* International Journal of Heat & Mass Transfer, Volume13 (7), Pages 1477-1482, 1988.

Siegel, R. and Howell, J.R. *Thermal Radiation Heat Transfer (Third Edition)*. Washington DC: Hemisphere Publishing Corporation, 1992.

Singh, S.S. and Gorski, L.M. *Ceramic Single Ended Recuperative Radiant Tube (Phase1)*. NTIS Document PB91222554, 1990.

Smith, T.E.; Sben, Z. E.; and A1-Turki A.M. *Radiative and Conductive Transfer in a Cylindrical Enclosure for a Real Gas.* Trans. ASME Journal of Heat Transfer, Volume 104, Pages 482-485, 1985.

Sobiesiak, A., Rahbar, S. and Becker, H.A. *Performance Characteristics of the Novel Low NO_X CGRI Burner for use with High Air Preheat.* Combustion and Flame, Volume 115, Pages 93-125, 1998.

Sparrow, E.M. and Cess, R.D. *Radiation Heat Transfer, Augmented Edition.* Washington DC: Hemisphere Publishing Corporation, 1978.

Tucker, Robert J. *How do I Predict Radiative Heat Transfer in Industrial Furnaces?* IFRF Combustion Handbook, File Number 65, Version 1, 2004.

Turns, S. R. *An Introduction to Combustion - Concepts and Applications (Second Edition).* New York: McGraw-Hill Inc., 2000.

United Nations. *Kyoto Protocol to the United Nations Framework Convention on Climate Change.* Retrieved October 2009: http://unfccc.int/resource/docs/convkp/kpeng.pdf, 1998.

U.S. Department of Energy (DOE) and Energy Information Administration (EIA). *Annual Energy Outlook 1999.* Washington, D.C.: U.S. DOE/EIA-0383, 1999.

U.S. Department of Energy (DOE). Industrial Combustion Vision: A Vision by and for the Industrial Combustion Community. Washington, D.C.: U.S. DOE, 1998.

U.S. Environmental Protection Agency (EPA). *Climate Change – Greenhouse Gas Emissions.* Retrieved September 2009: http://www.epa.gov/climatechange/emissions/, 2007.

U.S. Environmental Protection Agency (EPA). *Alternative Control Techniques Document — NOx Emissions from Utility Boilers*. EPA Report EPA-453/R-94-023, Research Triangle Park, NC, 1994.

Wang, X. and Wiser, G. *The implementation and compliance regimes under the climate change convention and its Kyoto Protocol*. Review of European Community and International Environmental Law, Vol. 11[2], Pages 181-198, 2002.

Webb, R. *On the Road to Recovery*. MRS Relay, British Gas, Pages 9-11, September 1983.

Wiebelt, J.A. *Engineering Radiation Heat Transfer.* New York: Holt, Rinehart and Winston, 1966.

Williams, S.J., Cuervo, L.A., and Chapman, M.A. *High-Temperature Industrial Process Heating: Oxygen-Gas Combustion and Plasma Heating Systems*. Gas Research Institute Report GRI-89/0256, Chicago, IL, July 1989.

WS Thermal Process Technology Inc. *Burners and Radiant Tubes.* Retrieved November 2009: http://www.flox.com/en/comp/company.html, 2004.

Wünning, J.G. *FLOX - Flameless Combustion.* Thermprocess Symposium, 2003.

Wünning, J.G. *Flameless Combustion in the Thermal Process Technology.* Second International Seminar on High Temperature Combustion, 2000.

Wünning, J.A. and Wünning, J.G. *Flameless Oxidation to Reduce Thermal NO-Formation.* Progress in Energy and Combustion Science, Volume 23, Pages 81-94, 1997.

Yang, K T. *Numerical Modeling of Natural Convection-Radiation Interactions in Enclosures.* In Proceedings of the 8th International Heat Transfer Conference (Washington, DC: Hemisphere) Volume 1, Pages 131-140, 1986.

Yimer, I. *Turbulent Mixing in a Low NOx Burner Model.* Ph.D. Thesis, Department of Chemical Engineering, Queen's University, Kingston, ON K7L 3N6, 1997.

Zeldovich, Y. B. *Acta Physicochimica.* U.R.S.S., Volume 21, Page 577, 1946.

Appendix A

SJ/WJ Furnace P&ID

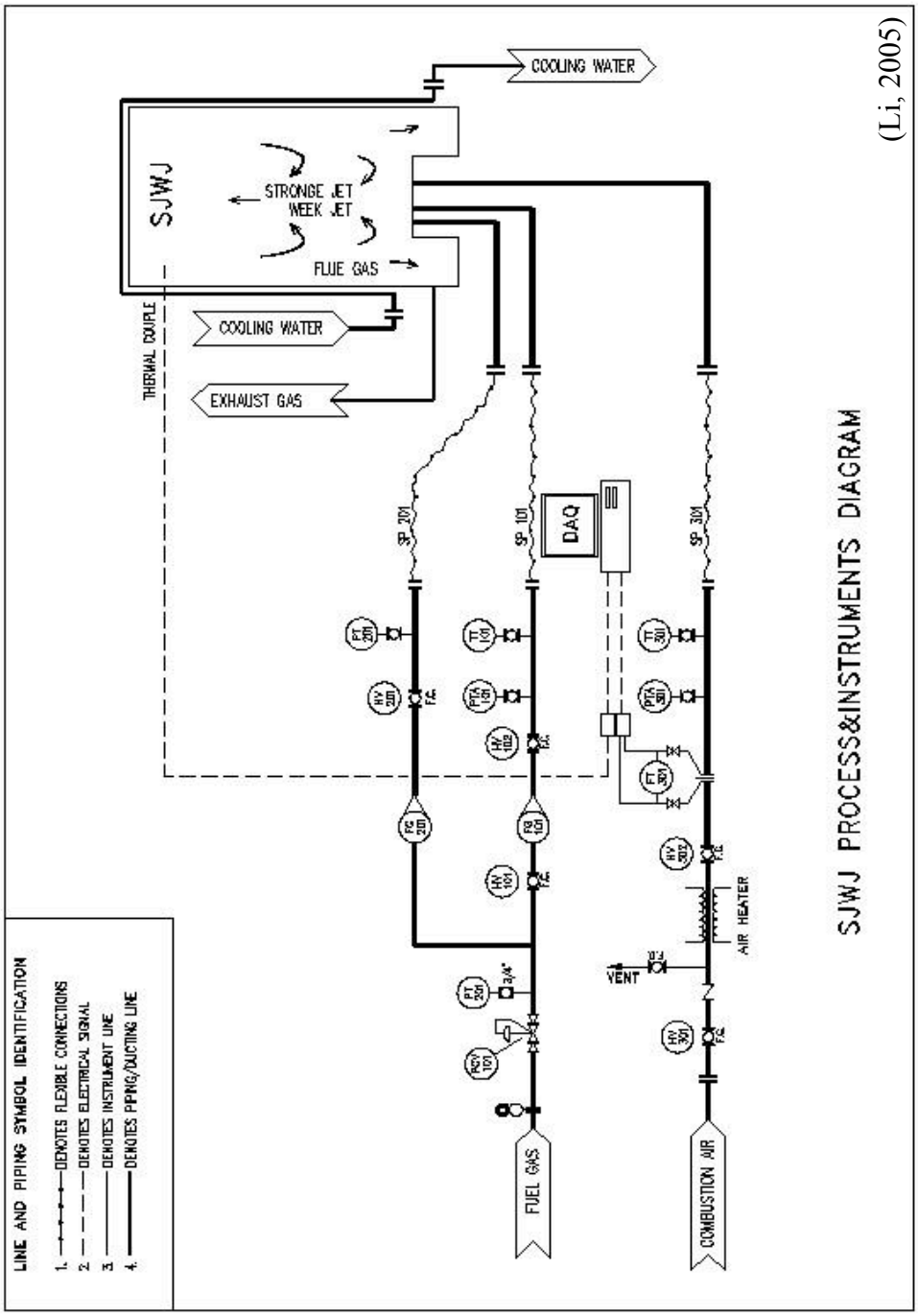

Appendix B

Nozzle Mix Burner Gas Train

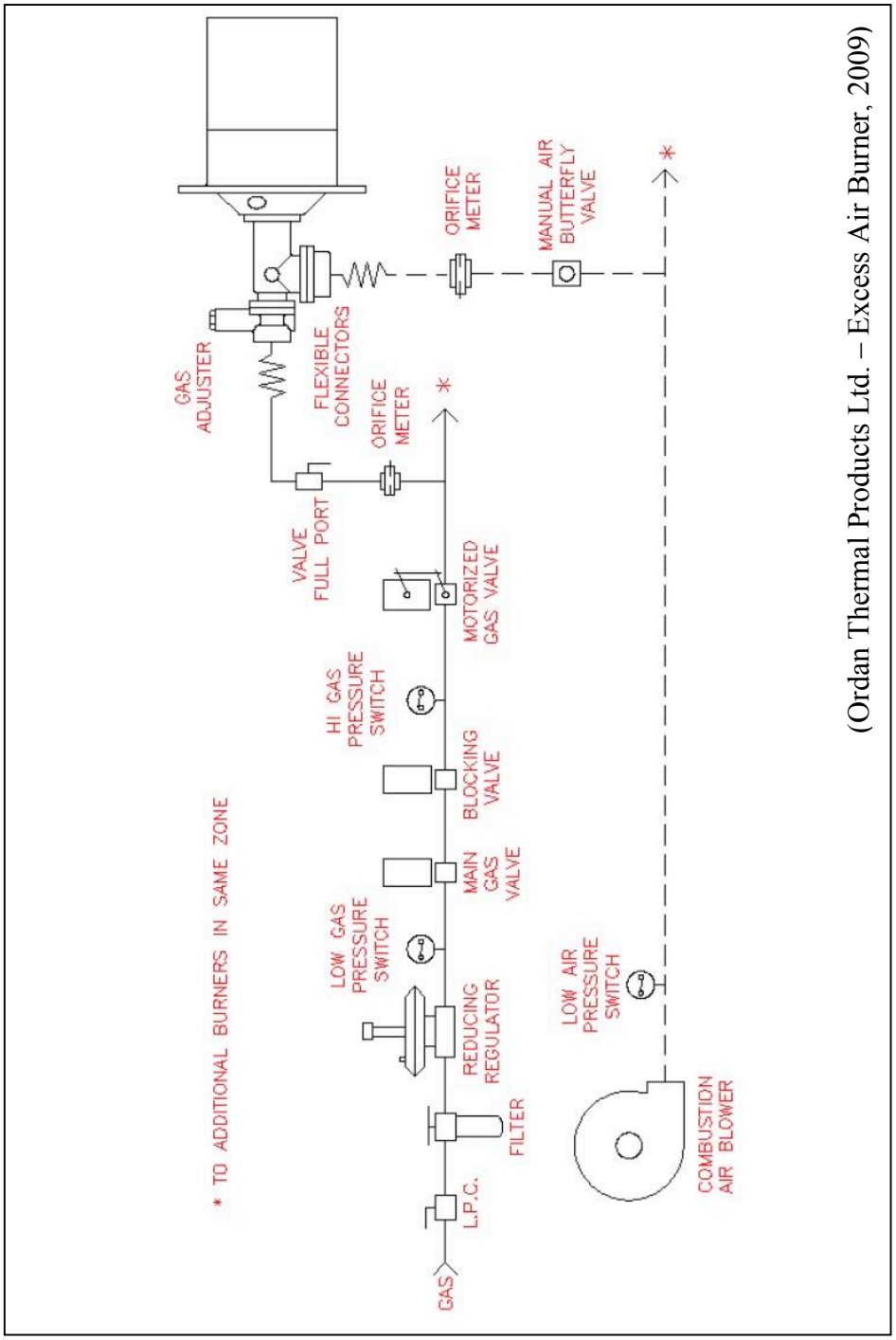

Appendix C

Emissivities of Various Surfaces as a Function of Temperature

Surface	Temperature (^{o}C)	Emissivity
A. Metals and their Oxides		
Aluminum		
Polished	100	0.095
Commercial sheet	100	.09
Heavily oxidized	95-505	0.20-0.31
Brass		
Highly polished		
73.2 Cu, 26.7 Zn	245-355	0.028-0.031
62.4 Cu, 36.8 Zn, 0.4 Pb, 0.3 Al	255-375	0.033-0.037
82.9 Cu, 17.0 Zn	275	0.030
Rolled plate, natural surface	20	0.06
Dull plate	50-350	0.22
Oxidized by heating at 600^{o}C	200-600	0.59-0.61
Copper		
Carefully polished electrolytic copper	80	0.018
Commercially polished but pits remain	20	0.030
Commercially scraped shiny but not mirrolike	20	0.072
Plate, heated for long time, covered with thick oxide layer	25	0.78
Molten copper	1075-1275	0.16-0.13
Gold		
Pure, highly polished	225-625	0.018-0.035
Iron and Steel (not including stainless steel)		
Electrolytic iron, highly polished	175-225	0.052-0.064
Steel, polished	100	0.066
Iron, polished	425-1025	0.14-0.38
Cast iron, polished	200	0.21
Cast iron, newly turned	20	0.44
Cast iron, turned and heated	880-988	0.60-0.70
Mild steel, cleaned with organic solvents	25	0.12, 0.15
Oxidized Surfaces		
Iron plate, pickled, then rusted red	20	0.61
Iron plate, completely rusted	20	0.69

Surface	Temperature (^oC)	Emissivity
Rolled sheet steel	20	0.66
Cast iron, oxidized at 600^oC	200-600	0.64-0.78
Steel, oxidized at 600^oC	200-600	0.79
Sheet Steel		
With rough oxide layer	25	0.80
With shiny oxide layer	25	0.82
Steel plate, rough	40-370	0.94-0.97
Molten surfaces		
Cast iron	1300-1400	0.29
Mild steel	1600-1800	0.28
Lead		
Pure (99.96%) unoxidized	125-225	0.057-0.075
Oxidized at 150^oC	200	0.63
Mercury	0-100	0.09-0.12
Nickel		
Electroplated, polished	25	0.045
Polished	100	0.072
Electroplated, not polished	20	0.11
Plate, oxidized by heating at 600^oC	200-600	0.37-0.48
Nickel Alloys		
Copper-nickel, polished	100	0.059
Nichrome wire, bright	50-1000	0.65-0.79
Platinum		
Pure polished plate	225-625	0.054-0.104
Silver		
Polished, pure	225-625	0.020-0.032
Stainless Steels		
Type 304 (8 Cr, 18 Ni) polished	100	0.074
Light silvery, rough, brown, after heating	215-490	0.44-0.36
After 42 hours at 525^oC	215-525	0.62-0.73
Thorium Oxide	275-825	0.21-0.58
Tin		
Bright	50	0.06
Commercial tin-plated sheet iron	100	0.07,0.08
Zinc		
Commercial 99.1% pure, polished	225-325	0.045-0.053
Oxidized by heating at 400^oC	400	0.11
Galvanized sheet iron, fairly bright	30	0.23
Galvanized sheet iron, gray oxidized	25	0.28

Surface	Temperature (°C)	Emissivity
B. Refractories, Building Materials, Paints, & Miscellaneous Materials		
Alumina (85-99.5 Al_2O_3; 0-12 SiO_2; 0-1 Fe_2O_3)		
Effect of mean grain size		
10 μm	1010-1565	0.18-0.30
50 μm		0.28-0.39
100 μm		0.40-0.50
Alumina-silica (showing effect of Fe)		
58-80 Al_2O_3; 16-38 SiO_2; 0.4 Fe_2O_3	1010-1570	0.43-0.61
26-36 Al_2O_3; 50-60 SiO_2; 1.7 Fe_2O_3		0.62-0.73
61 Al_2O_3; 35 SiO_2; 2.9 Fe_2O_3		0.68-0.78
Asbestos		
Board	25	0.96
Paper	40-370	0.93-0.94
Brick		
Red, rough but no gross irregularities	20	0.93
Building	1000	0.45
Fireclay	1000	0.75
Carbon		
Filament	1040-1405	0.526
Graphitized	100-320	0.75-0.76
Thin layer on iron plate	320-500	0.71-0.75
Thick coat	20	0.926-0.967
Glass		
Smooth	20	0.94
Magnesite refractory brick	1000	0.38
Paints, lacquers, varnishes		
Snow-white enamel varnish on iron plate	25	0.906
Black-shiny lacquer sprayed on iron	25	0.875
Radiator paint: white, cream, bleach	100	0.77-0.84
Plaster, rough line	10-90	0.91
Quartz		
Rough, fused	20	0.93
Glass, 1.98 mm thick	280-840	0.41-0.90
Glass, 6.88 mm thick	280-840	0.47-0.93
Silica (98 SiO_2; Fe-free), effect of grain size		
10 μm	1010-1565	0.33-0.42
70-600 μm		0.46-0.62
Water	0-100	0.95-0.963

From data tabulated by Hottel and Sarofim (1967).

Appendix D

Radiant View Factors for Important Geometries (Wiebelt, 1966)

Configuration A-1

This configuration consists of identical, parallel, directly opposed rectangles A_1 and A_2 (see figure). The configuration-fact or values are plotted in Figure A4.13 in terms of the parameters x and y, where $x = b/c$ and $y = a/c$.

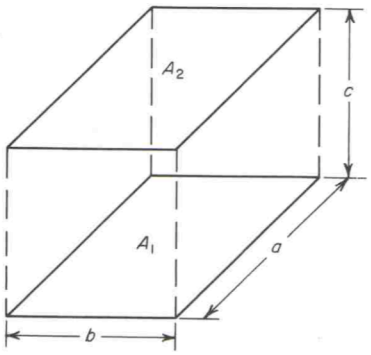

$$F_{12} = \frac{2}{\pi xy}\left\{\log_e\left[\frac{(1+x^2)(1+y^2)}{1+x^2+y^2}\right]^{1/2} + y\sqrt{1+x^2}\tan^{-1}\left(\frac{y}{\sqrt{1+x^2}}\right)\right.$$
$$\left. + x\sqrt{1+y^2}\tan^{-1}\left(\frac{x}{\sqrt{1+y^2}}\right) - y\tan^{-1} y - x\tan^{-1} x\right\}$$

$$\lim_{x\to\infty} F_{12} = \sqrt{1+\frac{1}{y^2}} - \frac{1}{y}$$

$$\lim_{y\to\infty} F_{12} = \sqrt{1-\frac{1}{x^2}} - \frac{1}{x}$$

$$\lim_{\substack{x\to\infty \\ y\to\infty}} F_{12} = 1$$

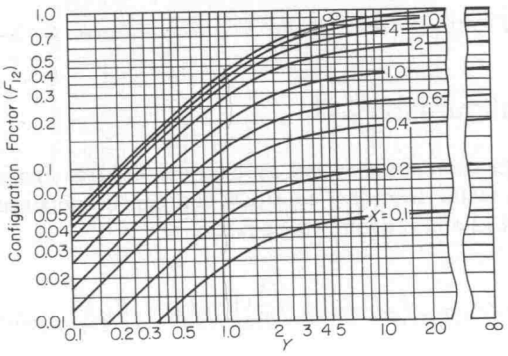

Figure A4.13 Configuration-factor Curves for A–1.

Configuration A-2

This configuration consists of two rectangles A_1 and A_2, with one common edge and an included angle between the two planes. The configuration factor

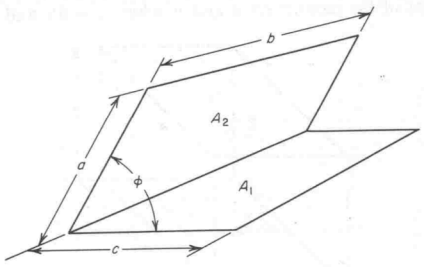

is plotted in Figure A4.14 as a function of N and L for various values of ϕ. $N = a/b$ and $L = c/b$ (see figure). For $\phi = 90°$,

$$F_{12} = \frac{1}{\pi L}\left(L\tan^{-1}\left(\frac{1}{L}\right) + N\tan^{-1}\left(\frac{1}{N}\right) - \sqrt{N^2+L^2}\tan^{-1}\left(\frac{1}{\sqrt{N^2+L^2}}\right)\right.$$

$$+\frac{1}{4}\log_e\left\{\left[\frac{(1+L^2)(1+N^2)}{(1+N^2+L^2)}\right]\left[\frac{L^2(1+L^2+N^2)}{(1+L^2)(L^2+N^2)}\right]^{L^2}\right.$$

$$\left.\left.\times\left[\frac{N^2(1+L^2+N^2)}{(1+N^2)(L^2+N^2)}\right]^{N^2}\right\}\right)$$

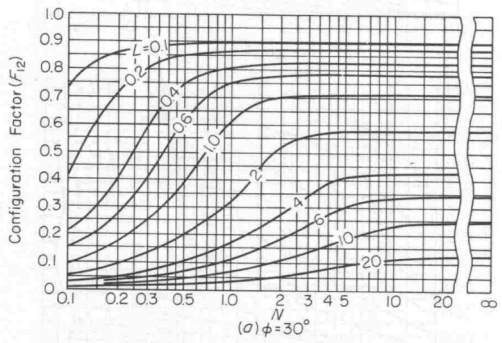

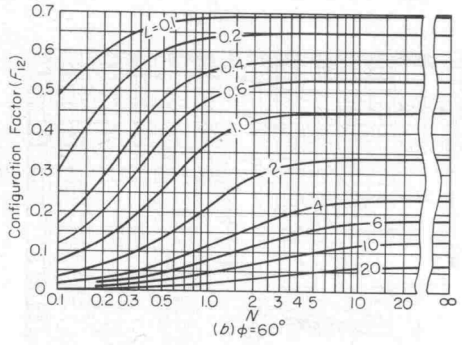

Figure A4.14 Configuration Curves for A–2 at Various Values of Φ. When $\phi = 0°$, $F_{12} = N/L$ for $N < L$ and 1 for $N > L$; when $\phi = 180°$, $F_{12} = 0$ for all values of N and L.

$$\lim_{N\to\infty} F_{12} = \frac{1}{\pi}\left[\tan^{-1}\left(\frac{1}{L}\right) + \frac{1}{4L}\log_e(1+L^2) - \frac{L}{4}\log_e\left(\frac{1+L^2}{L^2}\right)\right]$$

$$\lim_{L\to\infty} F_{12} = 0$$

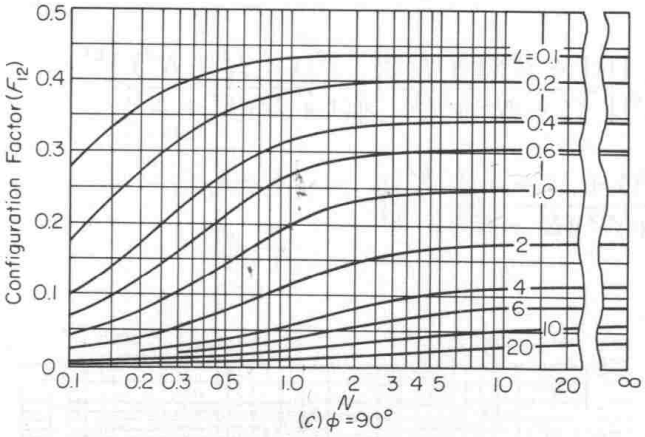

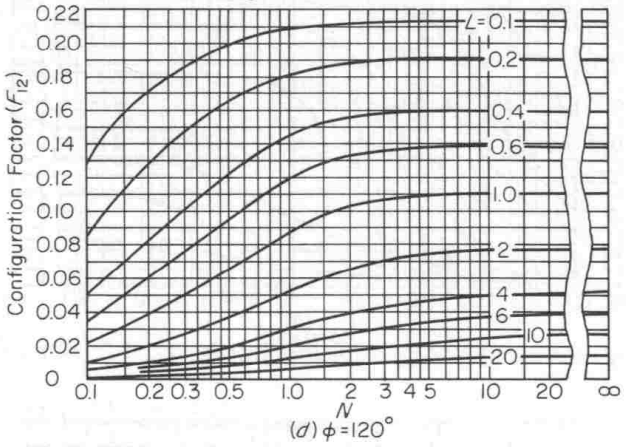

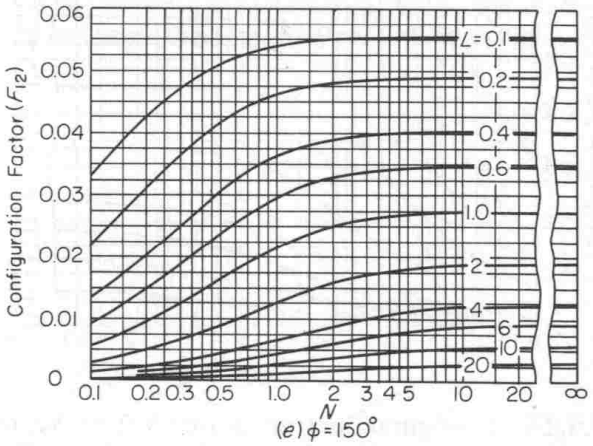

Figure A4.14 (continued)

Appendix E

Calculated Data for 14-Surface Grey Enclosure

First Principles Method

Input Data:

Surface	Area (m2)	Emittance	Reflectance	T (K)
1	0.0929	0.65	0.35	833
2	0.0929	0.65	0.35	333
3 -14	0.0619	0.65	0.35	444

Stefan Boltzmann Constant (σ):

5.7E-08 [$Wm^{-2}K^{-4}$]

View Factor Matrix:

F_{ij}	i = 1	2	3	4	5	6	7	8	9	10	11	12	13	14
j =1	0	0.069	0.024	0.070	0.255	0.024	0.070	0.255	0.024	0.070	0.255	0.024	0.070	0.255
2	0.069	0	0.255	0.070	0.024	0.255	0.070	0.024	0.255	0.070	0.024	0.255	0.070	0.024
3	0.016	0.170	0	0.000	0.000	0.171	0.048	0.009	0.148	0.089	0.028	0.171	0.048	0.009
4	0.047	0.047	0.000	0	0.000	0.048	0.171	0.048	0.089	0.148	0.089	0.048	0.171	0.048
5	0.170	0.016	0.000	0.000	0	0.009	0.048	0.171	0.028	0.089	0.148	0.009	0.048	0.171
6	0.016	0.170	0.171	0.048	0.009	0	0.000	0.000	0.171	0.048	0.009	0.148	0.089	0.028
7	0.047	0.047	0.048	0.171	0.048	0.000	0	0.000	0.048	0.171	0.048	0.089	0.148	0.089
8	0.170	0.016	0.009	0.048	0.171	0.000	0.000	0	0.009	0.048	0.171	0.028	0.089	0.148
9	0.016	0.170	0.148	0.089	0.028	0.171	0.048	0.009	0	0.000	0.000	0.171	0.048	0.009
10	0.047	0.047	0.089	0.148	0.089	0.048	0.171	0.048	0.000	0	0.000	0.048	0.171	0.048
11	0.170	0.016	0.028	0.089	0.148	0.009	0.048	0.171	0.000	0.000	0	0.009	0.048	0.171
12	0.016	0.170	0.171	0.048	0.009	0.148	0.089	0.028	0.171	0.048	0.009	0	0.000	0.000
13	0.047	0.047	0.048	0.171	0.048	0.089	0.148	0.089	0.048	0.171	0.048	0.000	0	0.000
14	0.170	0.016	0.009	0.048	0.171	0.028	0.089	0.148	0.009	0.048	0.171	0.000	0.000	0

View Factor Matrix:

F_{ij}	j = 1	2	3	4	5	6	7	8	9	10	11	12	13	14
i =1	0	0.069	0.016	0.047	0.170	0.016	0.047	0.170	0.016	0.047	0.170	0.016	0.047	0.170
2	0.069	0	0.170	0.047	0.016	0.170	0.047	0.016	0.170	0.047	0.016	0.170	0.047	0.016
3	0.024	0.255	0	0.000	0.000	0.171	0.048	0.009	0.148	0.089	0.028	0.171	0.048	0.009
4	0.070	0.070	0.000	0	0.000	0.048	0.171	0.048	0.089	0.148	0.089	0.048	0.171	0.048
5	0.255	0.024	0.000	0.000	0	0.009	0.048	0.171	0.028	0.089	0.148	0.009	0.048	0.171
6	0.024	0.255	0.171	0.048	0.009	0	0.000	0.000	0.171	0.048	0.009	0.148	0.089	0.028
7	0.070	0.070	0.048	0.171	0.048	0.000	0	0.000	0.048	0.171	0.048	0.089	0.148	0.089
8	0.255	0.024	0.009	0.048	0.171	0.000	0.000	0	0.009	0.048	0.171	0.028	0.089	0.148
9	0.024	0.255	0.148	0.089	0.028	0.171	0.048	0.009	0	0.000	0.000	0.171	0.048	0.009
10	0.070	0.070	0.089	0.148	0.089	0.048	0.171	0.048	0.000	0	0.000	0.048	0.171	0.048
11	0.255	0.024	0.028	0.089	0.148	0.009	0.048	0.171	0.000	0.000	0	0.009	0.048	0.171
12	0.024	0.255	0.171	0.048	0.009	0.148	0.089	0.028	0.171	0.048	0.009	0	0.000	0.000
13	0.070	0.070	0.048	0.171	0.048	0.089	0.148	0.089	0.048	0.171	0.048	0.000	0	0.000
14	0.255	0.024	0.009	0.048	0.171	0.028	0.089	0.148	0.009	0.048	0.171	0.000	0.000	0

D =

-0.265	0.006	0.001	0.004	0.016	0.001	0.004	0.016	0.001	0.004	0.016	0.001	0.004	0.016
0.00637	-0.265	0.016	0.004	0.001	0.016	0.004	0.001	0.016	0.004	0.001	0.016	0.004	0.001
0.00224	0.016	-0.177	0.000	0.000	0.011	0.003	0.001	0.009	0.006	0.002	0.011	0.003	0.001
0.00652	0.004	0.000	-0.177	0.000	0.003	0.011	0.003	0.006	0.009	0.006	0.003	0.011	0.003
0.02369	0.001	0.000	0.000	-0.177	0.001	0.003	0.011	0.002	0.006	0.009	0.001	0.003	0.011
0.00224	0.016	0.011	0.003	0.001	-0.177	0.000	0.000	0.011	0.003	0.001	0.009	0.006	0.002
0.00652	0.004	0.003	0.011	0.003	0.000	-0.177	0.000	0.003	0.011	0.003	0.006	0.009	0.006
0.02369	0.001	0.001	0.003	0.011	0.000	0.000	-0.177	0.001	0.003	0.011	0.002	0.006	0.009
0.00224	0.016	0.009	0.006	0.002	0.011	0.003	0.001	-0.177	0.000	0.000	0.011	0.003	0.001
0.00652	0.004	0.006	0.009	0.006	0.003	0.011	0.003	0.000	-0.177	0.000	0.003	0.011	0.003
0.02369	0.001	0.002	0.006	0.009	0.001	0.003	0.011	0.000	0.000	-0.177	0.001	0.003	0.011
0.00224	0.016	0.011	0.003	0.001	0.009	0.006	0.002	0.011	0.003	0.001	-0.177	0.000	0.000
0.00652	0.004	0.003	0.011	0.003	0.006	0.009	0.006	0.003	0.011	0.003	0.000	-0.177	0.000
0.02369	0.001	0.001	0.003	0.011	0.002	0.006	0.009	0.001	0.003	0.011	0.000	0.000	-0.177

det (D) = 6E-11

$_{s1}D_2'$ =

-0.2654	0.0000	0.0015	0.0043	0.0158	0.0015	0.0043	0.0158	0.0015	0.0043	0.0158	0.0015	0.0043	0.0158
0.0064	0.0064	0.0158	0.0043	0.0015	0.0158	0.0043	0.0015	0.0158	0.0043	0.0015	0.0158	0.0043	0.0015
0.0022	0.0015	-0.1769	0.0000	0.0000	0.0106	0.0030	0.0006	0.0092	0.0055	0.0017	0.0106	0.0030	0.0006
0.0065	0.0043	0.0000	-0.1769	0.0000	0.0030	0.0106	0.0030	0.0055	0.0092	0.0055	0.0030	0.0106	0.0030
0.0237	0.0158	0.0000	0.0000	-0.1769	0.0006	0.0030	0.0106	0.0017	0.0055	0.0092	0.0006	0.0030	0.0106
0.0022	0.0015	0.0106	0.0030	0.0006	-0.1769	0.0000	0.0000	0.0106	0.0030	0.0006	0.0092	0.0055	0.0017
0.0065	0.0043	0.0030	0.0106	0.0030	0.0000	-0.1769	0.0000	0.0030	0.0106	0.0030	0.0055	0.0092	0.0055
0.0237	0.0158	0.0006	0.0030	0.0106	0.0000	0.0000	-0.1769	0.0006	0.0030	0.0106	0.0017	0.0055	0.0092
0.0022	0.0015	0.0092	0.0055	0.0017	0.0106	0.0030	0.0006	-0.1769	0.0000	0.0000	0.0106	0.0030	0.0006
0.0065	0.0043	0.0055	0.0092	0.0055	0.0030	0.0106	0.0030	0.0000	-0.1769	0.0000	0.0030	0.0106	0.0030
0.0237	0.0158	0.0017	0.0055	0.0092	0.0006	0.0030	0.0106	0.0000	0.0000	-0.1769	0.0006	0.0030	0.0106
0.0022	0.0015	0.0106	0.0030	0.0006	0.0092	0.0055	0.0017	0.0106	0.0030	0.0006	-0.1769	0.0000	0.0000
0.0065	0.0043	0.0030	0.0106	0.0030	0.0055	0.0092	0.0055	0.0030	0.0106	0.0030	0.0000	-0.1769	0.0000
0.0237	0.0158	0.0006	0.0030	0.0106	0.0017	0.0055	0.0092	0.0006	0.0030	0.0106	0.0000	0.0000	-0.1769

$\det(_{s1}D_2') = -2.0E-12$

Total View Factor Matrix:

$\mathbb{F}_{ij}$	**j = 1**	**2**	**3**	**4**	**5**	**6**	**7**	**8**	**9**	**10**	**11**	**12**	**13**	**14**	$\sum_{j=1}^{n}\mathbb{F}_{ij}$
i =1	0.0373	0.0424	0.0158	0.0342	0.0926	0.0158	0.0342	0.0926	0.0158	0.0342	0.0926	0.0158	0.0342	0.0926	0.65
2	0.0424	0.0380	0.0926	0.0342	0.0158	0.0926	0.0342	0.0158	0.0926	0.0342	0.0158	0.0926	0.0342	0.0158	0.65
3	0.0239	0.1392	0.0269	0.0162	0.0087	0.0947	0.0343	0.0116	0.0854	0.0499	0.0184	0.0947	0.0343	0.0116	0.65
4	0.0508	0.0508	0.0162	0.0217	0.0162	0.0343	0.0890	0.0343	0.0499	0.0792	0.0499	0.0343	0.0890	0.0343	0.65
5	0.1392	0.0239	0.0087	0.0162	0.0269	0.0116	0.0343	0.0947	0.0184	0.0499	0.0854	0.0116	0.0343	0.0947	0.65
6	0.0239	0.1392	0.0947	0.0343	0.0116	0.0269	0.0162	0.0087	0.0947	0.0343	0.0116	0.0854	0.0499	0.0184	0.65
7	0.0508	0.0508	0.0343	0.0890	0.0343	0.0162	0.0217	0.0162	0.0343	0.0890	0.0343	0.0499	0.0792	0.0499	0.65
8	0.1392	0.0239	0.0116	0.0343	0.0947	0.0087	0.0162	0.0269	0.0116	0.0343	0.0947	0.0184	0.0499	0.0854	0.65
9	0.0239	0.1392	0.0854	0.0499	0.0184	0.0947	0.0343	0.0116	0.0269	0.0162	0.0087	0.0947	0.0343	0.0116	0.65
10	0.0508	0.0508	0.0499	0.0792	0.0499	0.0343	0.0890	0.0343	0.0162	0.0217	0.0162	0.0343	0.0890	0.0343	0.65
11	0.1392	0.0239	0.0184	0.0499	0.0854	0.0116	0.0343	0.0947	0.0087	0.0162	0.0269	0.0116	0.0343	0.0947	0.65
12	0.0239	0.1392	0.0947	0.0343	0.0116	0.0854	0.0499	0.0184	0.0947	0.0343	0.0116	0.0269	0.0162	0.0087	0.65
13	0.0508	0.0508	0.0343	0.0890	0.0343	0.0499	0.0792	0.0499	0.0343	0.0890	0.0343	0.0162	0.0217	0.0162	0.65
14	0.1392	0.0239	0.0116	0.0343	0.0947	0.0184	0.0499	0.0854	0.0116	0.0343	0.0947	0.0087	0.0162	0.0269	0.65

Heat Transfer Calculations for each Surface:

Surface Energies, $E_i = \sigma T_i^4$

Surface,*i*	1	2	3	4	5	6	7	8	9	10	11	12	13	14
E_i	27284.1	696.798	2202.23	2202.23	2202.23	2202.23	2202.23	2202.23	2202.23	2202.23	2202.23	2202.23	2202.23	2202.23

$$q_{i\to j} = \mathbb{F}_{ij} A_i E_i$$

q_{ij}	**j = 1**	**2**	**3**	**4**	**5**	**6**	**7**	**8**	**9**	**10**	**11**	**12**	**13**	**14**	$q_{net_i} = \sum_{i=1}^{n} q_{i\rightleftharpoons j}$
i =1	0	104.75	36.81	79.71	215.69	36.81	79.69	215.77	36.82	79.69	215.77	36.81	79.69	215.69	1433.69
2	-104.75	0	-12.95	-4.78	-2.21	-12.95	-4.78	-2.21	-12.95	-4.78	-2.21	-12.95	-4.78	-2.21	-184.51
3	-37.06	12.97	0	0	0	0	0	0	0	0	0	0	0	0	-24.09
4	-78.81	4.73	0	0	0	0	0	0	0	0	0	0	0	0	-74.08
5	-216.17	2.22	0	0	0	0	0	0	0	0	0	0	0	0	-213.94
6	-37.06	12.97	0	0	0	0	0	0	0	0	0	0	0	0	-24.09
7	-78.81	4.73	0	0	0	0	0	0	0	0	0	0	0	0	-74.08
8	-216.17	2.22	0	0	0	0	0	0	0	0	0	0	0	0	-213.94
9	-37.06	12.97	0	0	0	0	0	0	0	0	0	0	0	0	-24.09
10	-78.81	4.73	0	0	0	0	0	0	0	0	0	0	0	0	-74.08
11	-216.17	2.22	0	0	0	0	0	0	0	0	0	0	0	0	-213.94
12	-37.06	12.97	0	0	0	0	0	0	0	0	0	0	0	0	-24.09
13	-78.81	4.73	0	0	0	0	0	0	0	0	0	0	0	0	-74.08
14	-216.17	2.22	0	0	0	0	0	0	0	0	0	0	0	0	-213.94

Total View Factors Method

Coefficient Matrix:

$$\partial = \begin{vmatrix}
1.538 & -0.037 & -0.009 & -0.025 & -0.092 & -0.009 & -0.025 & -0.092 & -0.009 & -0.025 & -0.092 & -0.009 & -0.025 & -0.092 \\
-0.037 & 1.538 & -0.092 & -0.025 & -0.009 & -0.092 & -0.025 & -0.009 & -0.092 & -0.025 & -0.009 & -0.092 & -0.025 & -0.009 \\
-0.013 & -0.137 & 1.538 & 0.000 & 0.000 & -0.092 & -0.026 & -0.005 & -0.080 & -0.048 & -0.015 & -0.092 & -0.026 & -0.005 \\
-0.038 & -0.038 & 0.000 & 1.538 & 0.000 & -0.026 & -0.092 & -0.026 & -0.048 & -0.080 & -0.048 & -0.026 & -0.092 & -0.026 \\
-0.137 & -0.013 & 0.000 & 0.000 & 1.538 & -0.005 & -0.026 & -0.092 & -0.015 & -0.048 & -0.080 & -0.005 & -0.026 & -0.092 \\
-0.013 & -0.137 & -0.092 & -0.026 & -0.005 & 1.538 & 0.000 & 0.000 & -0.092 & -0.026 & -0.005 & -0.080 & -0.048 & -0.015 \\
-0.038 & -0.038 & -0.026 & -0.092 & -0.026 & 0.000 & 1.538 & 0.000 & -0.026 & -0.092 & -0.026 & -0.048 & -0.080 & -0.048 \\
-0.137 & -0.013 & -0.005 & -0.026 & -0.092 & 0.000 & 0.000 & 1.538 & -0.005 & -0.026 & -0.092 & -0.015 & -0.048 & -0.080 \\
-0.013 & -0.137 & -0.080 & -0.048 & -0.015 & -0.092 & -0.026 & -0.005 & 1.538 & 0.000 & 0.000 & -0.092 & -0.026 & -0.005 \\
-0.038 & -0.038 & -0.048 & -0.080 & -0.048 & -0.026 & -0.092 & -0.026 & 0.000 & 1.538 & 0.000 & -0.026 & -0.092 & -0.026 \\
-0.137 & -0.013 & -0.015 & -0.048 & -0.080 & -0.005 & -0.026 & -0.092 & 0.000 & 0.000 & 1.538 & -0.005 & -0.026 & -0.092 \\
-0.013 & -0.137 & -0.092 & -0.026 & -0.005 & -0.080 & -0.048 & -0.015 & -0.092 & -0.026 & -0.005 & 1.538 & 0.000 & 0.000 \\
-0.038 & -0.038 & -0.026 & -0.092 & -0.026 & -0.048 & -0.080 & -0.048 & -0.026 & -0.092 & -0.026 & 0.000 & 1.538 & 0.000 \\
-0.137 & -0.013 & -0.005 & -0.026 & -0.092 & -0.015 & -0.048 & -0.080 & -0.005 & -0.026 & -0.092 & 0.000 & 0.000 & 1.538
\end{vmatrix}$$

$$M = \begin{vmatrix}
-1 & 0.069 & 0.016 & 0.047 & 0.170 & 0.016 & 0.047 & 0.170 & 0.016 & 0.047 & 0.170 & 0.016 & 0.047 & 0.170 \\
0.069 & -1 & 0.170 & 0.047 & 0.016 & 0.170 & 0.047 & 0.016 & 0.170 & 0.047 & 0.016 & 0.170 & 0.047 & 0.016 \\
0.024 & 0.255 & -1 & 0.000 & 0.000 & 0.171 & 0.048 & 0.009 & 0.148 & 0.089 & 0.028 & 0.171 & 0.048 & 0.009 \\
0.070 & 0.070 & 0.000 & -1 & 0.000 & 0.048 & 0.171 & 0.048 & 0.089 & 0.148 & 0.089 & 0.048 & 0.171 & 0.048 \\
0.255 & 0.024 & 0.000 & 0.000 & -1 & 0.009 & 0.048 & 0.171 & 0.028 & 0.089 & 0.148 & 0.009 & 0.048 & 0.171 \\
0.024 & 0.255 & 0.171 & 0.048 & 0.009 & -1 & 0.000 & 0.000 & 0.171 & 0.048 & 0.009 & 0.148 & 0.089 & 0.028 \\
0.070 & 0.070 & 0.048 & 0.171 & 0.048 & 0.000 & -1 & 0.000 & 0.048 & 0.171 & 0.048 & 0.089 & 0.148 & 0.089 \\
0.255 & 0.024 & 0.009 & 0.048 & 0.171 & 0.000 & 0.000 & -1 & 0.009 & 0.048 & 0.171 & 0.028 & 0.089 & 0.148 \\
0.024 & 0.255 & 0.148 & 0.089 & 0.028 & 0.171 & 0.048 & 0.009 & -1 & 0.000 & 0.000 & 0.171 & 0.048 & 0.009 \\
0.070 & 0.070 & 0.089 & 0.148 & 0.089 & 0.048 & 0.171 & 0.048 & 0.000 & -1 & 0.000 & 0.048 & 0.171 & 0.048 \\
0.255 & 0.024 & 0.028 & 0.089 & 0.148 & 0.009 & 0.048 & 0.171 & 0.000 & 0.000 & -1 & 0.009 & 0.048 & 0.171 \\
0.024 & 0.255 & 0.171 & 0.048 & 0.009 & 0.148 & 0.089 & 0.028 & 0.171 & 0.048 & 0.009 & -1 & 0.000 & 0.000 \\
0.070 & 0.070 & 0.048 & 0.171 & 0.048 & 0.089 & 0.148 & 0.089 & 0.048 & 0.171 & 0.048 & 0.000 & -1 & 0.000 \\
0.255 & 0.024 & 0.009 & 0.048 & 0.171 & 0.028 & 0.089 & 0.148 & 0.009 & 0.048 & 0.171 & 0.000 & 0.000 & -1
\end{vmatrix}$$

Emissivity Matrix:

$$\varepsilon = \begin{vmatrix}
0.65 & 0 & 0 & 0 & 0 & 0 & 0 & 0 & 0 & 0 & 0 & 0 & 0 & 0 \\
0 & 0.65 & 0 & 0 & 0 & 0 & 0 & 0 & 0 & 0 & 0 & 0 & 0 & 0 \\
0 & 0 & 0.65 & 0 & 0 & 0 & 0 & 0 & 0 & 0 & 0 & 0 & 0 & 0 \\
0 & 0 & 0 & 0.65 & 0 & 0 & 0 & 0 & 0 & 0 & 0 & 0 & 0 & 0 \\
0 & 0 & 0 & 0 & 0.65 & 0 & 0 & 0 & 0 & 0 & 0 & 0 & 0 & 0 \\
0 & 0 & 0 & 0 & 0 & 0.65 & 0 & 0 & 0 & 0 & 0 & 0 & 0 & 0 \\
0 & 0 & 0 & 0 & 0 & 0 & 0.65 & 0 & 0 & 0 & 0 & 0 & 0 & 0 \\
0 & 0 & 0 & 0 & 0 & 0 & 0 & 0.65 & 0 & 0 & 0 & 0 & 0 & 0 \\
0 & 0 & 0 & 0 & 0 & 0 & 0 & 0 & 0.65 & 0 & 0 & 0 & 0 & 0 \\
0 & 0 & 0 & 0 & 0 & 0 & 0 & 0 & 0 & 0.65 & 0 & 0 & 0 & 0 \\
0 & 0 & 0 & 0 & 0 & 0 & 0 & 0 & 0 & 0 & 0.65 & 0 & 0 & 0 \\
0 & 0 & 0 & 0 & 0 & 0 & 0 & 0 & 0 & 0 & 0 & 0.65 & 0 & 0 \\
0 & 0 & 0 & 0 & 0 & 0 & 0 & 0 & 0 & 0 & 0 & 0 & 0.65 & 0 \\
0 & 0 & 0 & 0 & 0 & 0 & 0 & 0 & 0 & 0 & 0 & 0 & 0 & 0.65
\end{vmatrix}$$

Total View Factor Matrix:

$$\mathbb{F} = \begin{vmatrix}
0.0373 & 0.0424 & 0.0158 & 0.0342 & 0.0926 & 0.0158 & 0.0342 & 0.0926 & 0.0158 & 0.0342 & 0.0926 & 0.0158 & 0.0342 & 0.0926 \\
0.0424 & 0.0380 & 0.0926 & 0.0342 & 0.0158 & 0.0926 & 0.0342 & 0.0158 & 0.0926 & 0.0342 & 0.0158 & 0.0926 & 0.0342 & 0.0158 \\
0.0239 & 0.1392 & 0.0269 & 0.0162 & 0.0087 & 0.0947 & 0.0343 & 0.0116 & 0.0854 & 0.0499 & 0.0184 & 0.0947 & 0.0343 & 0.0116 \\
0.0508 & 0.0508 & 0.0162 & 0.0217 & 0.0162 & 0.0343 & 0.0890 & 0.0343 & 0.0499 & 0.0792 & 0.0499 & 0.0343 & 0.0890 & 0.0343 \\
0.1392 & 0.0239 & 0.0087 & 0.0162 & 0.0269 & 0.0116 & 0.0343 & 0.0947 & 0.0184 & 0.0499 & 0.0854 & 0.0116 & 0.0343 & 0.0947 \\
0.0239 & 0.1392 & 0.0947 & 0.0343 & 0.0116 & 0.0269 & 0.0162 & 0.0087 & 0.0947 & 0.0343 & 0.0116 & 0.0854 & 0.0499 & 0.0184 \\
0.0508 & 0.0508 & 0.0343 & 0.0890 & 0.0343 & 0.0162 & 0.0217 & 0.0162 & 0.0343 & 0.0890 & 0.0343 & 0.0499 & 0.0792 & 0.0499 \\
0.1392 & 0.0239 & 0.0116 & 0.0343 & 0.0947 & 0.0087 & 0.0162 & 0.0269 & 0.0116 & 0.0343 & 0.0947 & 0.0184 & 0.0499 & 0.0854 \\
0.0239 & 0.1392 & 0.0854 & 0.0499 & 0.0184 & 0.0947 & 0.0343 & 0.0116 & 0.0269 & 0.0162 & 0.0087 & 0.0947 & 0.0343 & 0.0116 \\
0.0508 & 0.0508 & 0.0499 & 0.0792 & 0.0499 & 0.0343 & 0.0890 & 0.0343 & 0.0162 & 0.0217 & 0.0162 & 0.0343 & 0.0890 & 0.0343 \\
0.1392 & 0.0239 & 0.0184 & 0.0499 & 0.0854 & 0.0116 & 0.0343 & 0.0947 & 0.0087 & 0.0162 & 0.0269 & 0.0116 & 0.0343 & 0.0947 \\
0.0239 & 0.1392 & 0.0947 & 0.0343 & 0.0116 & 0.0854 & 0.0499 & 0.0184 & 0.0947 & 0.0343 & 0.0116 & 0.0269 & 0.0162 & 0.0087 \\
0.0508 & 0.0508 & 0.0343 & 0.0890 & 0.0343 & 0.0499 & 0.0792 & 0.0499 & 0.0343 & 0.0890 & 0.0343 & 0.0162 & 0.0217 & 0.0162 \\
0.1392 & 0.0239 & 0.0116 & 0.0343 & 0.0947 & 0.0184 & 0.0499 & 0.0854 & 0.0116 & 0.0343 & 0.0947 & 0.0087 & 0.0162 & 0.0269
\end{vmatrix}$$

Heat Transfer between Surfaces

q =

0	104.75	36.81	79.71	215.69	36.81	79.69	215.77	36.82	79.69	215.77	36.81	79.69	215.69
-104.75	0	-12.95	-4.78	-2.21	-12.95	-4.78	-2.21	-12.95	-4.78	-2.21	-12.95	-4.78	-2.21
-37.06	12.97	0	0	0	0	0	0	0	0	0	0	0	0
-78.81	4.73	0	0	0	0	0	0	0	0	0	0	0	0
-216.17	2.22	0	0	0	0	0	0	0	0	0	0	0	0
-37.06	12.97	0	0	0	0	0	0	0	0	0	0	0	0
-78.81	4.73	0	0	0	0	0	0	0	0	0	0	0	0
-216.17	2.22	0	0	0	0	0	0	0	0	0	0	0	0
-37.06	12.97	0	0	0	0	0	0	0	0	0	0	0	0
-78.81	4.73	0	0	0	0	0	0	0	0	0	0	0	0
-216.17	2.22	0	0	0	0	0	0	0	0	0	0	0	0
-37.06	12.97	0	0	0	0	0	0	0	0	0	0	0	0
-78.81	4.73	0	0	0	0	0	0	0	0	0	0	0	0
-216.17	2.22	0	0	0	0	0	0	0	0	0	0	0	0

Camparison of results with those published by Clark and Korybalski (1974)

Surface, *i*	Net Heat Transfer Results, $q_{net,i}$ (Watts)		
	Author	Clark and Korybalski (1974)	Discrepancy
1	1433.69	1435.84	2.15
2	-184.51	-182.75	1.76
3	-24.09	-23.06	1.03
4	-74.08	-69.52	4.56
5	-213.94	-215.50	-1.56
6	-24.09	-23.06	1.03
7	-74.08	-69.52	4.56
8	-213.94	-215.50	-1.56
9	-24.09	-23.06	1.03
10	-74.08	-69.52	4.56
11	-213.94	-215.50	-1.56
12	-24.09	-23.06	1.03
13	-74.08	-69.52	4.56
14	-213.94	-215.50	-1.56